about Supporting Researchers

Kazuki Yoshizoe

Data Analysis Support Division, Data-Driven Innovation Initiative, Kyushu University

Research Institute for Information Technology, Kyushu University

Data Analysis Support Division

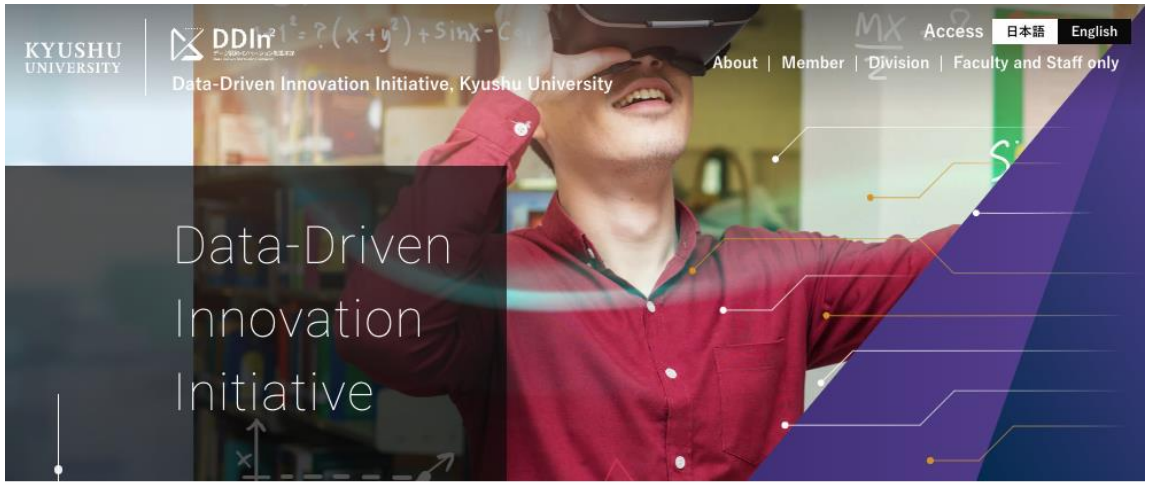

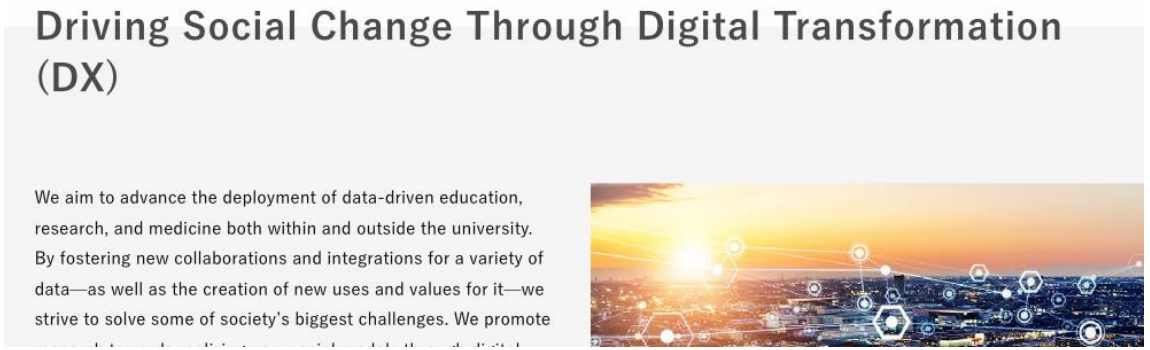

https://dx.kyushu-u.ac.jp/en/

DAS is one of the divisions in Data-Driven Innovation Initiative, Kyushu Univ (since this April).

We aim at accelerating early-stage applied data science researches.

- algorithms
- computing resources

Our activities

- Provide lectures / training sessions about
  - Statistical tools
  - Data Science software
  - Hands-on sessions for supercomputer usage
- Examples of the topics
  - Supercomputer training sessions
  - “GPU minicamp”
  - Statistics Lectures
  - Quantum Computer software
  - Game develop engine

Kyushu-U Supercomputer “Genkai”

We also aim at providing computing resources at a reasonable cost.

玄界 Genkai

Part of the members of the division are supercomputer experts. (Including me)

High Performance Computing

Simplify access to HPC for Diverse Research

computing resource

CPU nodes / GPU nodes

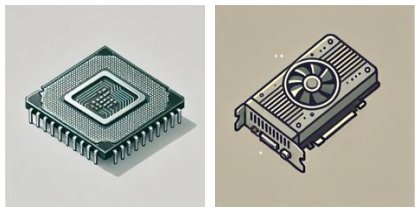

Large size memory

Large or Fast storage

suitable for various usage
e.g. “AI + HPC”

Easy-to-use

supporting software

Open OnDemand

NextCloud

Users can use supercomputers from the browsers
e.g., launching Jupyter

File sharing is also easy

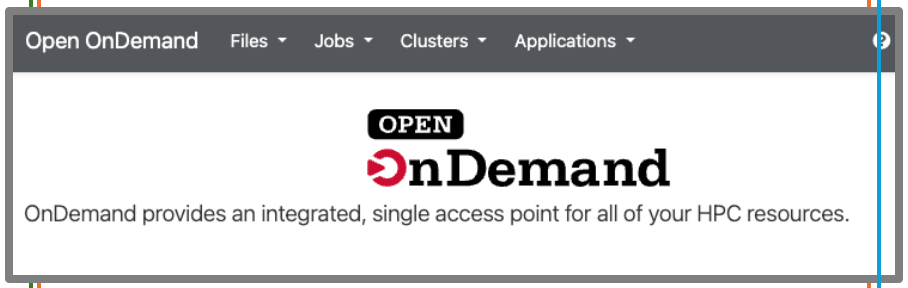

welcome new users

Hands-on sessions which supports various research projects.

Find Molecules by **HPC**, **AI**, and **Search**

Parallel Search Algorithm

Search space of (small) organic compounds

Monte-Carlo Tree Search

2003 nicolas p. rougier (CC BY-SA 4.0)

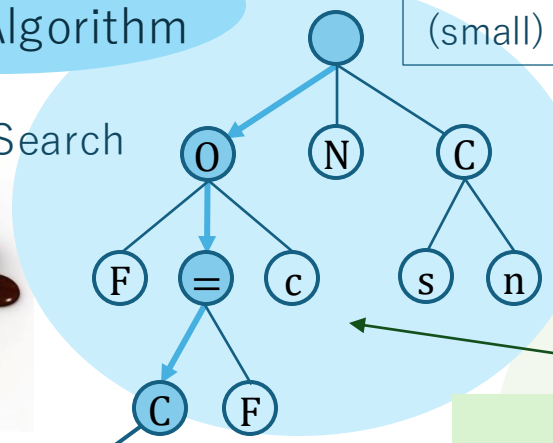

HPC
High Performance Computing

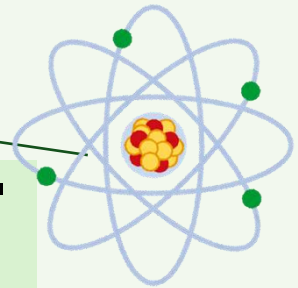

Calculate reward using Simulators or ML models

Fast, approx.: Machine Learning Models
Slower, Accurate: Simulators

DNN Models

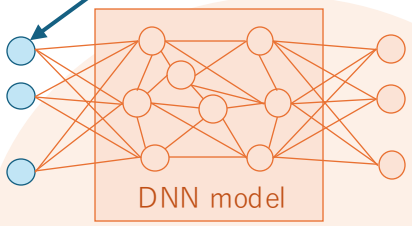

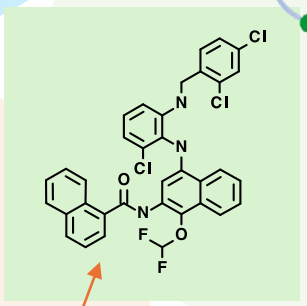

Sample promising molecules

O=**C**(Nc1cc(Nc2c(Cl)cccc2NCc2ccc(Cl)cc2Cl)c2ccccc2c1OC(F)F)c1cccc2ccccc12

Generate molecules as strings using DNN models trained on chemistry databases

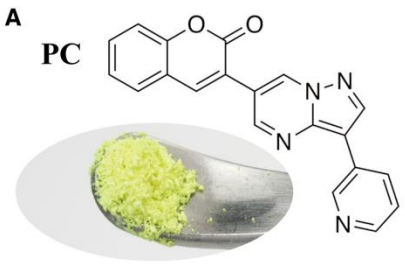

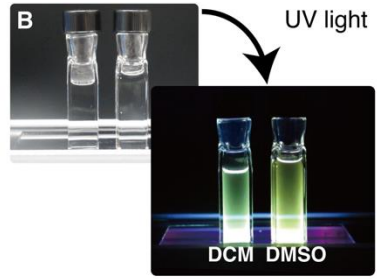

Novel fluorescent molecules [Sumita+2022, Fig. 5]

Your voice matters

- How you started?
- The cost?
- How you manage data?
- How did you overcome the difficulties?
- Any future demands? Complaints?

- Your opinion helps us improve our systems / services.

International Institute for Carbon-Neutral Energy Research

Characterize Geometry Structure of Porous Formation via Random Walks

Supported by JST-CREST Grant Number JPMJCR15D3 project on Topological Data Analysis

Nguyen Thi Hoai Linh

Multiscale Science and Engineering for Energy and the Environment Thrust, CESD, WPI - I²CNER, Kyushu University

WIS 2024

Ito Campus, Kyushu University

November 28-29, 2024

KYUSHU UNIVERSITY

wpi World Premier International Research Center Initiative

ILLINOIS

Objective

Join work with Prof. Tomoyuki Shirai (IMI, Kyushu University),
Prof. Takeshi Tsuji (I2CNER, University of Tokyo),

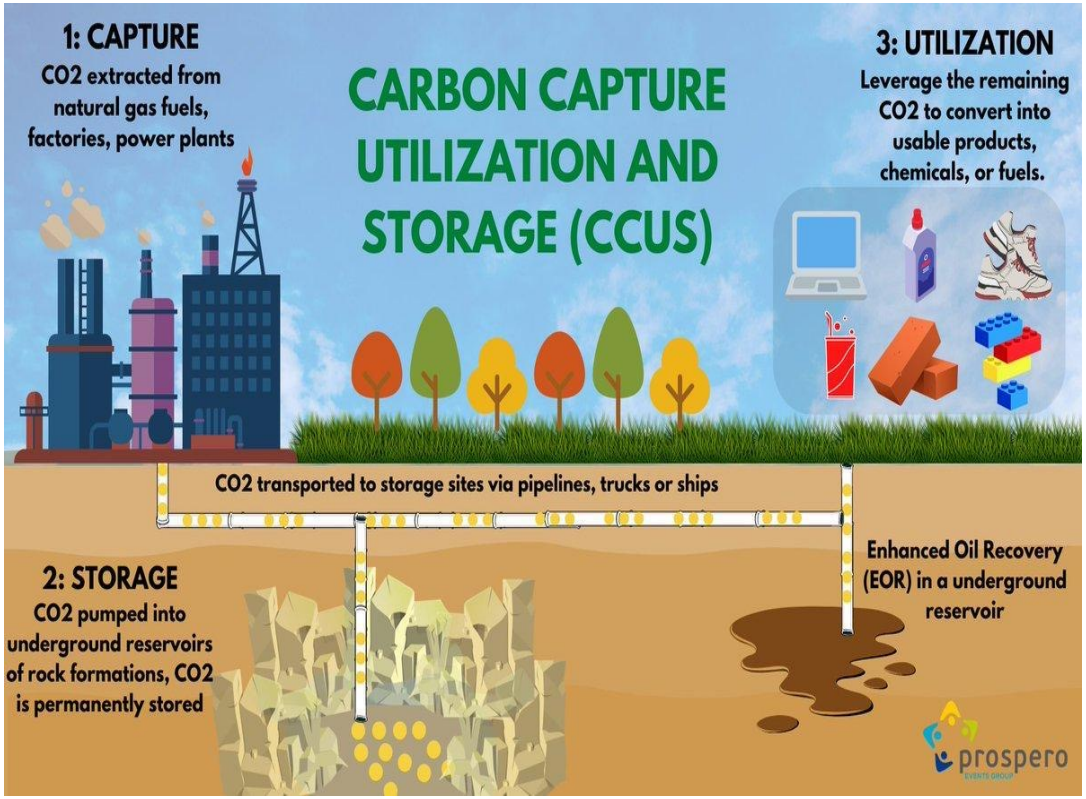

https://www.nextias.com/current-affairs/30-11-2022/carbon-capture-utilisation-and-storage-ccus-policy-framework

* Special Report on Carbon Dioxide Capture and Storage, Intergovernmental Panel on Climate Change (IPCC) 2005, B. Metz et al. ed Cambridge University Press

Motivation

- Geological sequestration of CO_2 – important technology on Carbon capture, utilization, and storage (CCUS).
- Among geological sequestration, mineral trapping is a promising solution contributed to negative emission by 2050.
- Geological storage capacity worldwide is likely (probability 60%~90%) at least about 2,000 $GtCO_2$.

Geological sequestration

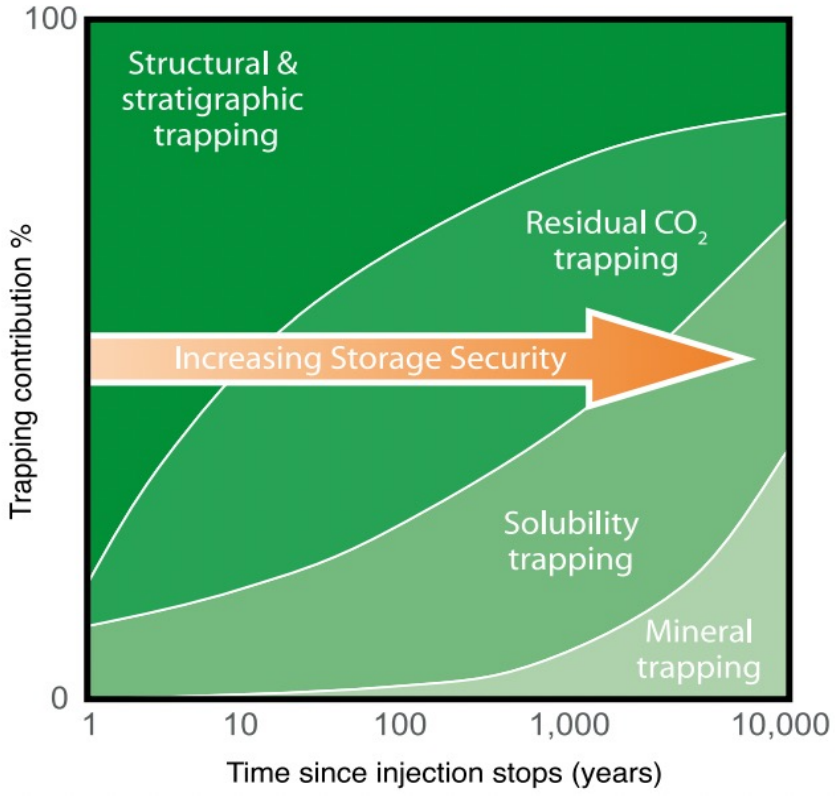

IPCC 2005: Storage security depends on a combination of physical and geochemical trapping

Geological sequestration: inject captured CO_2 into natural geological formations such as saline aquifers, oil and gas reservoirs and storing it permanently and safely there.

Security and efficency of CO_2 storage are ensured by several trapping mechanisms.

Challenging

- Geological sequestration has complicated mechanisms, depending on interplay between geomechanical, thermal, hydraulic and geochemical processes occurring as injected CO_2 migrates, dissolves in formation fluid, and reacts with formation bed rock.
- The trapping mechanisms (physical, residual, adsorption, solubility, mineral trapping,…) depend on several factors:
  - Injection conditions
  - Fluid properties
  - Characteristics of porous materials
- Trapping mechanisms occurs on different spatial and temporal scales and exhibit different degree of permanency.

Mathematical approach

Effective mathematical models can simulate a broad range of reservoir-relevant conditions within an acceptable period of time with use of improved computational resources.

- Study geometric structure of natural porous formation: ***graph notation, Random walk, Curve fitting***.
- Develop a nano-scale mathematical model: ***Random walk method***.
- Propose two ***probabilistic strategies for precipitation***.
- Obtain optimal injection conditions, rock formation favor fluid flow through simulation studies.

Study of effect of geometric structure to the fluid flow and precipitation process

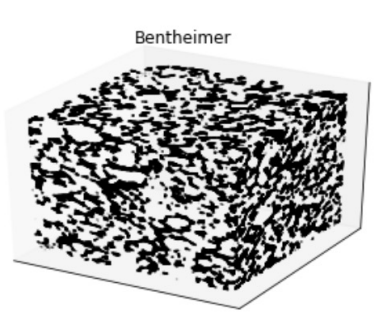

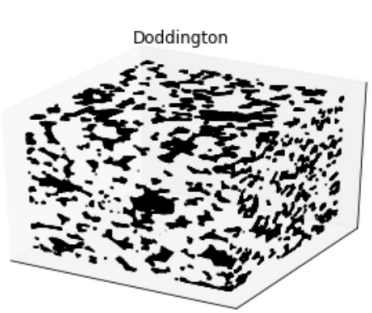

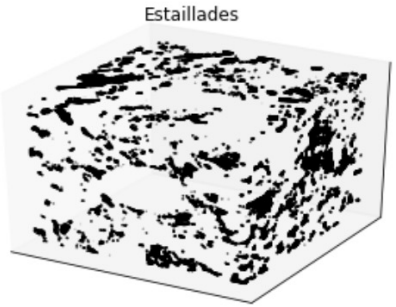

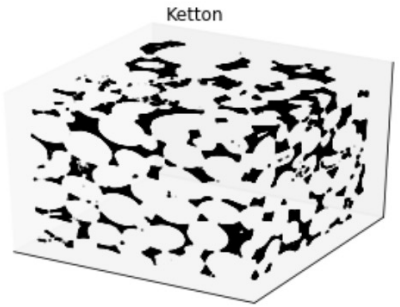

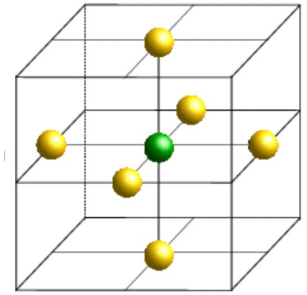

Binary rock extracted by high-resolution micro-computed tomography (CT): 1000x1000x1000 voxels, representing physical rock volume of approximately 3.2x3.2x3.2 mm.

6-lattice neighbors:

$$\mathcal{N}(x_t) = \{(i \pm 1, j, k), (i, j \pm 1, k), (i, j, k \pm 1)\}. \quad (1)$$

$$\mathcal{N}_p(x_t) = \mathcal{N}(x_t) \cap \mathcal{P}, \quad (2)$$

Connected component concept

Table: Statistics on void structure

	Bentheimer	Doddington	Estaillades	Ketton
Porosity	0.217	0.196	0.127	0.133
No. connected components	33,920	280	14,8329	39,190
No. passable components	1	1	1	1
Account for	99.764%	99.484%	85.668%	99.002%

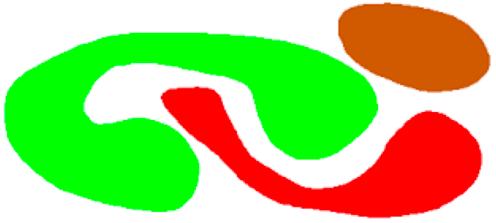

Particle flow through pore space

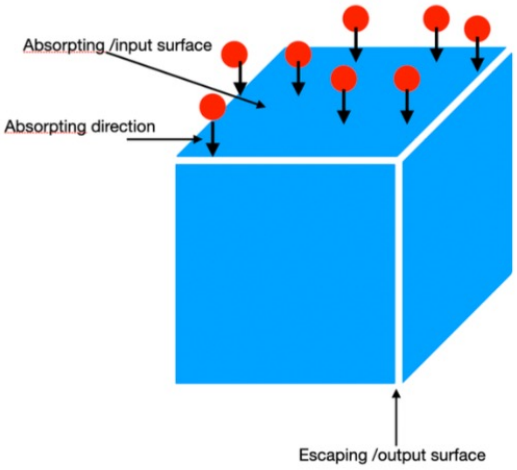

Random walk rule governing particle movement:

- Injected particle invades into pore space under the pressure gradient between the inlet and the outlet surfaces
- Particles' movement is driven by random walk rule:

The transition probability of a particle at position x_t to move to a position y is

	$\mathcal{N}_p(x_t) = \emptyset$	$\mathcal{N}_p(x_t) \neq \emptyset$
$y = x_t$	1	0
$y \in \mathcal{N}_p(x_t)$	0	specified as in (3) & (4)

$$p(x_t \to y) = \frac{g(x_t, y)}{\sum_{z \in \mathcal{N}_p(x_t)} g(x_t, z)}, \tag{3}$$

where

$$g(x_t, z) = \begin{cases} v + d & \text{if } x_t \to z \text{ is absorption direction} \\ d & \text{otherwise.} \end{cases} \tag{4}$$

Fluid flow invading

Evolution of particle flow propagation

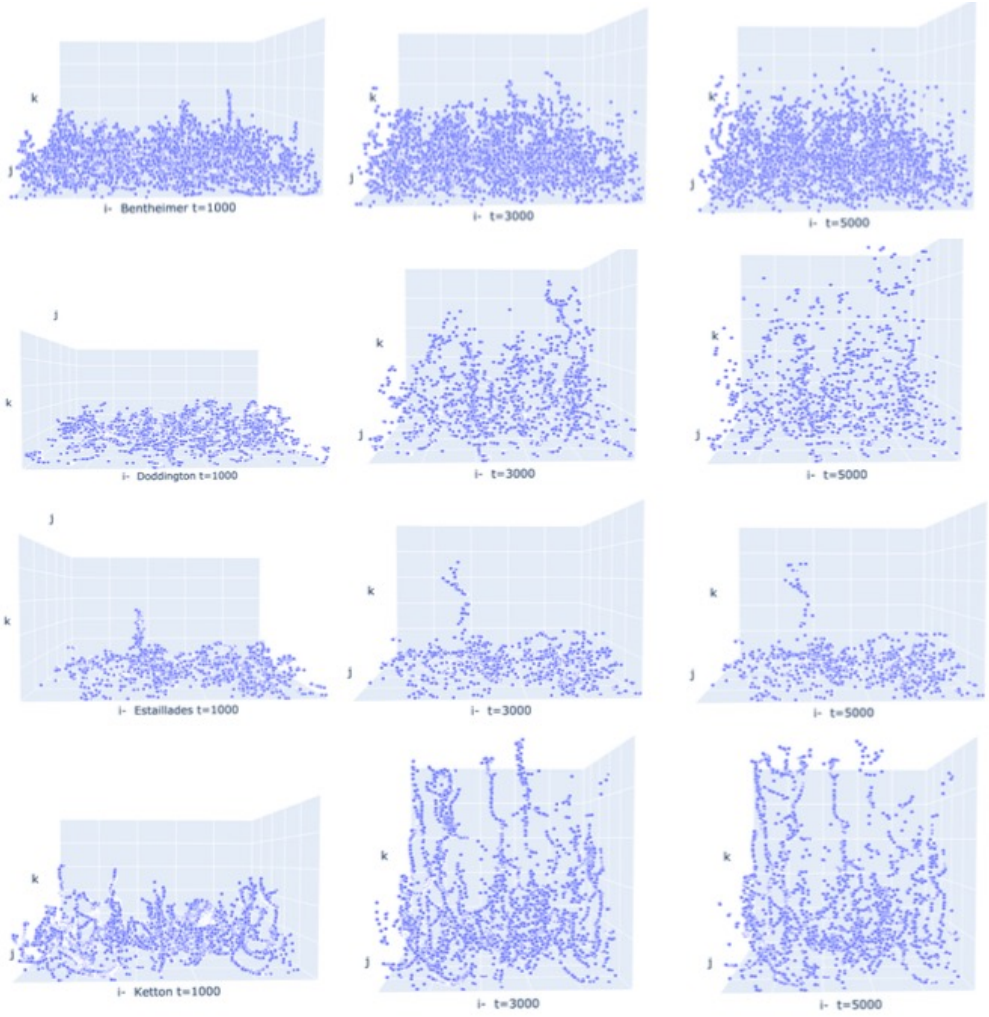

Particle distribution

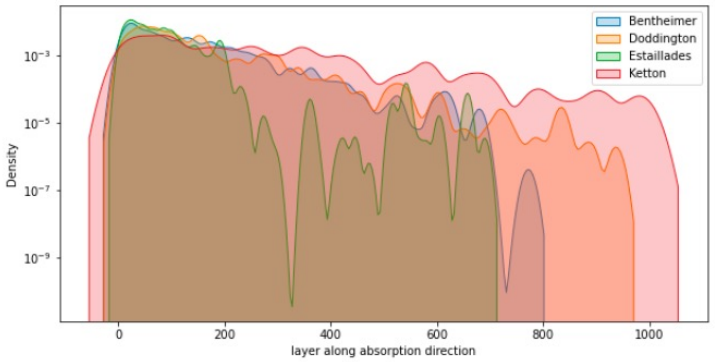

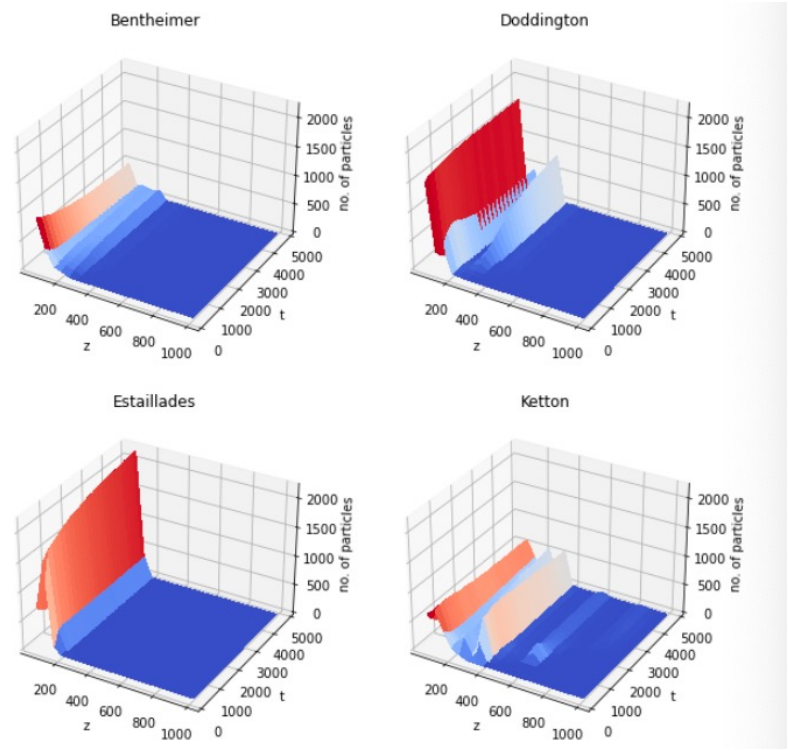

Fluid flow invading

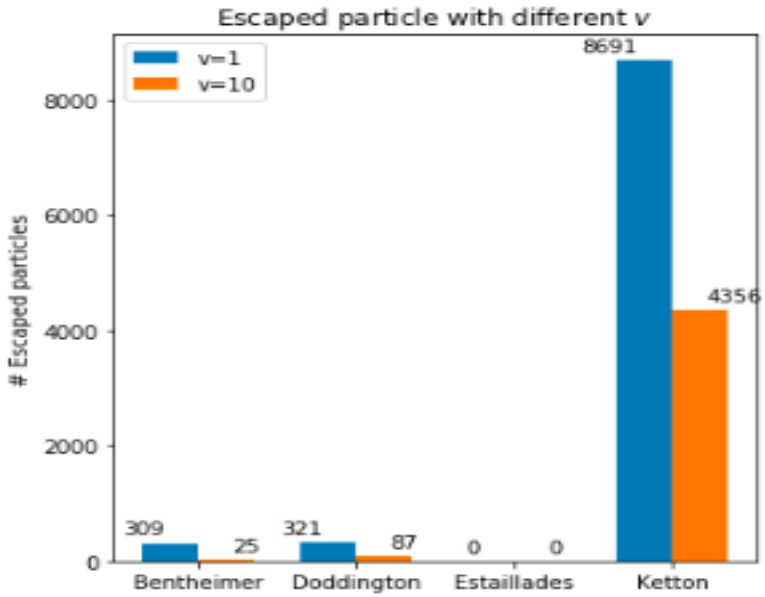

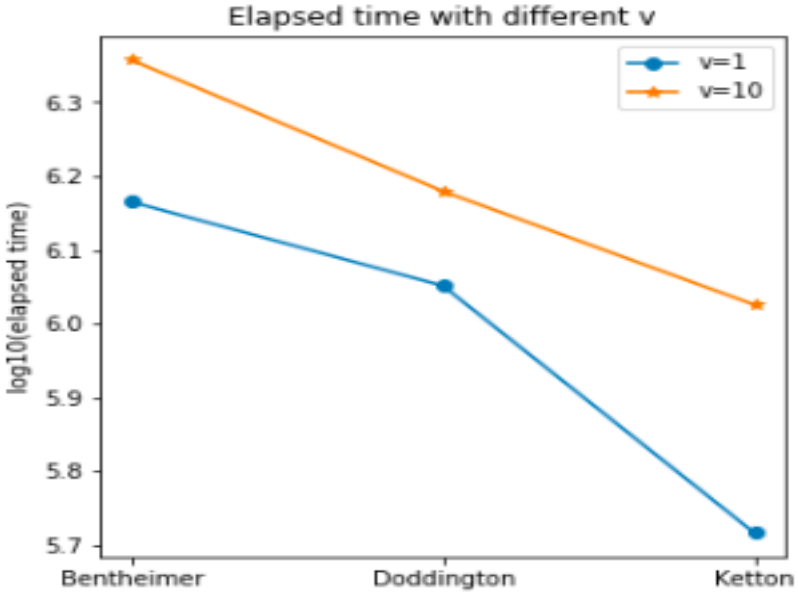

- Kettons shows the highest permeability
- Increasing pressure gradient does not necessarily increase the invading process
- Large pressure makes particles lose their flexibility to disperse to avoid obstacels.
- Pressure parameter should be appropriately chosen for maximizing fluid flow.

Precipitation rule

Rock voxel update: each pore voxel become grain voxel with probability:

$$\sum_{i=1}^{p}(1-q)^{i-1}q, \qquad (5)$$

$q \in [0,1]$: $probability\ of\ precipitation$,
p: number of time that particles have passed through the corresponding pore position

Single phase precipitation

Regression model:

$$\text{porosity decrease} = \exp(aq) + b$$

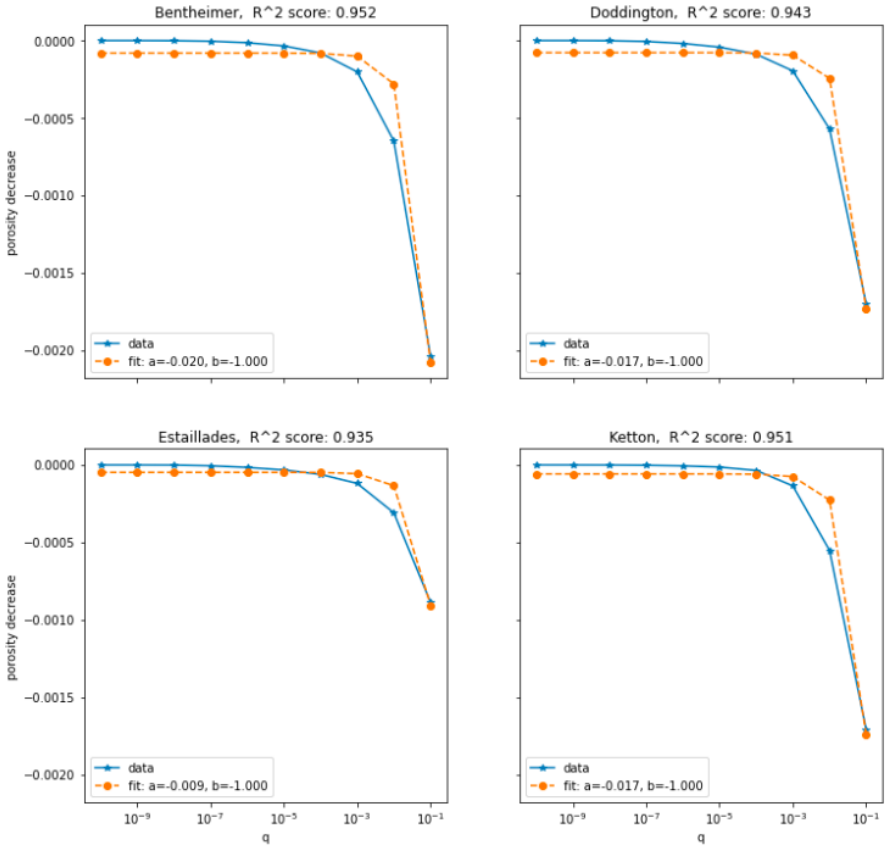

|a| describes the speed of the precipitation process:
Bentheimer => Doddington,
Ketton => Estaillades.

Multi-phase precipitation

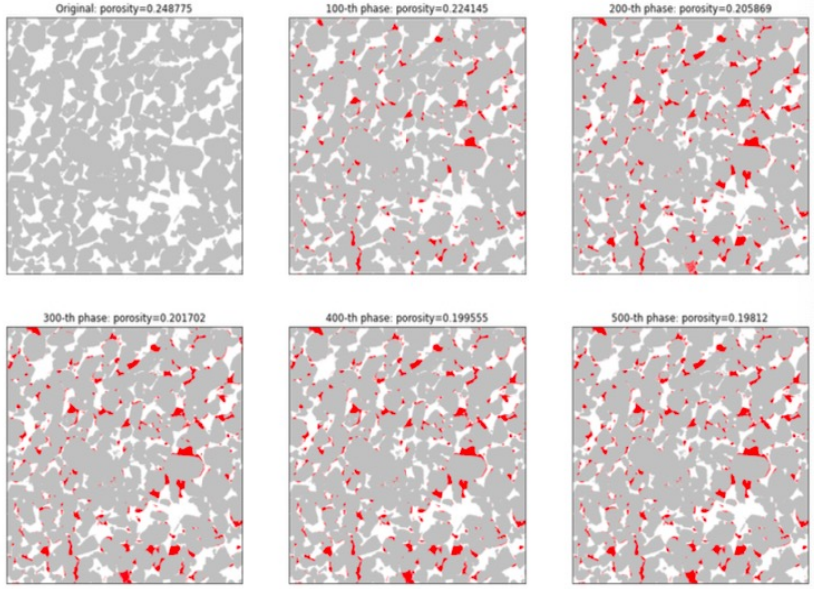

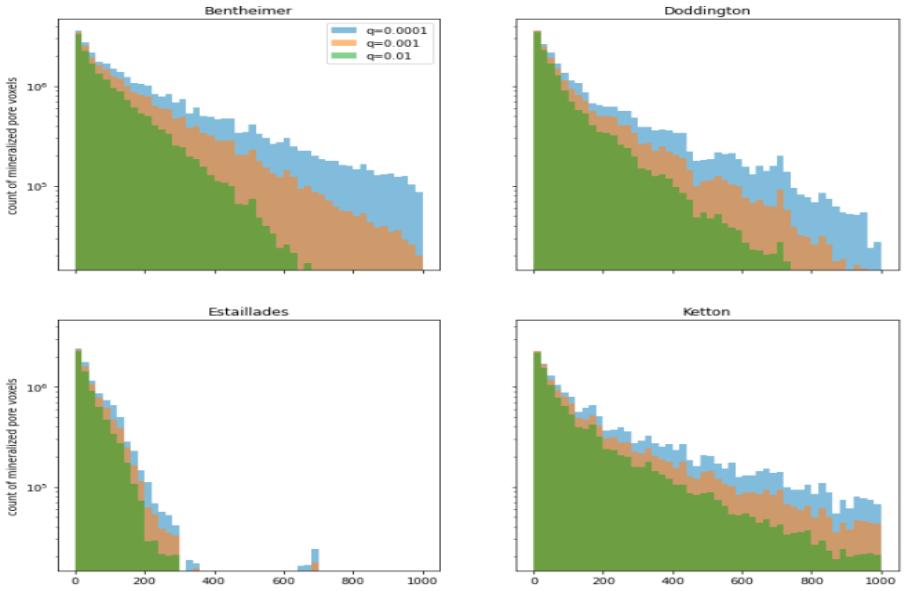

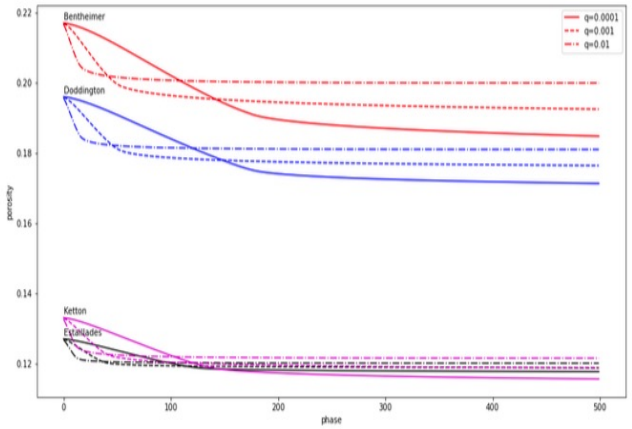

- Porosity decrease is no longer a monotonically non-increasing function of *q*.
- *When q is large, precipitation happens rapidly near the inlet surface, therefore narrows down or obturates the capillaries and prevents particles from invading deeper into the pore space.*

Future research direction

Research on carbon storage and management using the earth

Field-scale models for CO_2 storage

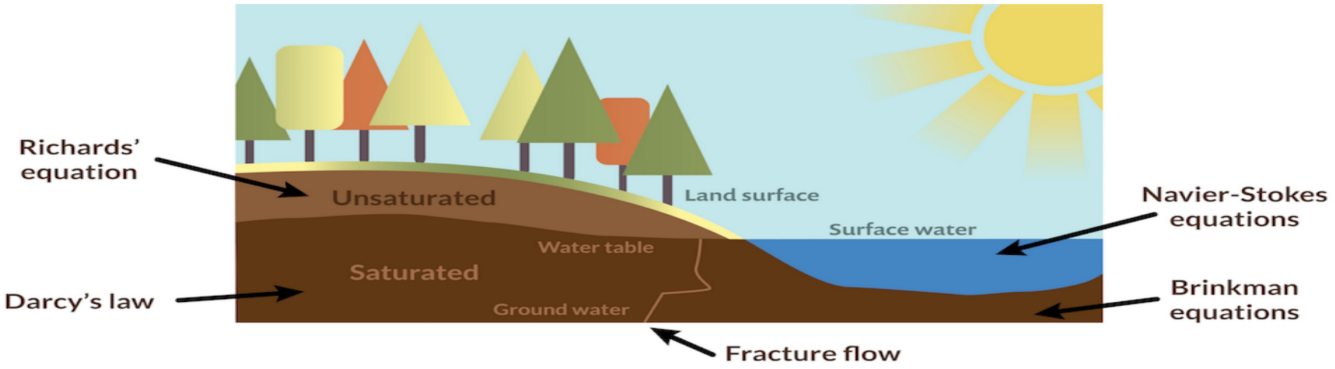

Estimates of spatial and temporal scales associated with CO_2 storage
(Nordbotten, JM, Celia, MA, *Geological Storage of CO2 Modeling Approaches for Large-Scale Simulation, Wiley, 2012*)

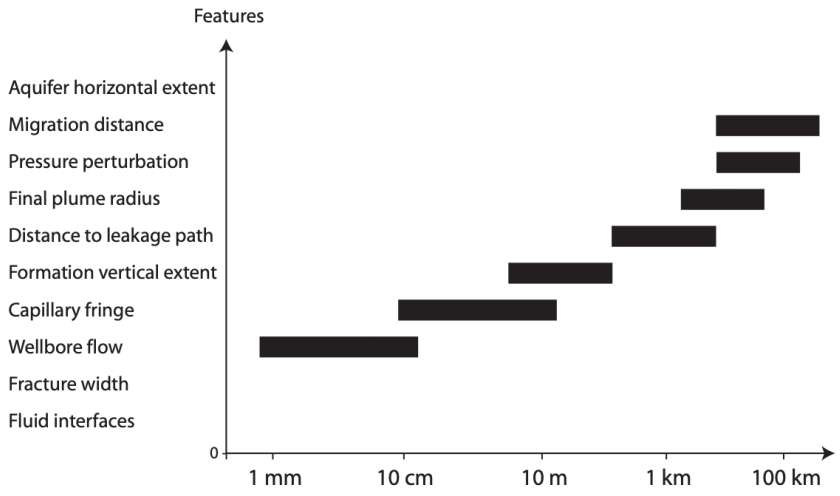

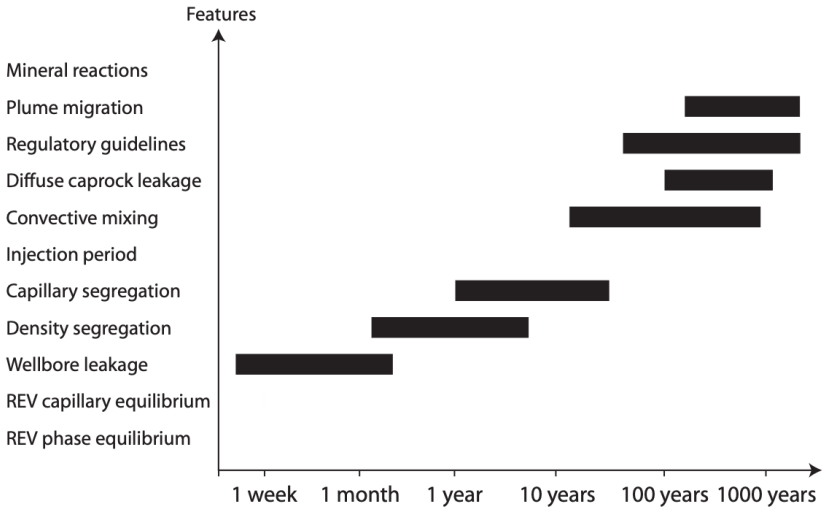

Future research direction

Research on carbon storage and management using the earth

Field-scale models for CO_2 storage

Equations for standard two-fluid system (micro and meso scales)[1]

$$\rho_\alpha \phi \frac{\partial s_\alpha}{\partial t} + s_\alpha \rho_\alpha c_\alpha \frac{\partial p_\alpha}{\partial t} + \nabla \cdot [\rho_\alpha \mathbf{u}_\alpha] = \Psi_\alpha,$$

$$\mathbf{u}_\alpha = -\lambda_\alpha \mathbf{k}(\nabla p_\alpha - \rho_\alpha \mathbf{g}), \quad (\alpha = w, n),$$

$$\sum_\alpha s_\alpha = s_w + s_n = 1,$$

$$p_n - p_w = p^{\mathrm{cap}}(s_w).$$

Heterogeneous Multiscale Method (HMM)[2]

Large-scale coarse-scale model

Combined challenge of

- nonlinear partial differential equation
- heterogeneous parameters

=> impossible for finding the exact solution at fine scales of resolution.

Approximate solutions

Model reduction

Numerical discretization

My approach

[1]Nordbotten, JM, Celia, MA, *Geological Storage of CO2 Modeling Approaches for Large-Scale Simulation, Wiley, 2012.*

[2]Weinan, E, Engquist, B, The heterogeneous multi-scale methods, Communications in Mathematical Science, 1, 87-133, 2003.

Future research direction

Research on carbon storage and management using the earth

Field-scale models for CO_2 storage

Topic 2: Injected CO_2 leakage model

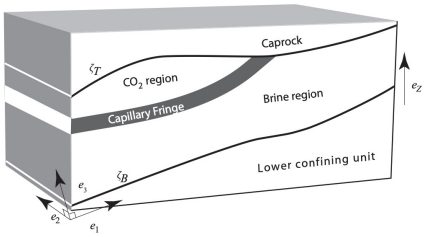

The imperfection in the caprock, including natural faults or fractions as well as old oil and gas wells, may allow for fluid leakage out of the injection formation. These need to be taken into account.

Fluid flow through aquifer (macro scales)

$$\frac{\partial M^i}{\partial t} + \nabla_{||} \cdot \mathbf{F}^i = \Psi^i_\Sigma,$$

M^i: mass of component i in $[\zeta_B, \zeta_T]$ per unit area
$\mathbf{F}^i$: coarse mass flux
Ψ^i_Σ: coarse source

$$M^i = C^i_M m^i \equiv \sum_\alpha \int_{\zeta_B}^{\zeta_T} \rho_\alpha \phi s_\alpha m^i_\alpha dx_3 = \int_{\zeta_B}^{\zeta_T} m^i dx_3,$$

$$\mathbf{F}^i = \mathbf{e}_{||} \cdot \sum_\alpha \int_{\zeta_B}^{\zeta_T} \rho_\alpha \mathbf{u}_\alpha m^i_\alpha dx_3,$$

$$\Psi^i_\Sigma = \int_{\zeta_B}^{\zeta_T} \psi^i dx_3 + \Psi^i_B - \Psi^i_T,$$

$$\mathbf{u}_\alpha = -\lambda_\alpha(s_\alpha)\mathbf{k}(\nabla p_\alpha - \rho_\alpha g),$$

m^i: mass of component i per volume of total porous medium.

Fluid flow through Wells and Fractures

$$U_{\alpha,3} = - \wedge_{\alpha,3}(S_\alpha) K_3 \Phi(\zeta_B, p_\alpha, \varrho_\alpha, h_{T,B}),$$

K_3: upscaled coefficients,

$$K_3 \equiv \left(\int_{\zeta_B}^{\zeta_T} k_3^{-1} dx_3 \right)^{-1} h_{T,B},$$

$$\wedge_{\alpha,3} \equiv \left(\int_{\zeta_B}^{\zeta_T} \lambda^{-1}_{\alpha,3} k_3^{-1} dx_3 K_3 \right)^{-1} h_{T,B},$$

$$\varrho_\alpha \equiv \frac{1}{h_{T,B}} \int_{\zeta_B}^{\zeta_T} \rho_\alpha dx_3.$$

Summary

- A tool to study geometric structure of porous rock formation.
- Developed nano-scale random walk models to investigate particle flow propagation within pore space
- Introduced a probabilistic rule for precipitation
- Our study suggests that geometry structure of Bentheimer, Doddington, and Ketton would be potentially appropriate for CO_2 storage, while Estaillades would not

The study proposed methods for characterizing the porous rock formation, which is important for storage site selection and provide knowledge of which conditions favour or disfavour injection process, can aid long-term prediction of the fate of injected CO_2

ADVANCING BIRD CLASSIFICATION: HARNESSING PSA-DENSENET FOR CALL-BASED

SONG TIANYU TA VIET TON

INTRODUCTION

MOTIVATION

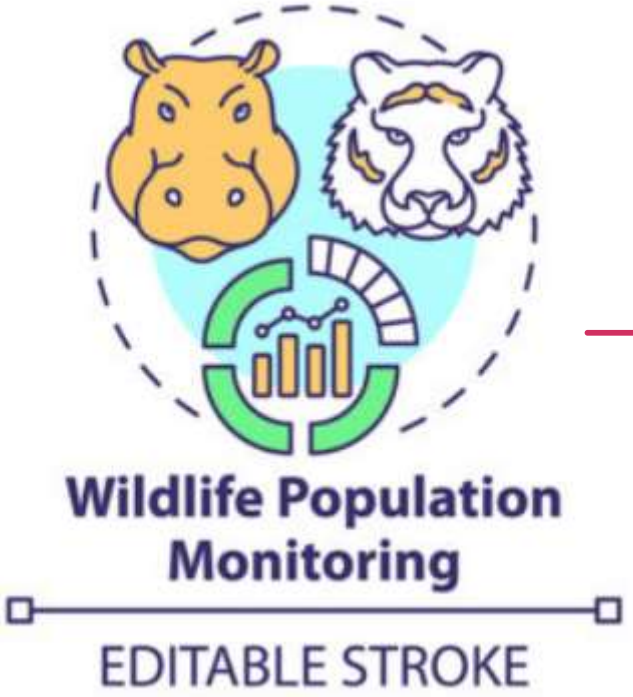

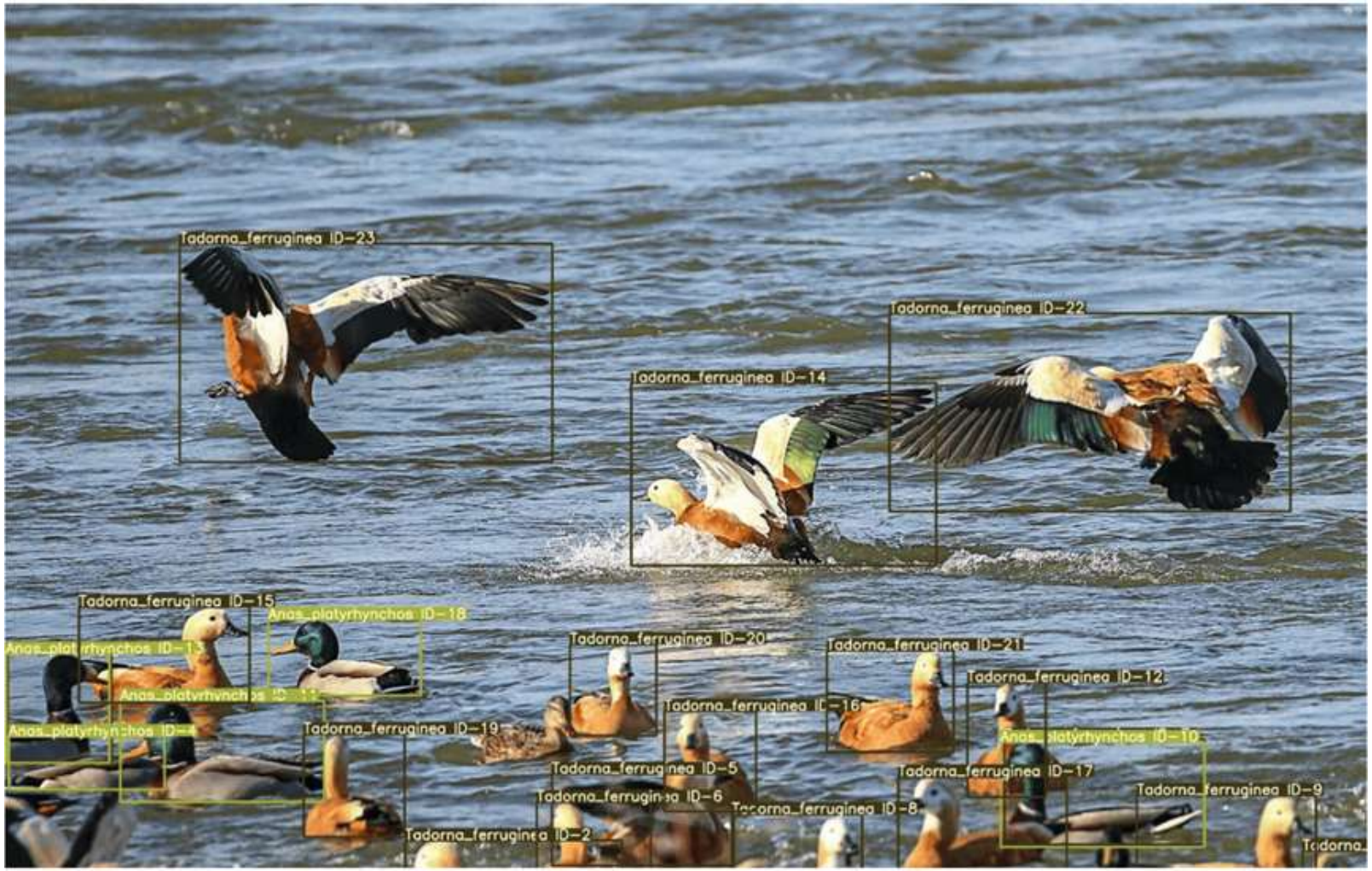

Chen X, Pu H, He Y, et al. An Efficient Method for Monitoring Birds Based on Object Detection and Multi-Object Tracking Networks[J]. Animals, 2023, 13(10): 1713.

MOTIVATION

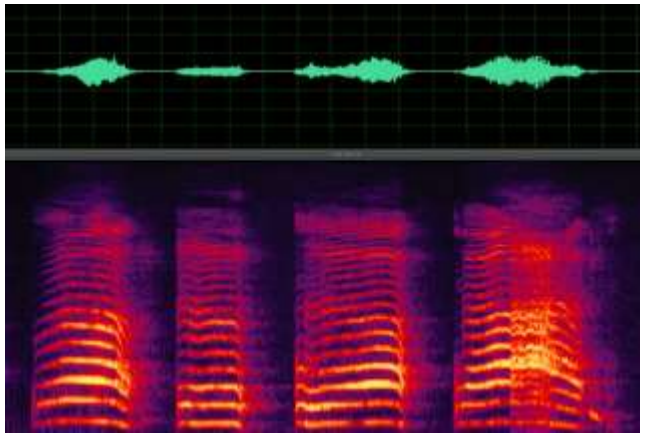

Bird Population Monitoring

Bird-call Recognition

DATASET

Sparrow

Redshank

Woodcock

Teal

Grey Partridge

Grey Heron

Bird Name	Number
Sparrow	1195
Cormorant	852
Grey Heron	850
Red-throated Diver	835
Wood Sandpiper	825
Stone-curlew	814
Mute Swan	800
Pheasant	797
Redshank	790
Black-winged Stilt	786
Mallard	766
Greylag Goose	759
Quail	738
Common Buzzard	733
Bar-tailed Godwit	710
Western Water Rail	680
Teal	602
Woodcock	460
Eurasian Sparrowhawk	290
Grey Partridge	29

METHODS

SOUND RECOGNITION

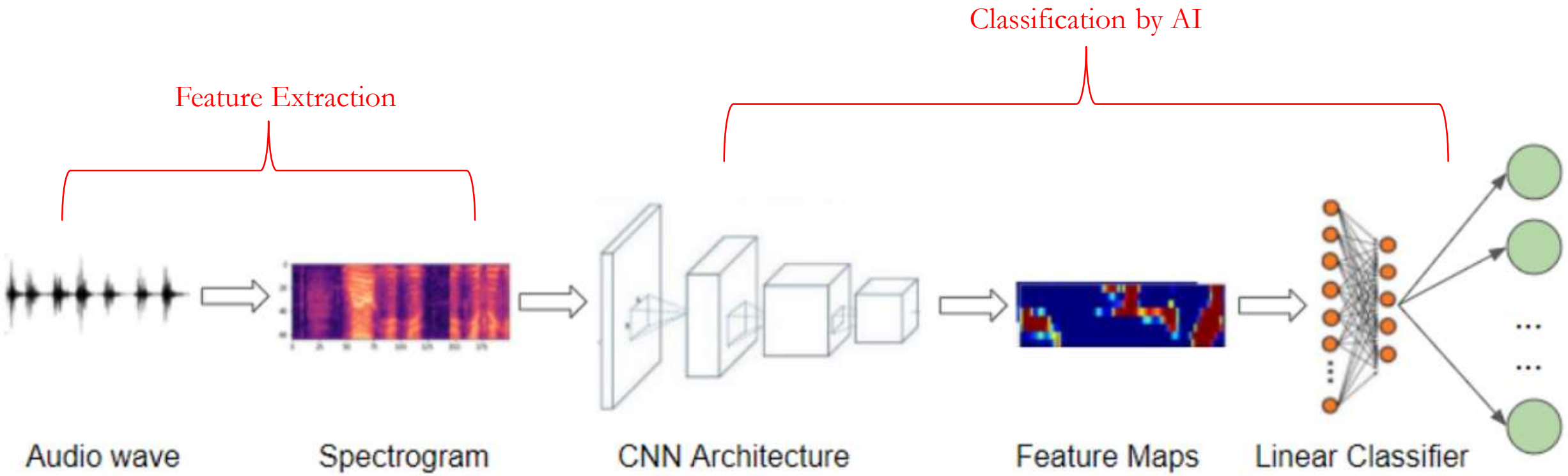

FEATURE EXTRACTION

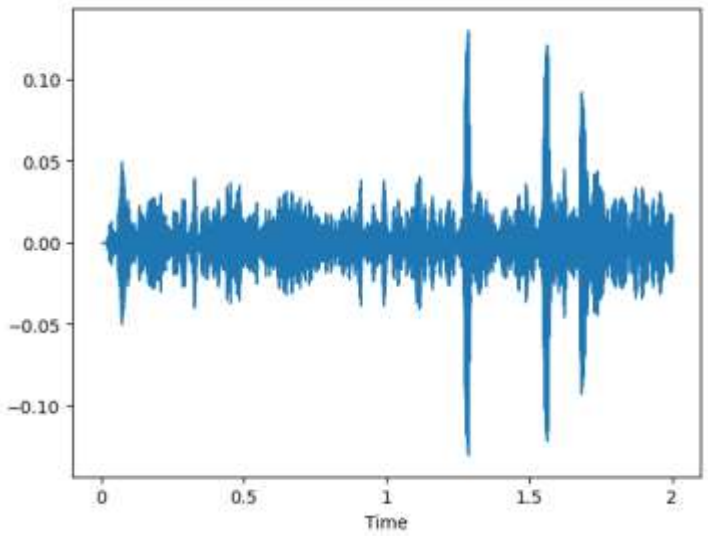

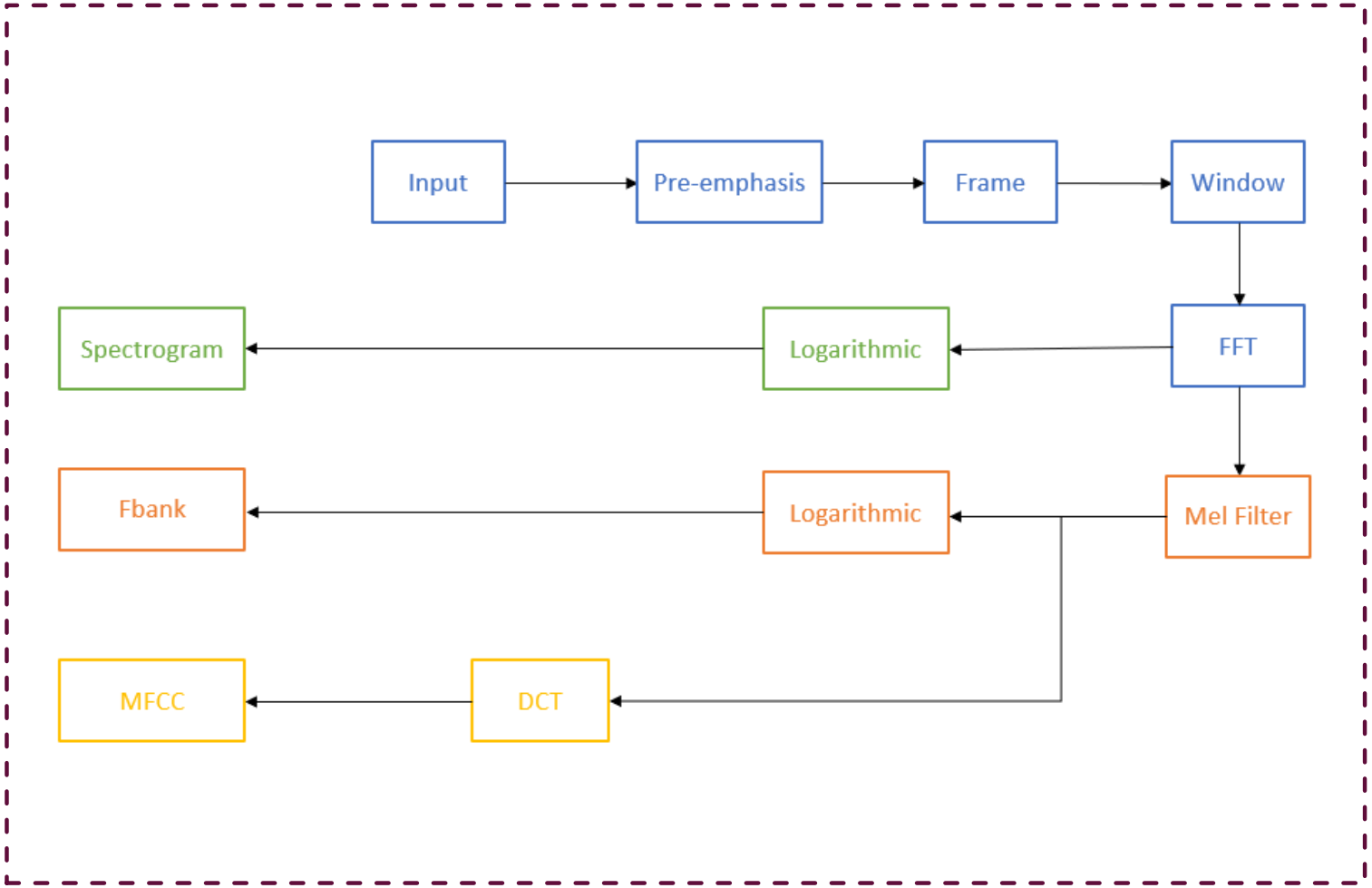

Conversion process of three feature extraction methods

FEATURE EXTRACTION

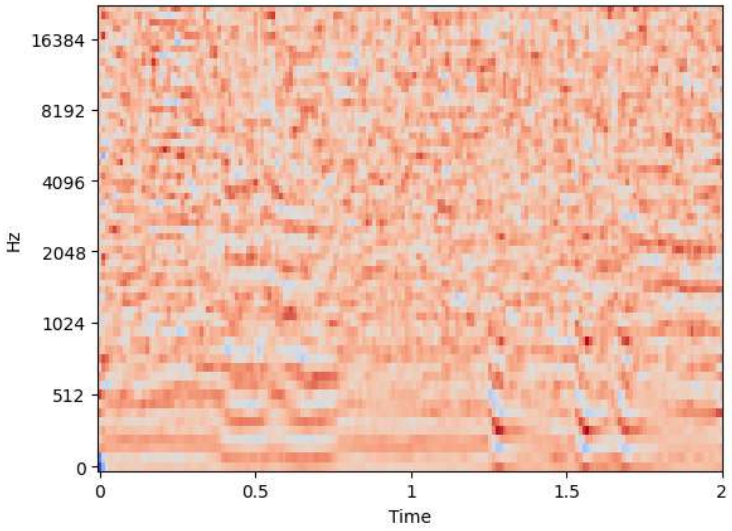

MFCC

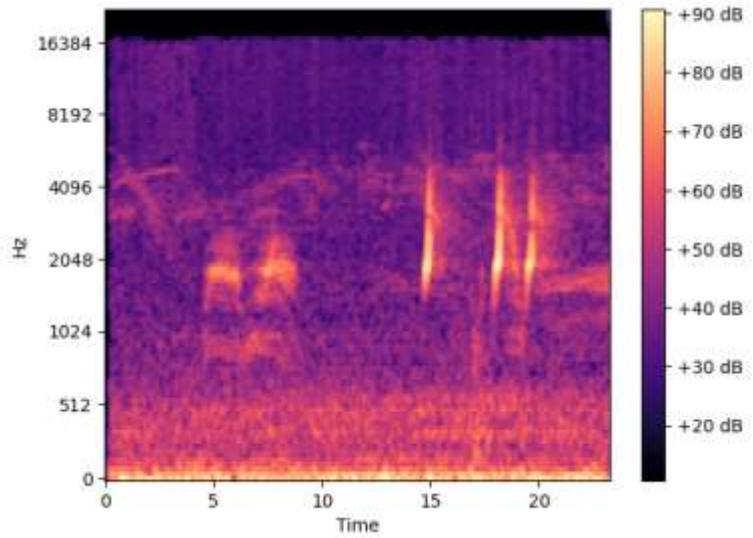

Fbank

Method	DenseNet			ResNet		
	Accuracy	Recall	Cost time	Accuracy	Recall	Cost time
Fbank	84.2%	84.4%	2076.79 sec	85.2%	84.5%	2122.07 sec
MFCC	89.9%	88.3%	1476.07 sec	89.2%	86.5%	1567.89sec

Comparison of two feature extraction methods.

DEEP LEARNING MODEL ---- DENSENET

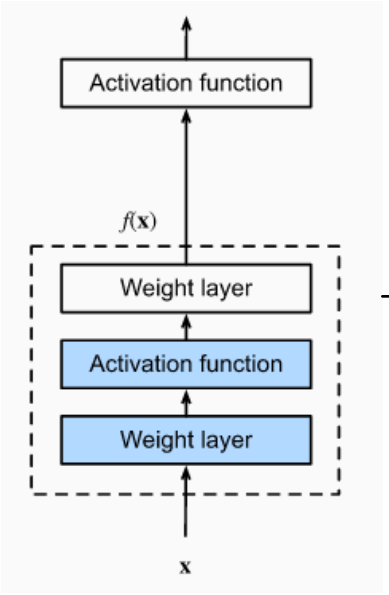

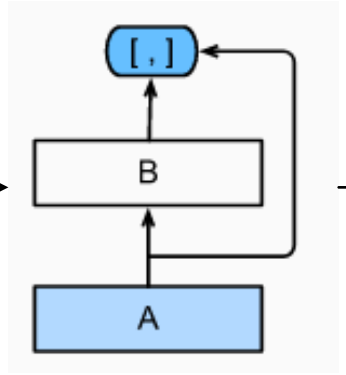

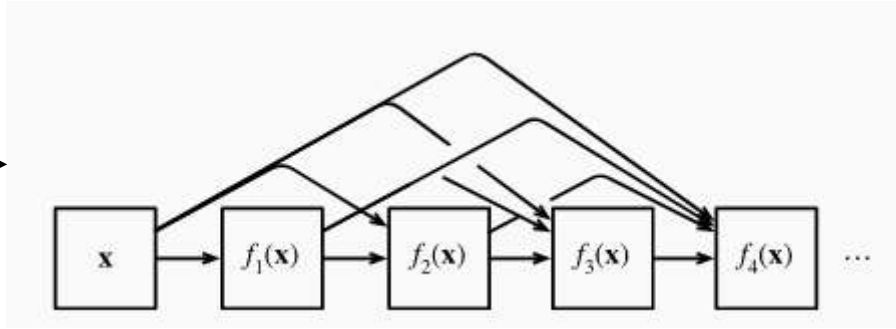

Combining multiple blocks to build a DenseNet

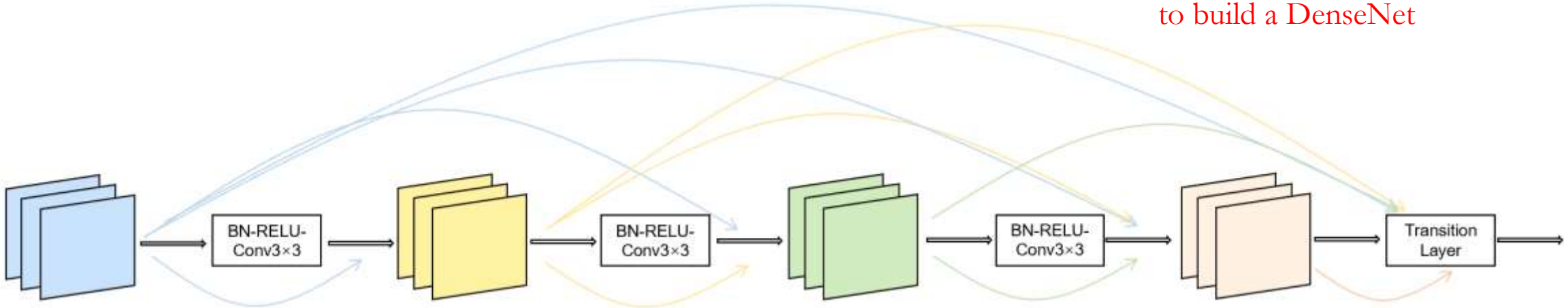

DEEP LEARNING MODEL ---- CONVOLUTION

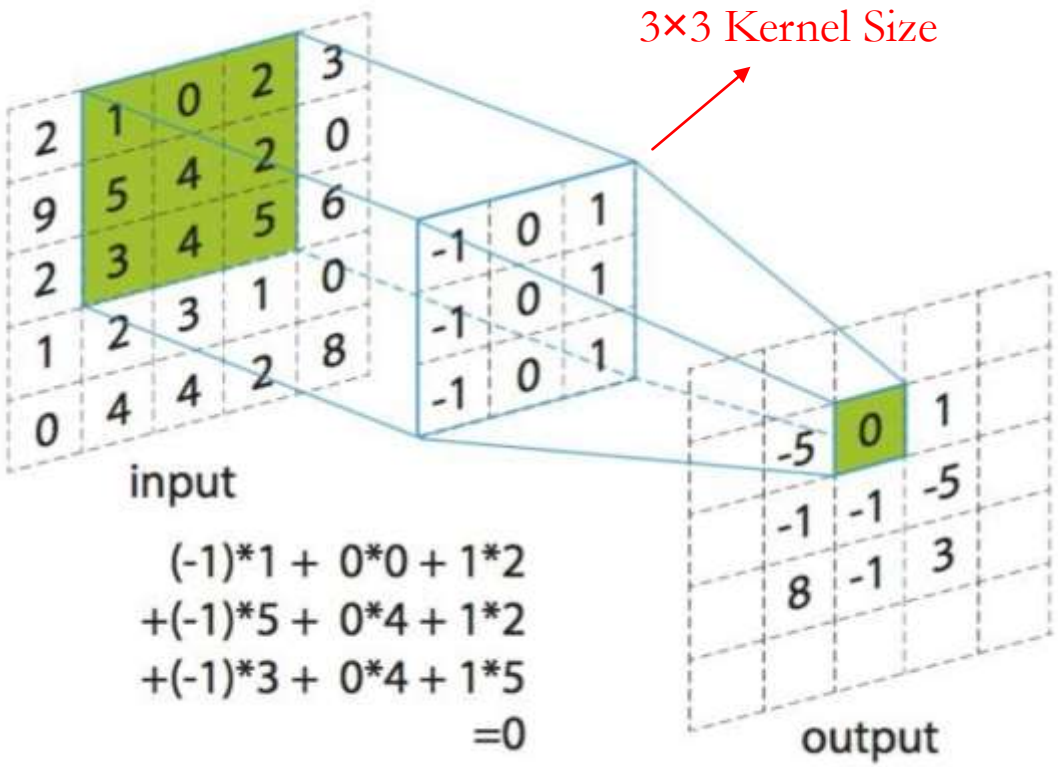

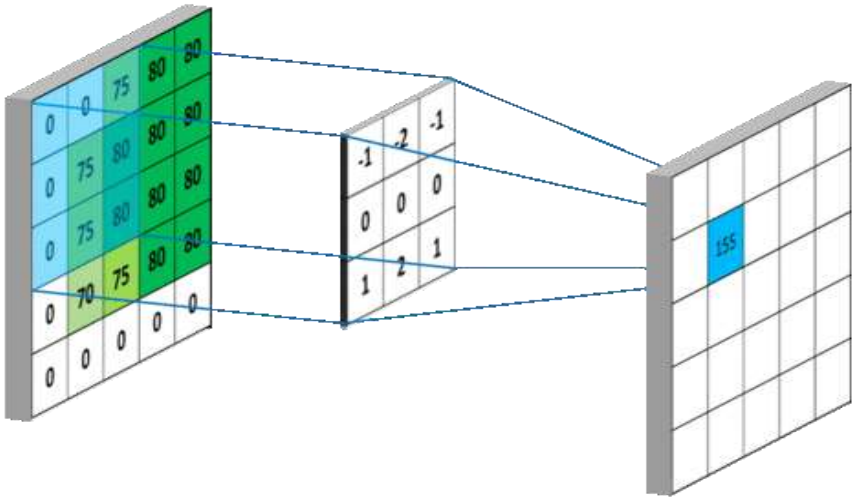

DEEP LEARNING MODEL --- PSAMODULE

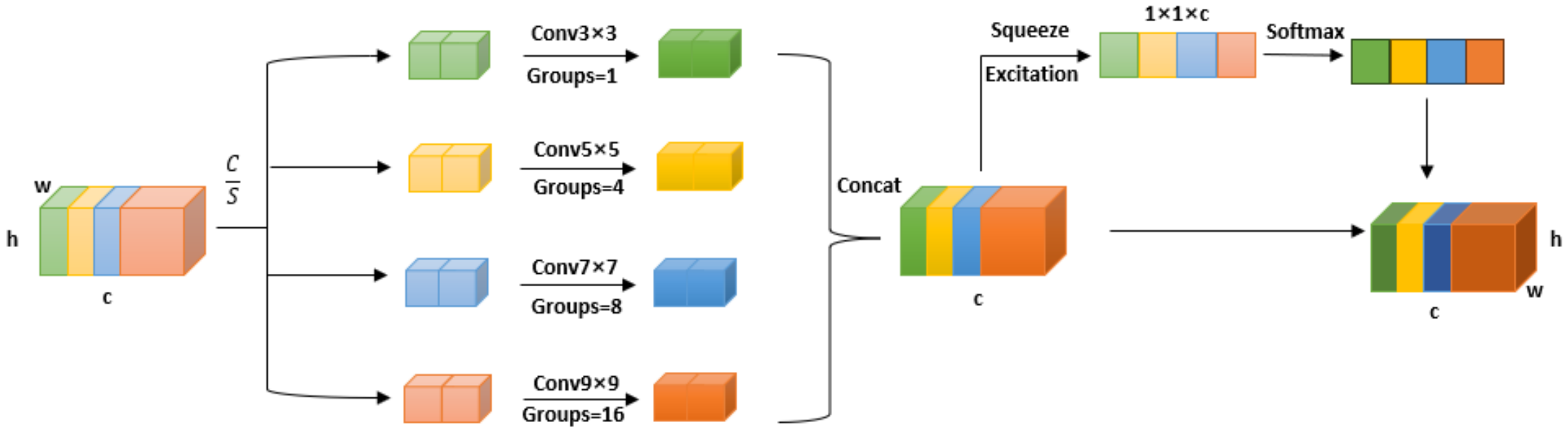

For groups of different scales, convolution operations are performed using convolution kernels of different sizes to capture spatial information of different scales.

DEEP LEARNING MODEL --- PSAMODULE

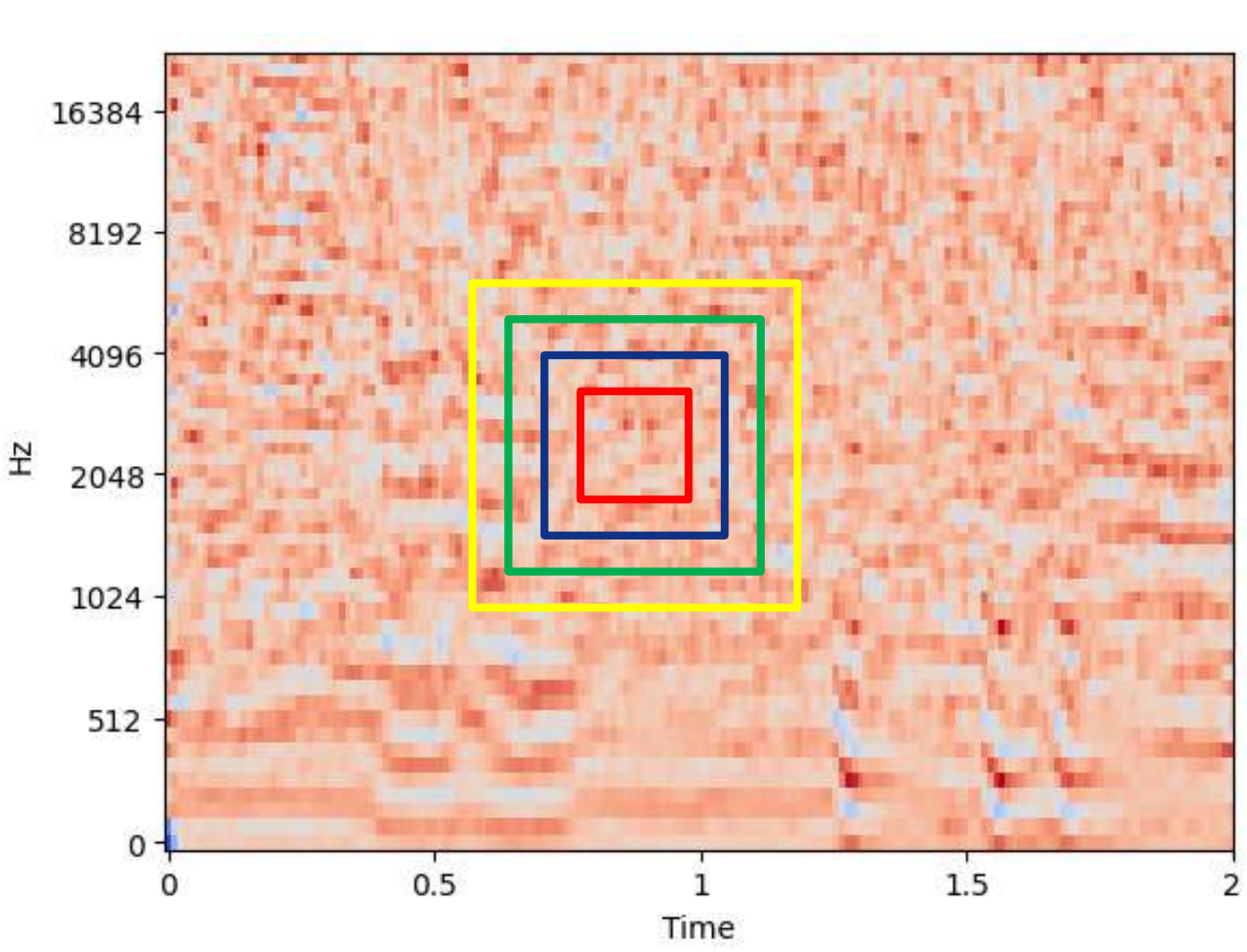

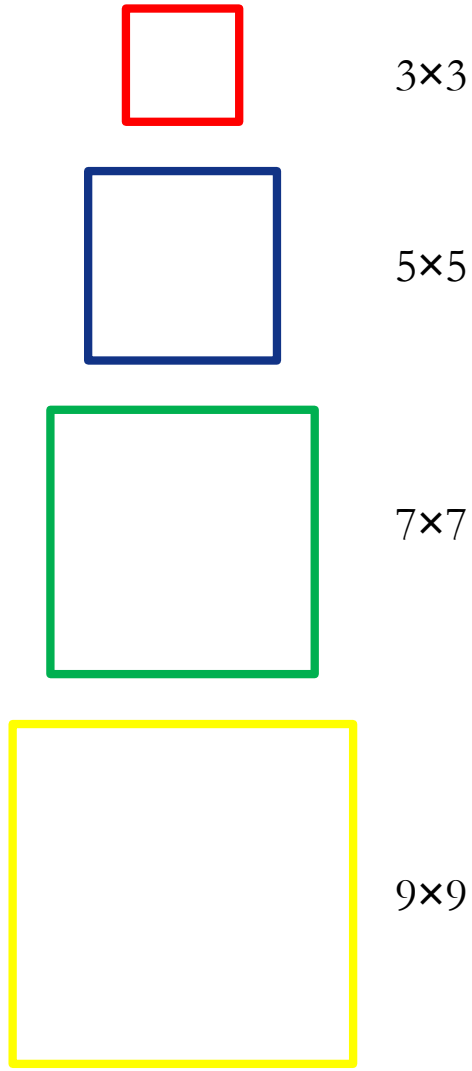

DEEP LEARNING MODEL ---- PSA-DENSENET

Layers	PSA-DenseNet	Output Size
Convolution	7×7, stride 2, 64 channels	32×86
Block 1	$\begin{bmatrix} 1 \times 1 Conv \\ PSAModule \end{bmatrix} \times 6, 448 channels$	16×43
Transition Layer 1	$\begin{bmatrix} 1 \times 1 Conv \\ AvgPool(size = 2) \end{bmatrix}, 224 channels$	16×43
Block 2	$\begin{bmatrix} 1 \times 1 Conv, 256 \\ PSAModule \end{bmatrix} \times 12, 992 channels$	8×21
Transition Layer 2	$\begin{bmatrix} 1 \times 1 Conv \\ AvgPool(size = 2) \end{bmatrix}, 496 channels$	8×21
Block 3	$\begin{bmatrix} 1 \times 1 Conv, 256 \\ PSAModule \end{bmatrix} \times 24, 2032 channels$	4×10
Transition Layer 3	$\begin{bmatrix} 1 \times 1 Conv \\ AvgPool(size = 2) \end{bmatrix}, 1016 channels$	4×10
Block 4	$\begin{bmatrix} 1 \times 1 Conv, 256 \\ PSAModule \end{bmatrix} \times 16, 1400 channels$	2×5
Classification Layer	GlobalAvgPool(size=1)	1×1
	20d fc, Softmax	

Structure of PSA-DenseNet model.

RESULTS

RESULTS
-- CONFUSION MATRIX

Bird Name	Probability
Sparrow	93.20%
Cormorant	99.43%
Grey Heron	100.00%
Red-throated Diver	96.53%
Wood Sandpiper	98.04%
Stone-curlew	96.34%
Mute Swan	97.95%
Pheasant	97.55%
Redshank	95.51%
Black-winged Stilt	98.42%
Mallard	98.72%
Greylag Goose	92.59%
Quail	98.56%
Common Buzzard	93.62%
Bar-tailed Godwit	99.24%
Western Water Rail	85.29%
Teal	89.74%
Woodcock	100.00%
Eurasian Sparrowhawk	90.57%
Grey Partridge	100.00%

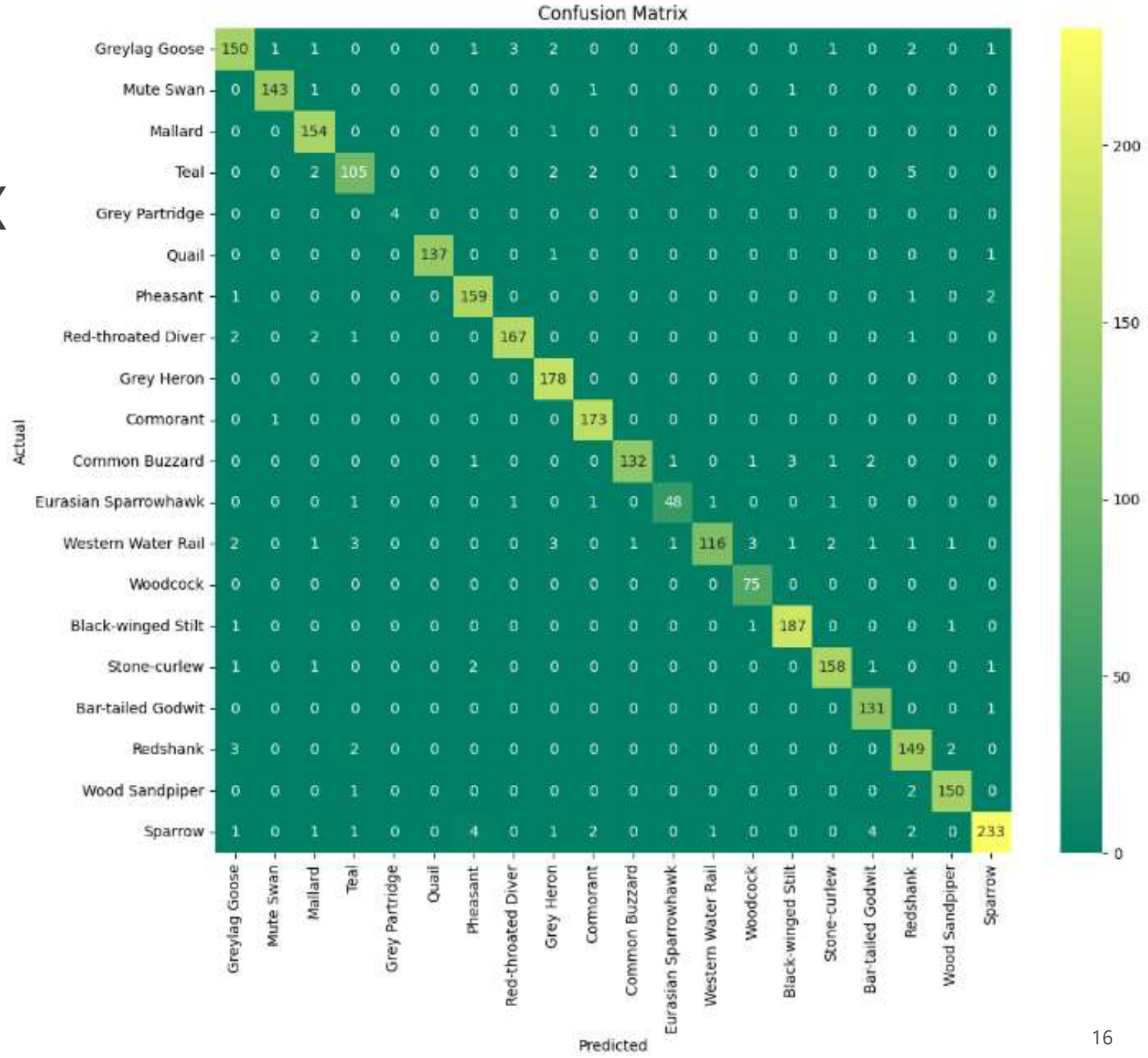

RESULTS
-- MODEL COMPARISON

Model	F_1 Macro	Recall	Accuracy
PSA-DenseNet	94.7%	94.8%	95.8%
DenseNet	87.6%	88.3%	89.9%
MobileNetV2	87.6%	88.4%	90.9%
ResNet	85.8%	86.5%	89.2%
EPSANet	88.9%	87.9%	89.5%

Performance of models.

		Predicted	
		Negative **(N)** -	Positive **(P)** +
Actual	Negative -	True Negative **(TN)**	**False Positive (FP) Type I Error**
	Positive +	**False Negative (FN) Type II Error**	True Positive **(TP)**

CONCLUSION

CONCLUSION

① We compare two commonly used audio feature extraction methods and use MFCC as a final method to extract features from raw audio and study call-based bird classification.

② We use the PSA-DenseNet model for a large dataset of calls from 20 distinct bird species, our investigation shows the remarkable efficacy of PSA-DenseNet in tasks pertaining to call-based bird classification, surpassing the performance of existing models including DenseNet, MobileNet V2, ResNet, and EPSANet.

③ PSA-DenseNet potential applicability in a broader spectrum of audio feature learning tasks, such as music classification, in future researches.

④ PSA-DenseNet does face challenges associated with its extensive parameter count and prolonged training duration. Consequently, future researches may explore the development of lighter models based on this foundation.

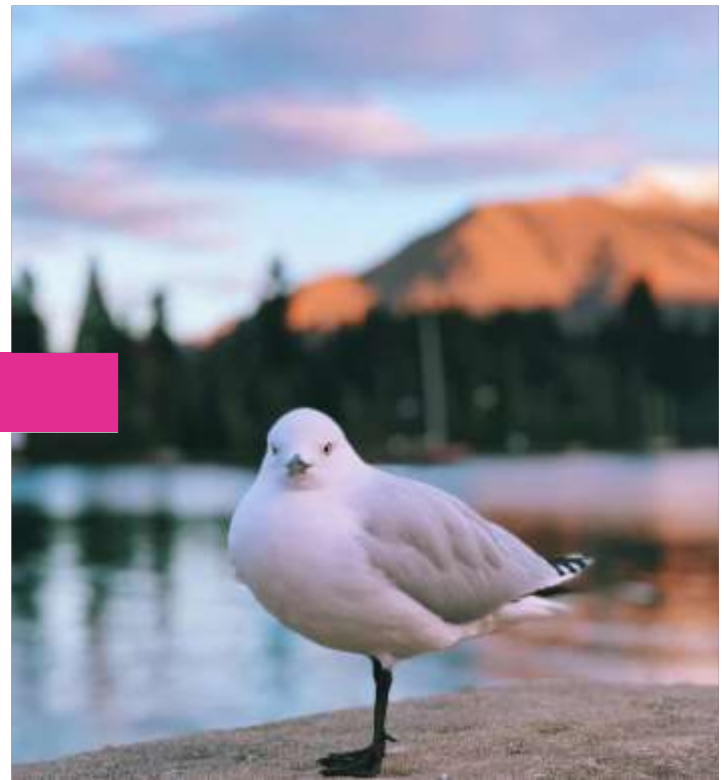

THANK YOU

[1] Tianyu Song, Linh Thi Hoai Nguyen, Ton Viet Ta, MPSA-DenseNet: A novel deep learning model for English accent classification. Computer Speech & Language, 2025, 89.

[2] Tianyu Song, Ton Viet Ta, Advancing Bird Classification: Harnessing PSA-DenseNet for Call-Based Recognition. The Proceedings of the Fifth Workshop on Interdisciplinary Sciences, 2023.

The Sixth Workshop on Interdisciplinary Sciences (WIS 2024)
November 28, 2024

Single and combined applications of bacteriophage and cinnamon oil against pathogenic *Listeria monocytogenes* in milk and chicken meat

Aye Thida Maung, Yoshimitsu Masuda, Ken-ichi Honjoh, Takahisa Miyamoto*

Graduate School of Bioresource and Bioenvironmental Sciences
Laboratory of Food Hygienic Chemistry
Faculty of Agriculture, Kyushu University

Introduction

Listeria monoytogenes

- Gram positive, rod-shaped bacterium
- 13 serotypes, serotype 1/2a, 1/2b, 4b: causes 90% human listeriosis
- **Symptoms:** meningitis, encephalitis, septicaemia, abortion
- **High motility rate:** 20-30% (the elderly, fetus)

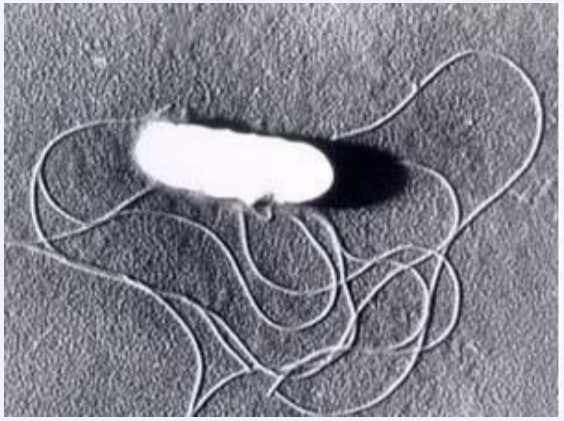

Antimicrobial resistance (AMR)

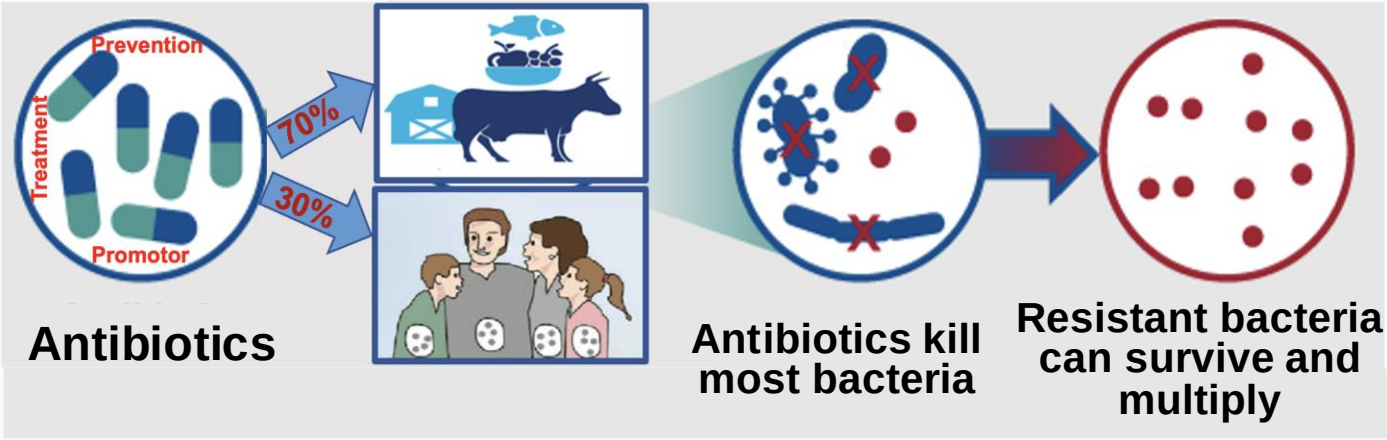

(WHO, 2019)

Alternative antimicrobial agents

Introduction

Bacteriophage (Phage)

- Bacterial virus
- High host specificity
- Abundant in natural environment
- Harmless to humans

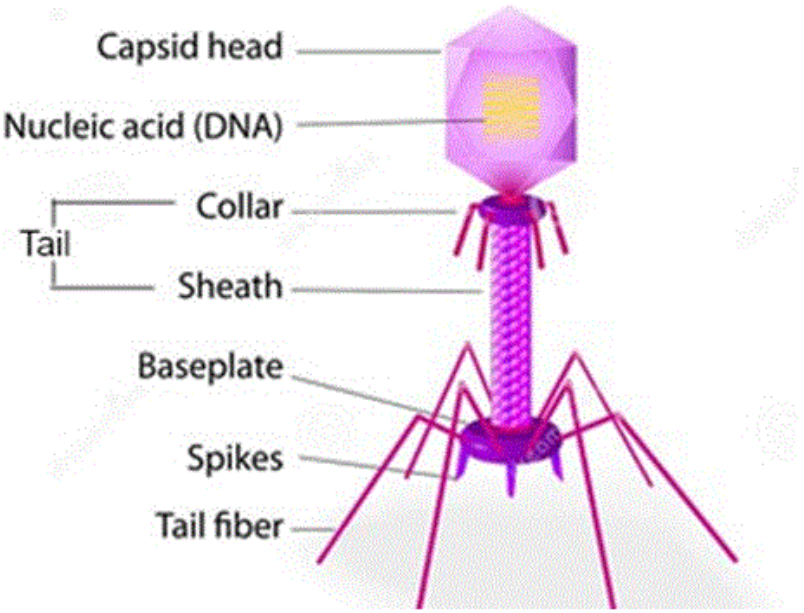

Essential oils (EOs)

- Compounds extracted from plants
- Antimicrobial activity
- Antioxidant activity
- Health benefits

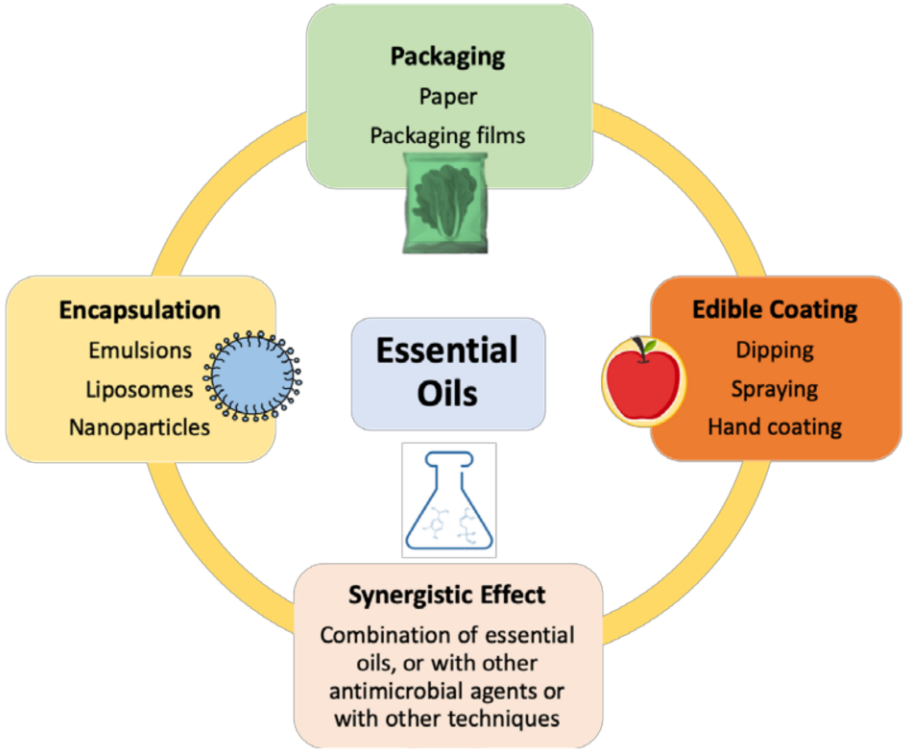

Objectives

1. Isolation and characterization of **bacteriophages** specific to *L. monocytogenes*.
2. Evaluation of natural antimicrobial substances (**essential oils**) against *L. monocytogenes*.
3. Determination of the effects of **phage and/or cinnamon oils** against *L. monocytogenes* in liquid and solid foods.

Objectives

1. Isolation and characterization of **bacteriophages** specific to *L. monocytogenes*.

2. Evaluation of natural antimicrobial substances (**essential oils**) against *L. monocytogenes*.

3. Determination of the effects of **phage and/or cinnamon oils** against *L. monocytogenes* in liquid and solid foods.

Isolation of bacteriophages

Method

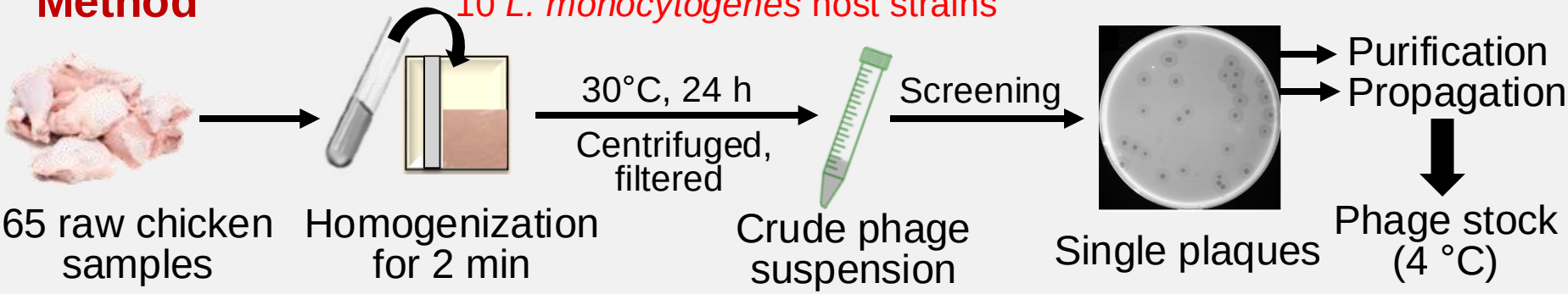

Result

Phages isolated from chicken samples

No.	Phage name	Sample code	Sources	Titer (PFU/mL)
1	PLM1	CM-4	Chicken wing	1.7×10^{10}
2	PLM2	CM-6	Chicken ovary and oviduct	7.9×10^{9}
3	PLM3	CM-7	Chicken thigh cartilage	1.7×10^{10}
4	PLM4	CM-8	Chicken thigh fillet	4.9×10^{9}
5	PLM5	CM-9	Chicken liver	8.2×10^{9}
6	PLM6	CM-21	Chicken chopped meat	6.1×10^{9}
7	PLM7	CM-59	Chicken breast (sasami)	5.8×10^{9}
8	PLM8	CM-60	Chicken skin	2.6×10^{9}
9	PLM9	CM-61	Chicken chopped meat	9.5×10^{9}

- Nine phages were isolated with the target host (*L. monocytogenes* 193).

Characterization (Host range determination)

Method

➢ **Spot test**

Phage stock (10^8 PFU/mL)

↓ Spotted

bacteria lawn

↓ 30°C, overnight

Checked clear zone

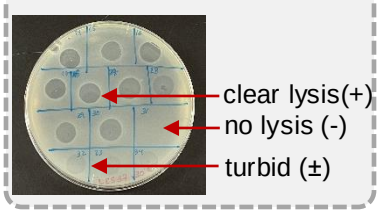

Result

Bacterial strains	Serotype	Phages								
		PLM1	PLM2	PLM3	PLM4	PLM5	PLM6	PLM7	PLM8	PLM9
LM S8HC	1/2a	-	-	-	-	-	-	-	-	-
LM S4HO	1/2a	±	±	±	±	±	±	±	±	+
LM S25FC	1/2b	-	-	-	-	-	-	-	-	-
LM S38HC	1/2a	-	-	-	-	-	-	-	-	-
LM 8FO	1/2b	-	-	-	-	-	-	-	-	-
LM 76HA	1/2a	+	+	+	+	+	+	+	+	+
LM 11FA	ND	+	+	+					+	+
LM 38FO	ND	±	+							+
LM 26FA	4b	-	-							-
LM 152	1/2c	-	-							-
LM174	1/2a	-	-	-	-	-	-	-	-	-
LM 178	1/2b	-	-	-	-	-	-	-	-	-
LM 185	4b	+	+	+	+	+	+	+	+	+
LM 193*	4b	+	+	+	+	+	+	+	+	+
LM ATCC 15313^T		-	-	-	-	-	-	-	-	-
L. innocua ATCC 33090		+	+	+	+	+	+	+	+	+
L. innocua Wild strain		+	+	+	+	+	+	+	+	+
L. ivanovii ATCC 19119		-	-	-	-	-	-	-	-	-
L. seeligeri ATCC 35967		+	+	+	+	+	+	+	+	+
L. seeligeri Wild strain		-	-	-	-	-	-	-	-	-
L. welshimeri ATCC 35897		+	+	+	+	+	+	+	+	+
L. welshimeri Wild strain		+	+	+	+	+	+	+	+	+
L. grayi ATCC 25401		+	+	+	+	+	+	+	+	+
(+) clear lysis		10	11	11	10	10	10	11	10	12
(±) turbid		2	1	1	2	2	2	1	2	0

Phage PLM9 was selected for further characterization.

The lytic activity showed in various *Listeria* spp.

All of the phages are inactive against *S. aureus*, *B. cereus*, *B. thuringiensis*, S. Typhimurium, S. Enteritidis.

Stability test

Method

Phage PLM9 (10^8 PFU/mL) → Temperature (4-90°C), 1 h → **Checked the phage titers** ← SM buffer (pH 2-10), 4 & 25 °C, 24 h ← Phage PLM9 (10^8 PFU/mL)

Result

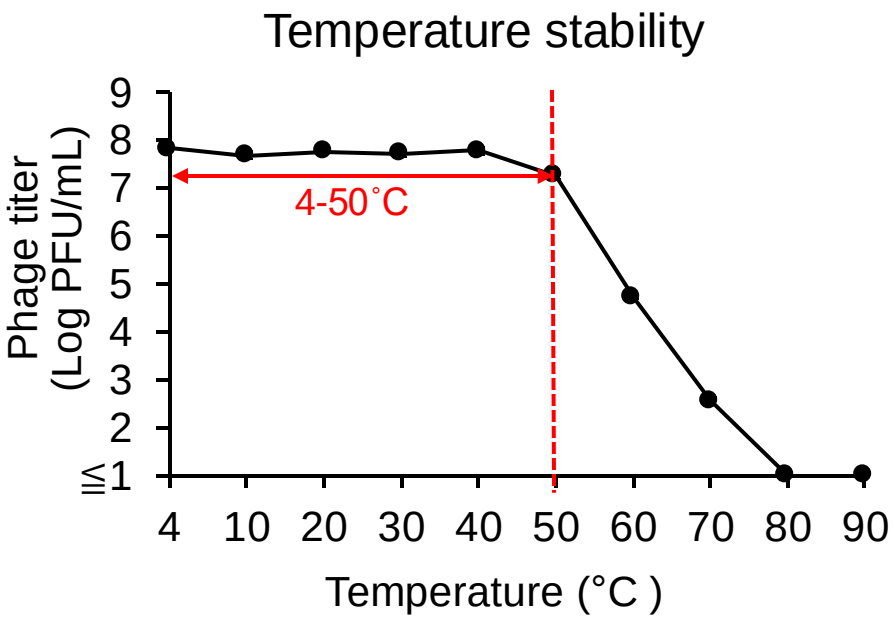

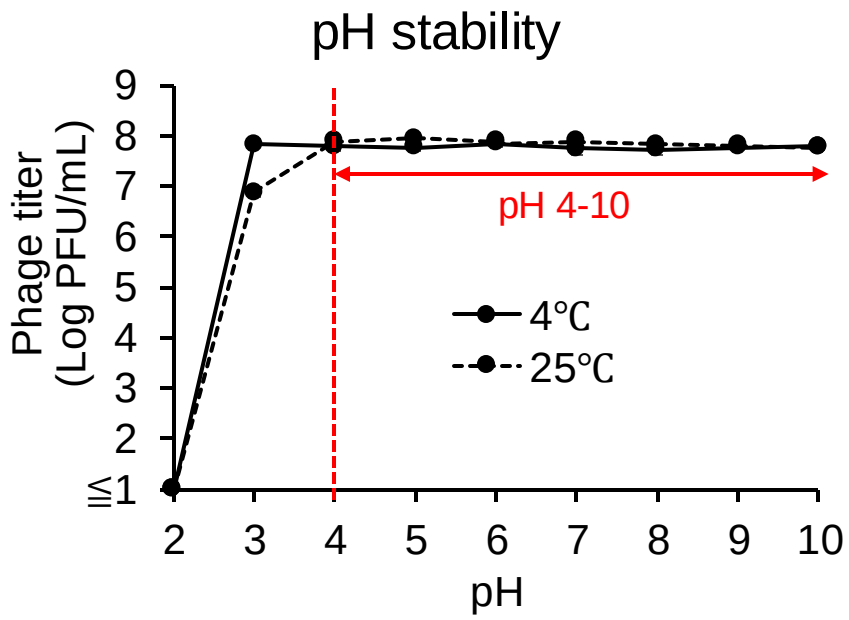

- Phage PLM9 was stable at temperatures (4-50˚C) and pH (4-10).

Whole genomic sequence analysis

Method

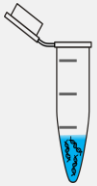

DNA extraction
(Hi Viral Nucleic Acid Kit)

Whole genomic DNA sequencing

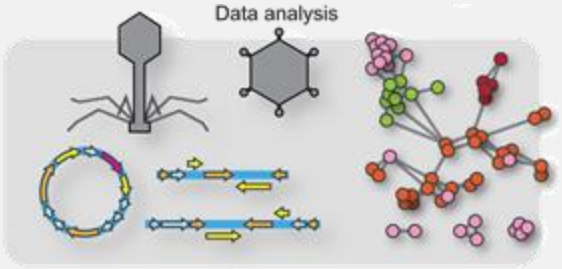

Bioinformatic analysis

Result

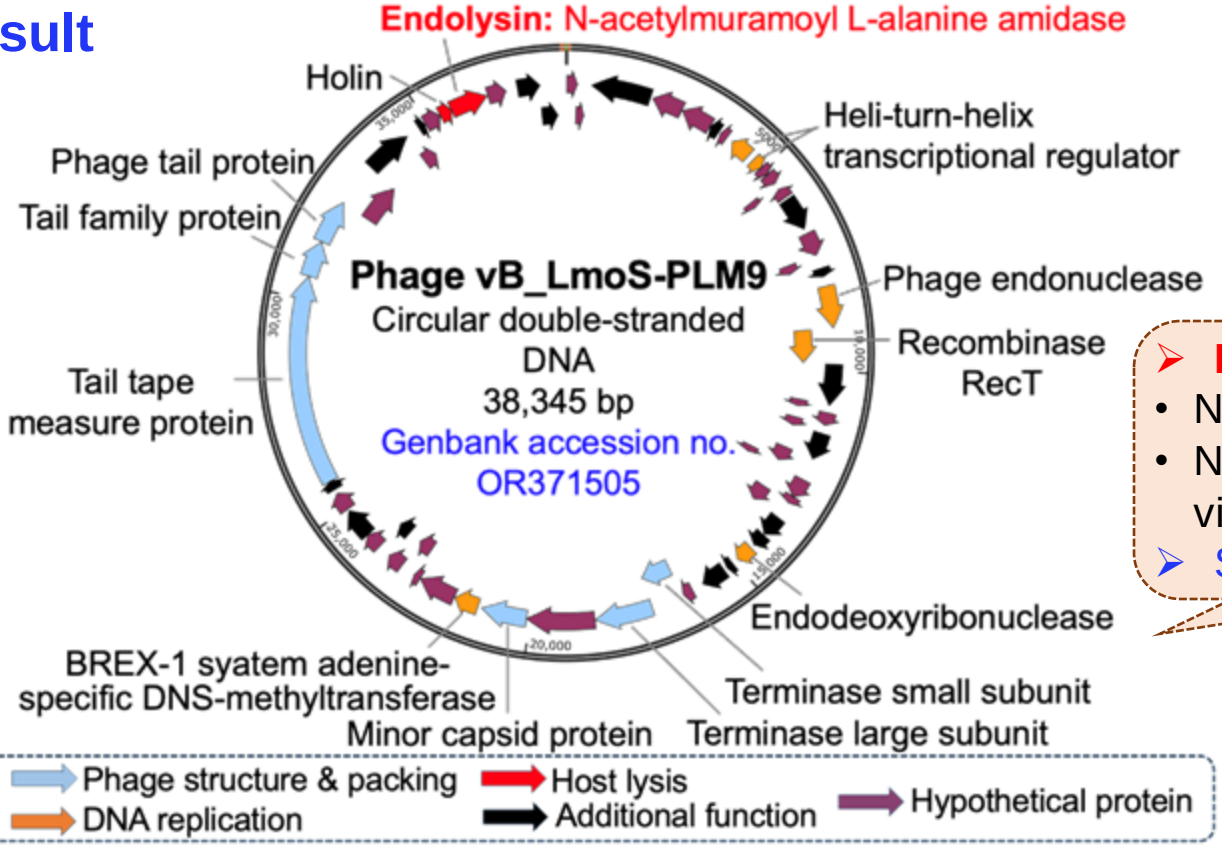

➢ **Lytic phage**

- No lysogenic-related gene.
- No antibiotic resistance, virulence, or toxic genes.

➢ Safe for food applications.

Objectives

1

- Isolation and characterization of **bacteriophages** specific to *L. monocytogenes*.

2

- Evaluation of natural antimicrobial substances (**essential oils**) against *L. monocytogenes*.

3

- Determination of the effects of **phage and/or cinnamon oils** against *L. monocytogenes* in liquid and solid foods.

Essential oils tested in this study

- According to the Generally Recognized as Safe (GRAS) list, which permits certain EOs for use in food products by the US FDA, 8 EOs were selected.

Clove
(*Eugenia caryophyllius*)

Cinnamon bark (C.b)
(*Cinnamomum zeylanicium*)

Cinnamon cassia (C.c)
(*Cinnamomum cassia*)

Ginger
(*Zingiber officinale)*

Turmeric
(*Ciurcuma longa*)

Basil
(*Ocimum basilicum*)

Lemon
(*Citrus limon*)

Lemon grass
(*Cymbopogon flexuosus*)

Antibacterial activity of essential oils

Method: Disc diffusion method

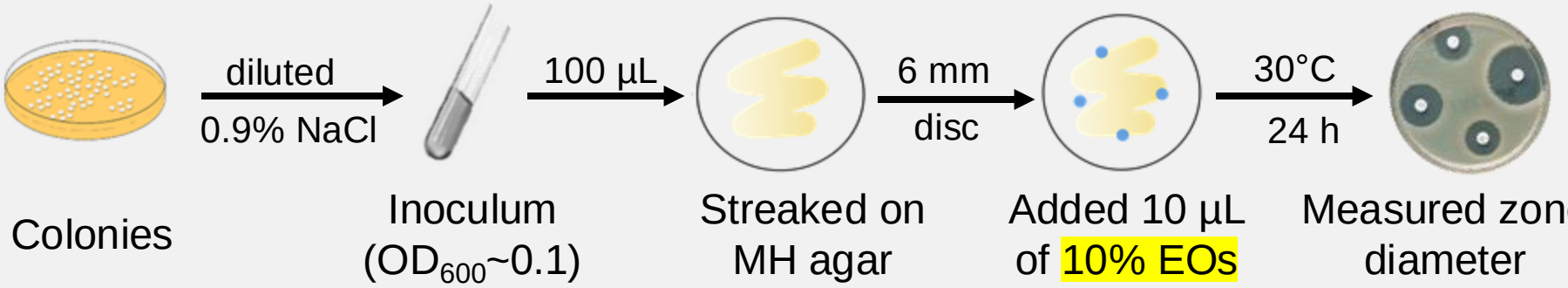

Result

Listeria spp.	Zone diameter (Mean ± S.D. mm)			
	C.b	C.c	Clove	Lemon grass
L. monocytogenes 193*	26.7±1.2^{c}	21.7±1.5^{b}	9.7±1.2^{a}	9.7±0.6^{a}
L. monocytogenes ATCC 15313^{T}	25.5±0.9^{c}	30.2±0.8^{d}	8.2±0.3^{a}	12.0±1.0^{b}
L. innocua ATCC 33090	32.0±1.0^{b}	32.7±0.6^{b}	10.3±0.6^{a}	9.7±0.6^{a}
L. innocua LIS31	24.3±0.6^{c}	28.2±0.8^{d}	7.7±0.6^{a}	9.7±0.6^{b}
L. ivanovii ATCC 19119	30.3±0.6^{b}	29.3±0.6^{b}	8.7±0.6^{a}	10.0±1.0^{a}
L. seeligeri ATCC 35967	31.3±0.6^{b}	33.7±2.5^{b}	11.7±1.5^{a}	11.7±1.2^{a}
L. seeligeri LIS34	30.3±0.6^{b}	33.8±01.9^{c}	10.7±0.6^{a}	10.7±0.6^{a}
L. welshimeri ATCC 35897	24.3±1.5^{b}	24.7±0.6^{b}	9.7±0.6^{a}	10.7±0.6^{a}
L. welshimeri LIS36	23.6±1.5^{b}	22.0±2.0^{b}	0	11.3±0.6^{a}
L. grayi ATCC 25401	20.0±1.0^{b}	25.7±1.5^{c}	9.8±0.8^{a}	10.7±1.2^{a}

No inhibition was observed in 10% ginger, turmeric, basil, and lemon.

$^{a\text{-}c}$Significant differences ($P < 0.05$) among EOs in each row.

MIC and MBC of cinnamon oils

Method: Microbroth dilution method

4, 2, 1, 0.5, 0.25, 0.125, 0.0625, 0.03, 0.015 %

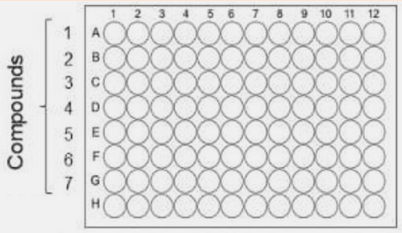

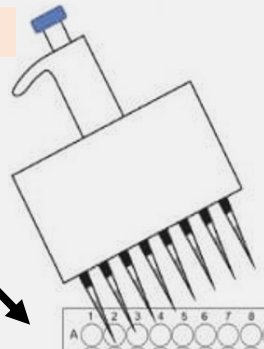

(-) ve control- only broth
(+) ve control- only cell suspension

2-fold serial dilution of cinnamon oils in microdilution plate

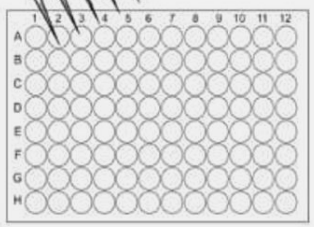

30°C
24 h

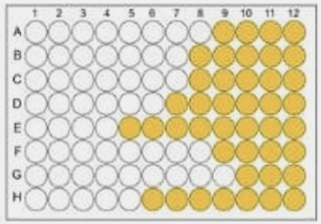

100 µL

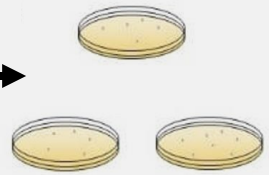

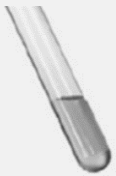

Bacterial suspension (10^6 CFU/mL)

Mixed 100 µL of bacterial inoculum and 100 µL of different concentrations of C.b or C.c oil

Measured OD_{600} to determine MIC concentration

Determined the MBC on TSA

Result

EOs	MIC (%)	MBC (%)
Cinnamon bark	0.0625	0.125
Cinnamon cassia	0.0625	0.125

MIC- Minimum Inhibitory Concentration
MBC- Minimum Bactericidal Concentration

Objectives

1

- Isolation and characterization of **bacteriophages** specific to *L. monocytogenes*.

2

- Evaluation of natural antimicrobial substances (**essential oils**) against *L. monocytogenes*.

3

- Determination of the effects of **phage and/or cinnamon oils** against *L. monocytogenes* in liquid and solid foods.

Effects of phage and/or cinnamon oils against *L. monocytogenes* in broth

Method

500 µL culture (10^6 CFU/mL)

500 µL phage and/or EOs (broth as control)

30°C

4 mL BHI broth

Viable counts (0, 2, 4, 6, 8, 10, 24 h) on TSA

Result

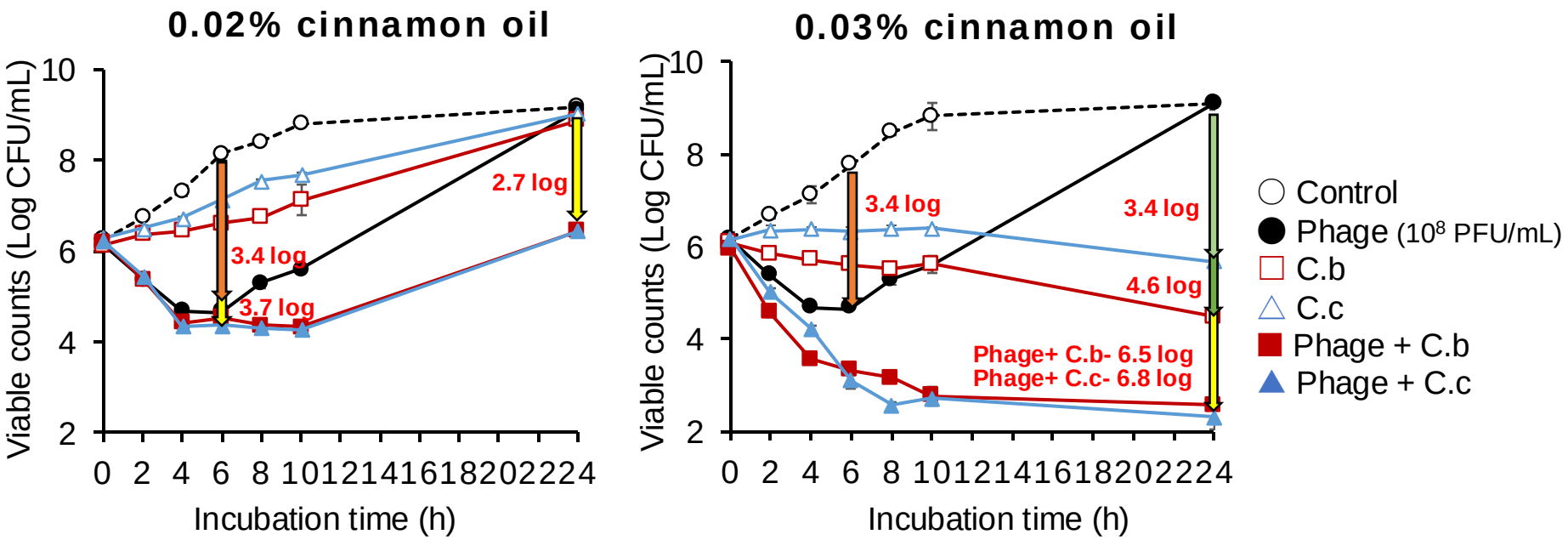

Effects of phage and/or cinnamon oils against *L. monocytogenes* in milk

Method

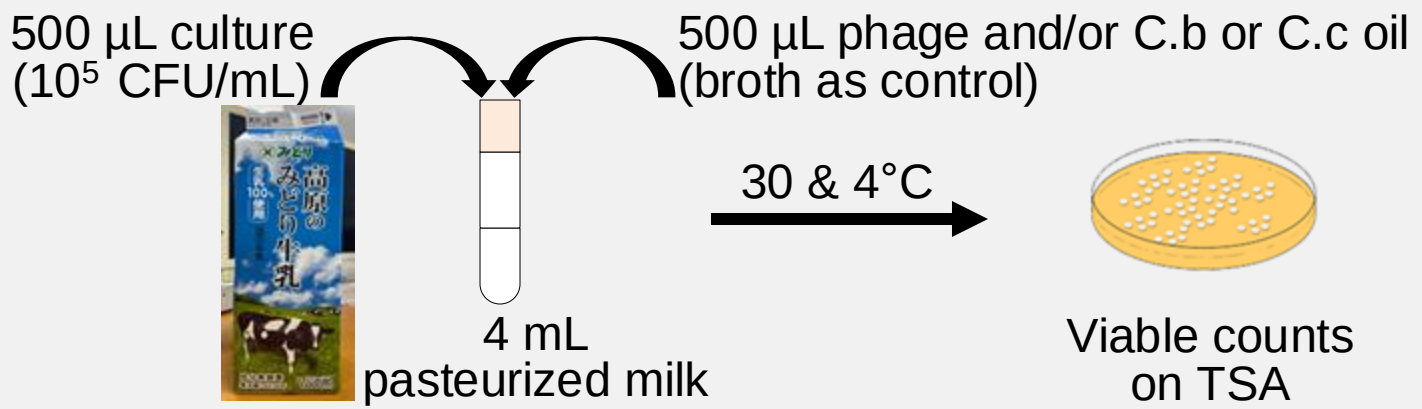

Result

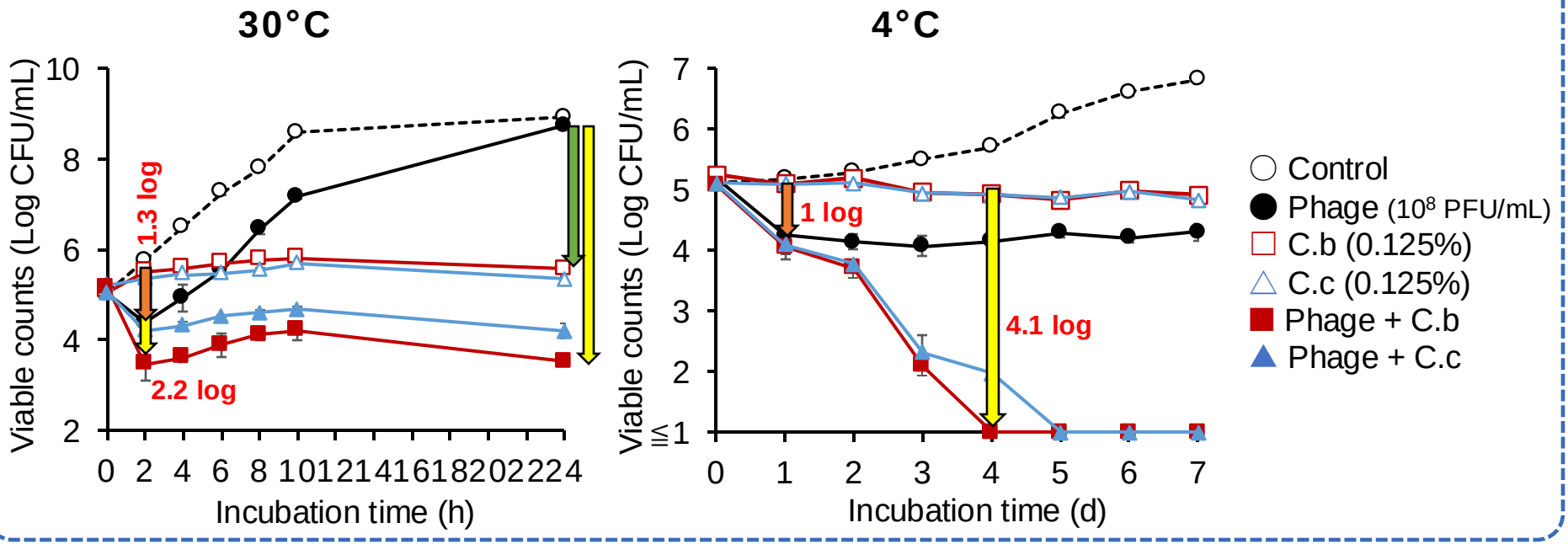

Effects of phage and/or cinnamon oil against *L. monocytogenes* on chicken meat

Method

Result

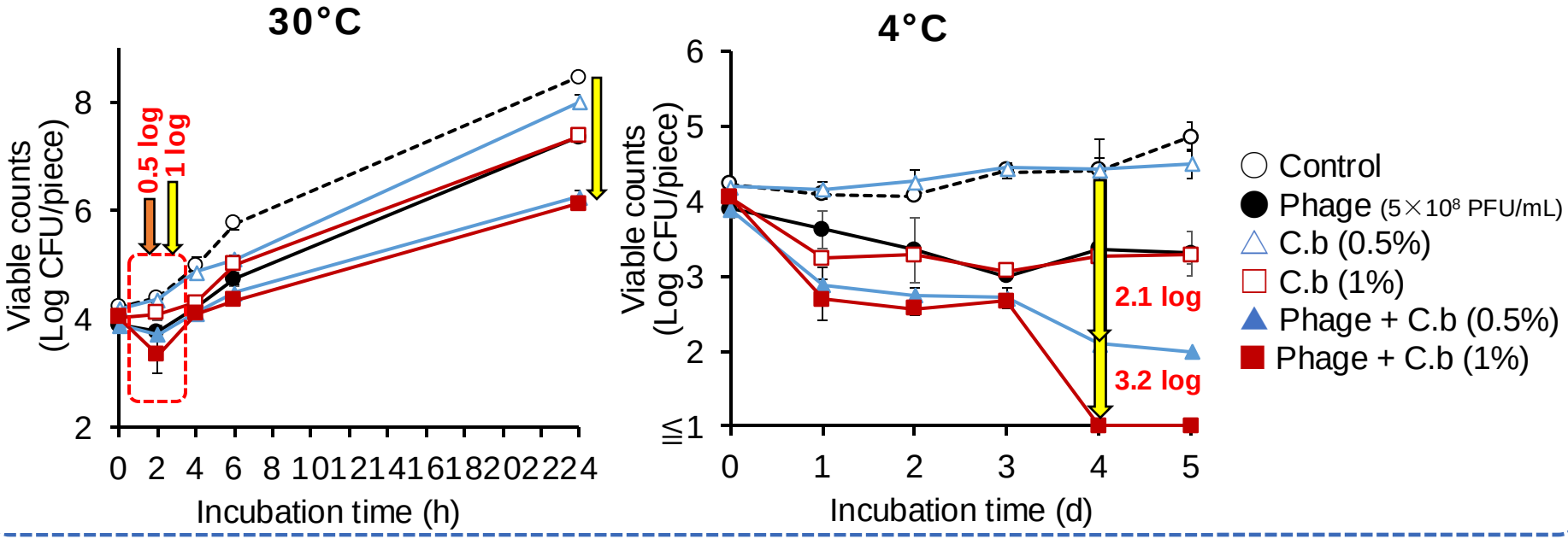

Conclusion

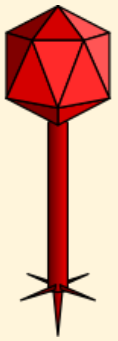

Phage vB_LmoS-PLM9

Active against 5 species of *Listeria* including *L. monocytogenes.*

+

Cinnamon oils

Strongest anti-listerial activity among 8 essential oils.

MIC : 0.0625%
MBC: 0.125%

- **Decreased viable counts of *L. monocytogenes* by more than 4 log in milk, and 3 log on chicken at 4°C.**
- **Prevented regrowth of resistant cells of *L. monocytogenes* at 4°C.**

The combined use of phage and cinnamon oil is a promising candidate for controlling *L. monocytogenes* in liquid and solid foods.

Publication

https://doi.org/10.1016/j.ijfoodmicro.2024.110797

International Journal of Food Microbiology 421 (2024) 110797

Contents lists available at ScienceDirect

International Journal of Food Microbiology

journal homepage: www.elsevier.com/locate/ijfoodmicro

Single and combined application of bacteriophage and cinnamon oils against pathogenic *Listeria monocytogenes* in milk and smoked salmon

Aye Thida Maung [a,b], Marwa Nabil Sayed Abdelaziz [a], Tahir Noor Mohammadi [c], Su Zar Chi Lwin [a], Mohamed El-Telbany [a], Junxin Zhao [a,d], Chen Wang [a], Yunzhi Lin [a], Cunkuan Shen [e], Mahmoud Zayda [f], Yoshimitsu Masuda [a], Ken-ichi Honjoh [a], Takahisa Miyamoto [a,*]

[a] *Department of Bioscience and Biotechnology, Graduate School of Bioresource and Bioenvironmental Science, Kyushu University, 744 Motooka, Nishi-ku, Fukuoka 819-0395, Japan*
[b] *Department of Animal Science, University of Veterinary Science, Yezin, Nay Pyi Taw, Myanmar*
[c] *Biology Department, San Diego State University, San Diego, CA, United States*
[d] *State Key Laboratory of Food Science and Technology, Nanchang University, Nanchang 330047, China*
[e] *College of Biological and Environmental Science, Zhejiang Wanli University, Ningbo, Zhejiang 315100, China*
[f] *Department of Food Hygiene and Control, Faculty of Veterinary Medicine, University of Sadat City, Sadat City, Monofiya Governorate, Egypt*

ARTICLE INFO

Keywords:
Listeria monocytogenes
Phage
Cinnamon oil
Milk
Smoked salmon

ABSTRACT

Nowadays, the discovery of alternative natural antimicrobial substances such as bacteriophages, essential oils, and other physical and chemical agents is developing in the food industry. In this study, nine bacteriophages were isolated from various parts of raw chickens and exhibited lytic activities against *L. monocytogenes* and various *Listeria* spp. The characterization of phage vB_LmoS-PLM9 was stable at 4 to 50 °C and pH range from 4 to 10. Phage vB_LmoS-PLM9 had a circular, double-stranded genomic DNA with 38,345 bp having endolysin but no antibiotic resistance or virulence genes. Among the eight essential oils tested at 10 %, cinnamon bark, and cassia oils showed the strongest antilisterial activities. The combined use of phage vB_LmoS-PLM9 and cinnamon oils indicated higher efficiency than single treatments. The combination of phage (MOI of 10) and both cinnamon oils (0.03 %) reduced the viable counts of *L. monocytogenes* and inhibited the regrowth of resistant cell populations in broth at 30 °C. Furthermore, treatment with the combination of phage (MOI of 100) and cinnamon oil (0.125 %) was effective in milk, especially at 4 °C by reducing the viable count to less than lower limit of detection. These results suggest combining phage and cinnamon oil is a potential approach for controlling *L. monocytogenes* in milk.

Thanks for your kind attention!

Aye Thida Maung, PhD
Lecturer, University of Veterinary Science, Myanmar
E.mail: dr.ayethidamaung@gmail.com

Study on the release behavior of aroma components from rhizome starches - added agar emulsion gel

Truong Minh Hang[1], Prof. Noriyuki Igura[2], Assoc.Prof. Tsubaki Shuntaro[2]

[1]Division of Biotechnology, Biochemistry and Post-Harvest Technology, The Western Highlands of Agriculture and Forestry Science Institute, Vietnam

[2] Laboratory of Food Process Engineering, Graduate School of Bioresource and Bioenvironmental Sciences, Kyushu University

INTRODUCTION - DYSPHAGIA

Dysphagia (difficulty in swallowing) is an impairment of swallowing that may result from a variety of medical conditions (acute or progressive neurological conditions, trauma, disease or surgery) (Leslie P et al., BMJ 2003).

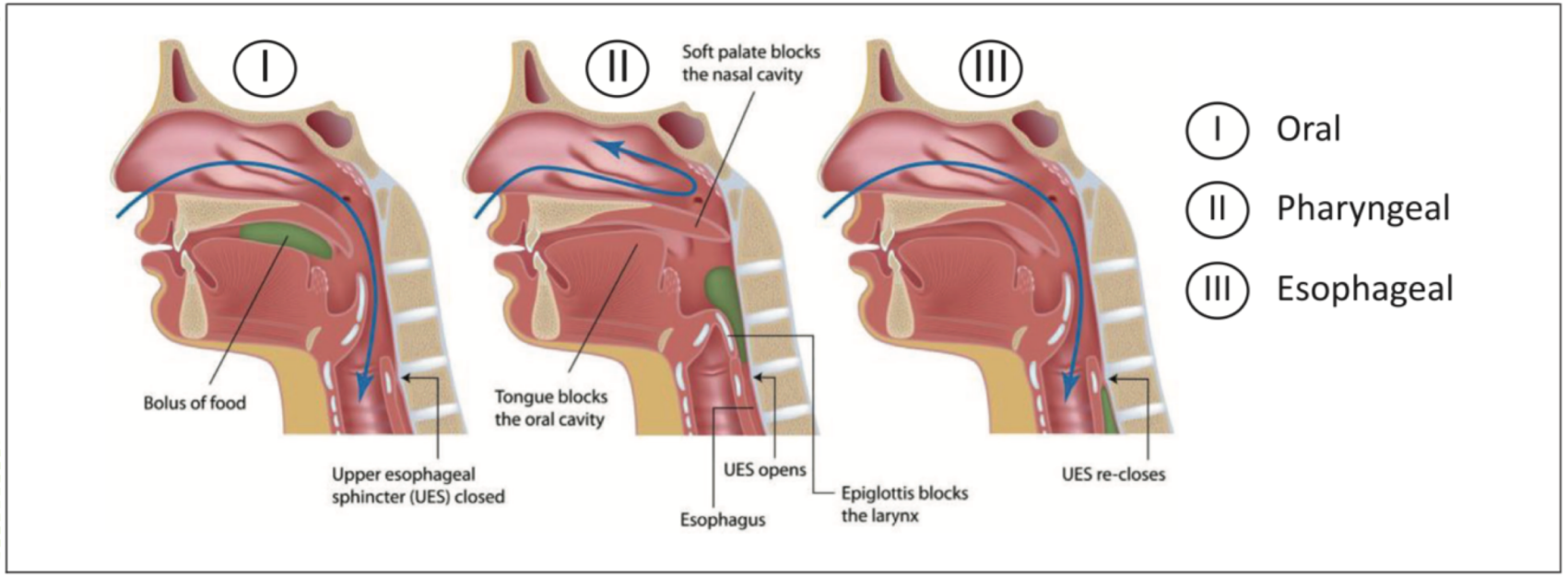

(Fujiso et al., PloS One, 2018)

Affect about 8% of the world's population, higher prevalence among the elderly.

COVID - 19 patients are in relation to potential dysphagia problems (Mohan R. et al., Turkish Journal of Physical Medicine and Rehabilitation, 2020)

INTRODUCTION – DYSPHAGIA DIETS

Texture

- Food texture recommended for dysphagia diets should be soft, moist, elastic, smooth, and easy to swallow.
- Main textural parameters determined in Textural modified foods are hardness, adhesiveness and cohesiveness (Aguilera & Park, Trends in Food Science & Technology, 2016).

Flavor

- 70% of food taste is determined by aroma.
- Preferable scent promotes saliva secretion.

  → Easy to swallow (Karami et al., International Journal of Dentistry, 2011)

INTRODUCTION - AGAR EMULSION GEL (AEG)

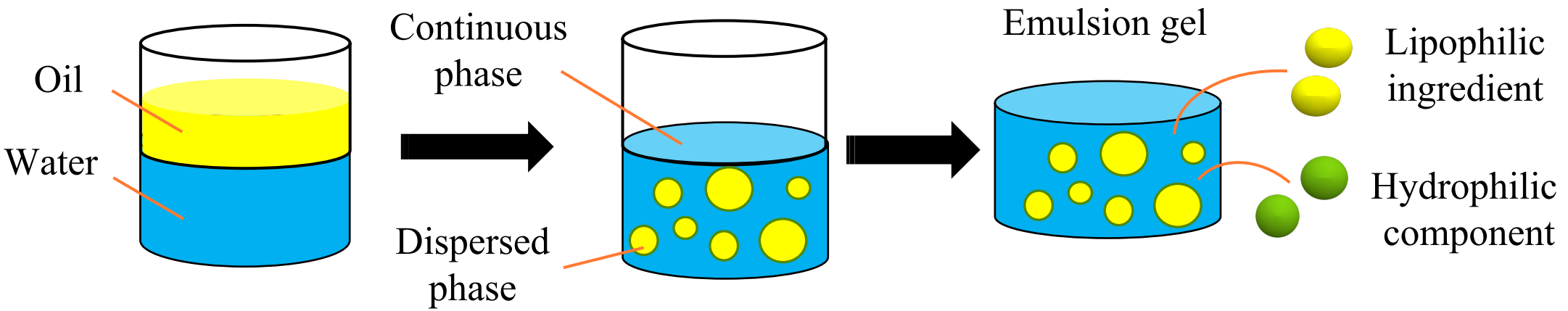

Agar emulsion gel

- Have effective delivery of functional ingredients
- Slow release of lipophilic flavour compounds
- Easiest to swallow among the food forms

(Mao, Roos, and Miao, Journal of Agricultural & Food Chemistry, 2014)

INTRODUCTION - RHIZOME STARCHES

(Viet Nam Cassava Association)

Government News - Socialist Republic of Viet Nam

Cassava, Potato, Sweet potato

- Safe emulsion stabilizers
- Can change the rheological properties
- Abundant, common, low processing cost

→ Excellent emulsion stabilizers, and are widely used for food applications

PREVIOUS STUDY RESULTS

- The textural characteristics of the AEG was influenced by the addition of starch: Hardness went down while cohesiveness and adhesiveness increased.
- For dysphagia diet, potato starch at the percentage lower than 1.5 wt% in AEG gave better result compared to the other starches.

EXPANDED RESEARCH

Will the addition of starch to emulsion gel affect the flavor of the product?

PURPOSES

The study aims to investigate the aroma release behavior of agar emulsion gel (AEG) when adding different type of rhizome starches

MATERIALS & METHODS

AROMA RELEASE BEHAVIOR

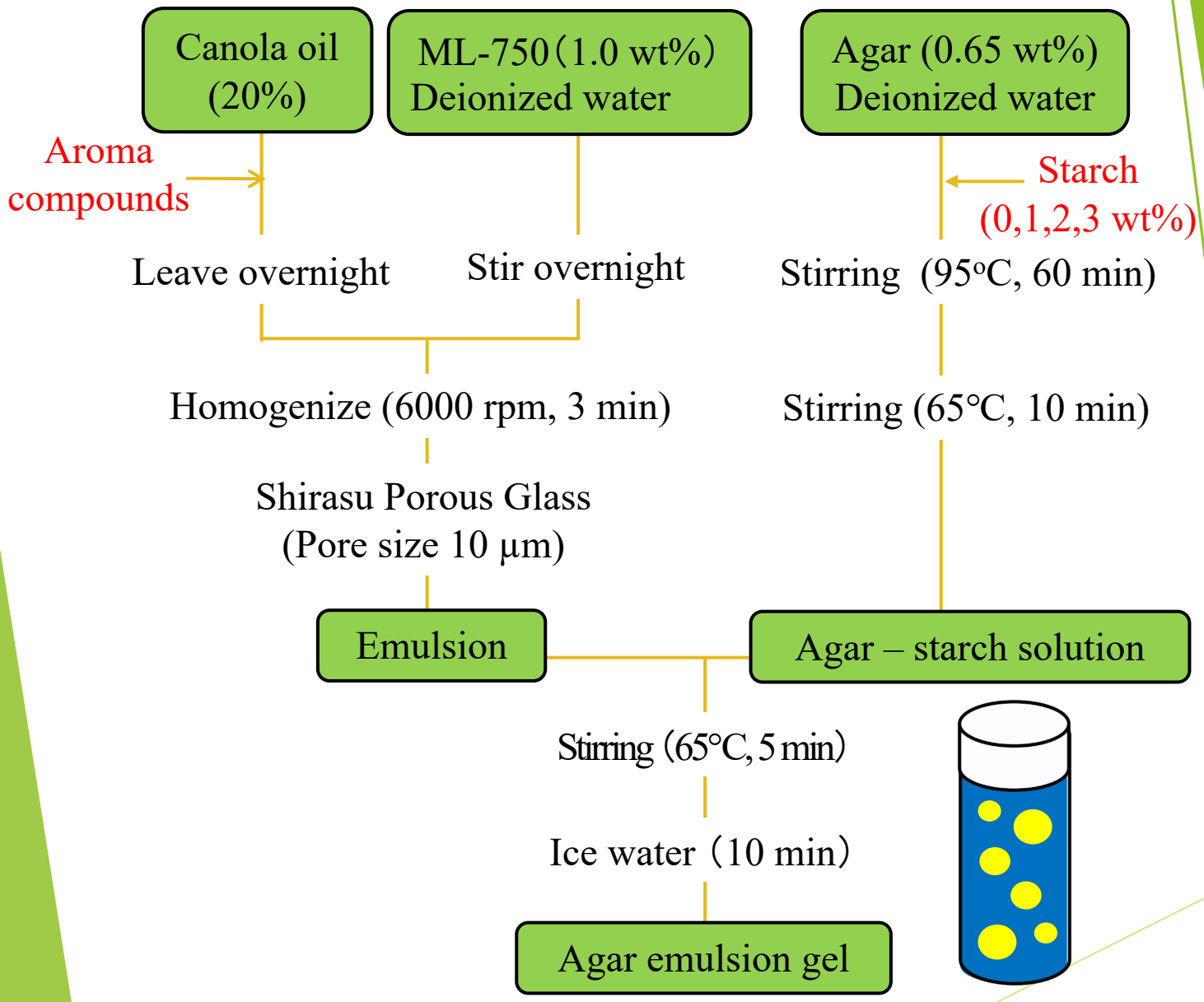

Aroma compound	$logP_{ow}$
2-Methyl pyrazine	0.21
Benzyl alcohol	1.10
Hexanal	1.78
Ethyl hexanoate	2.83
Linalool	2.97
Decanal	3.76
Ethyl decanoate	4.79

GC Analysis

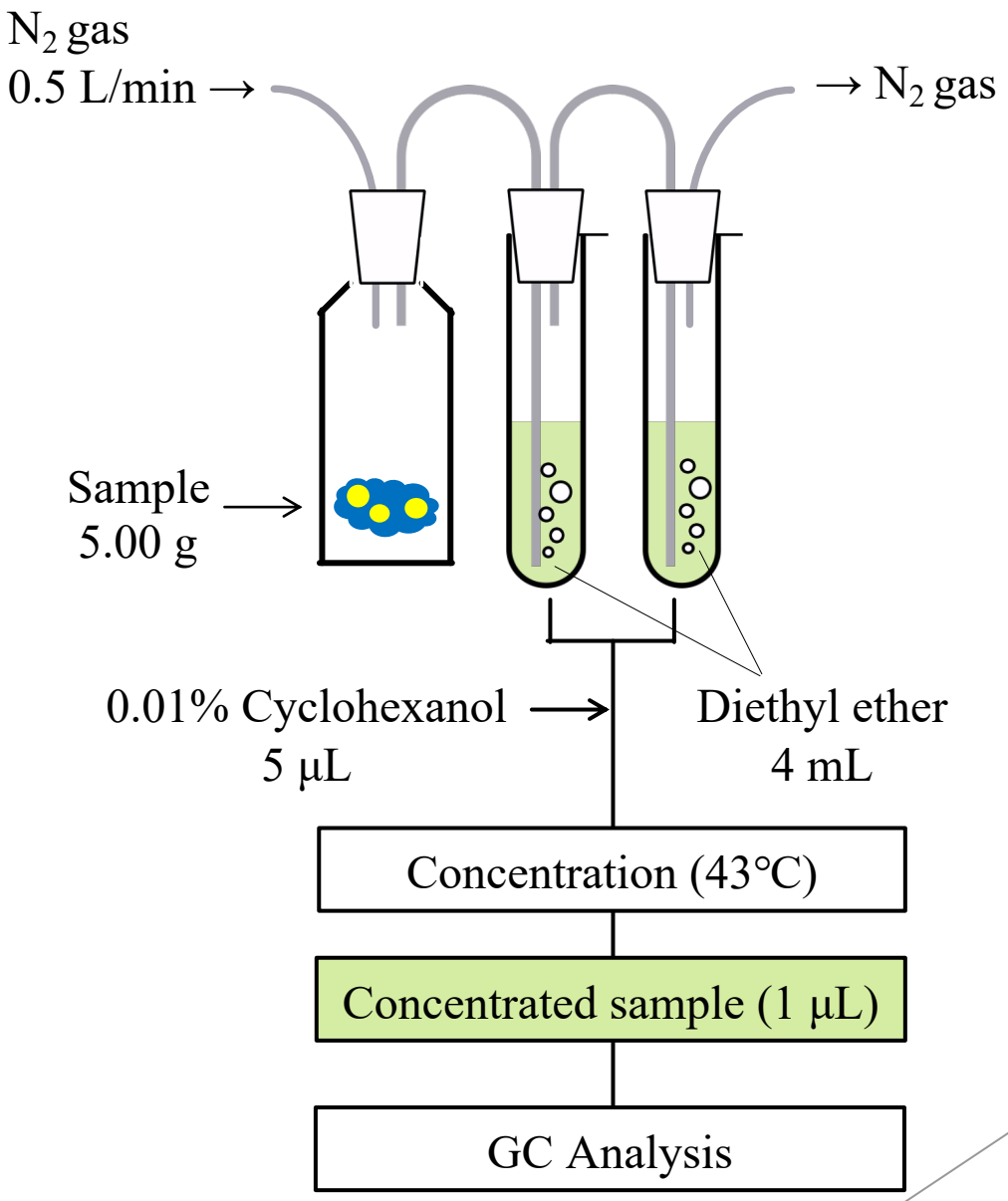

GC Analysis conditions	
Device	GC-2025 (SHIMADZU)
Column	DB-WAX (30 m×0.25 mm i.d., 0.5 µm)
Temperature rising	40℃ → 10℃/min → 230℃, 2 min
Vaporization chamber temperature	250℃
Sample injection method	Splitless
Column flow rate	Helium, 1.8 mL/min
Detector	Flame ionization detector
Detector temperature	250℃

RESULT & DISCUSSION

Amount of aroma compounds release from AEG

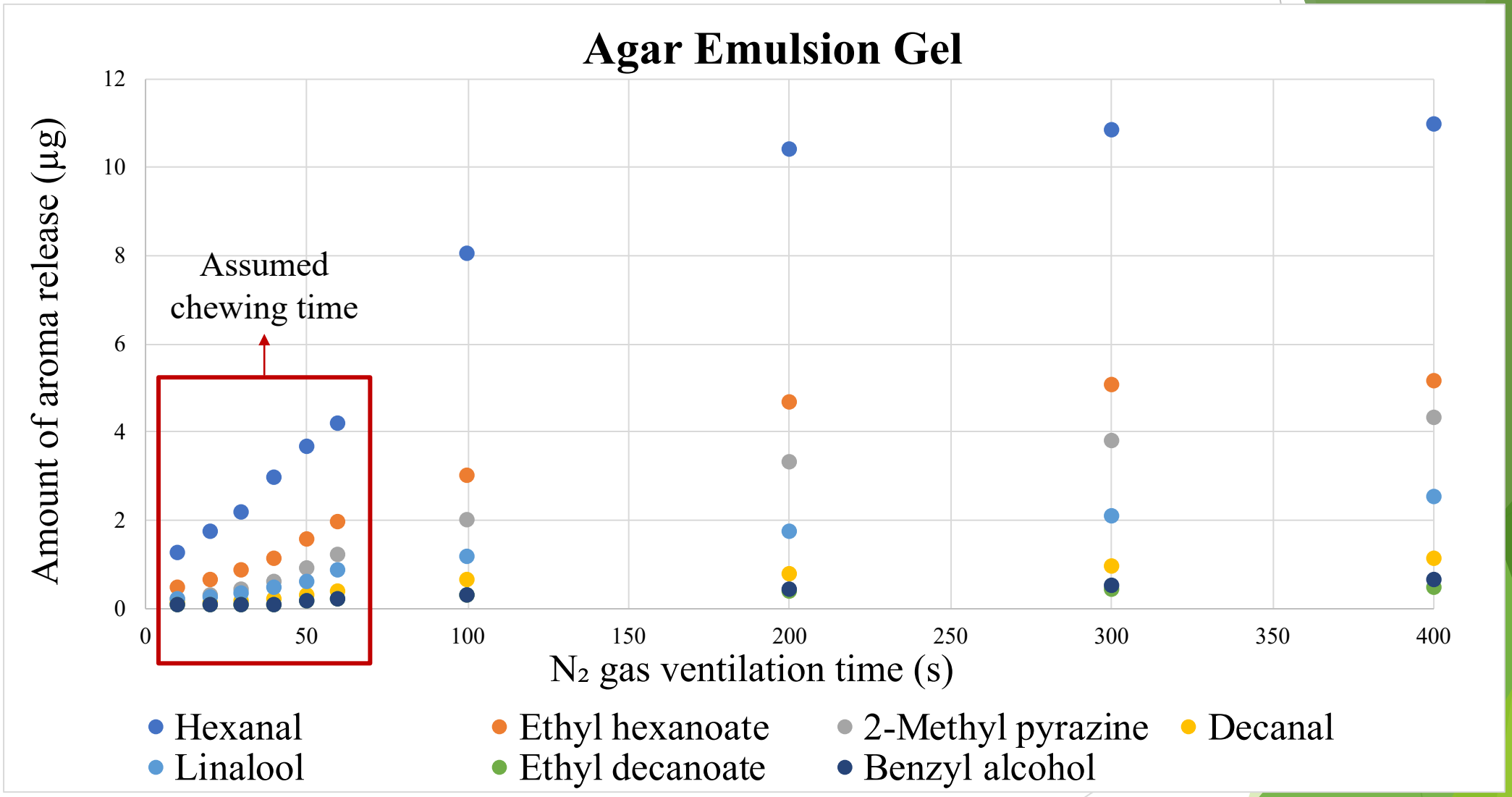

Amount of aroma compounds release from starch added AEG

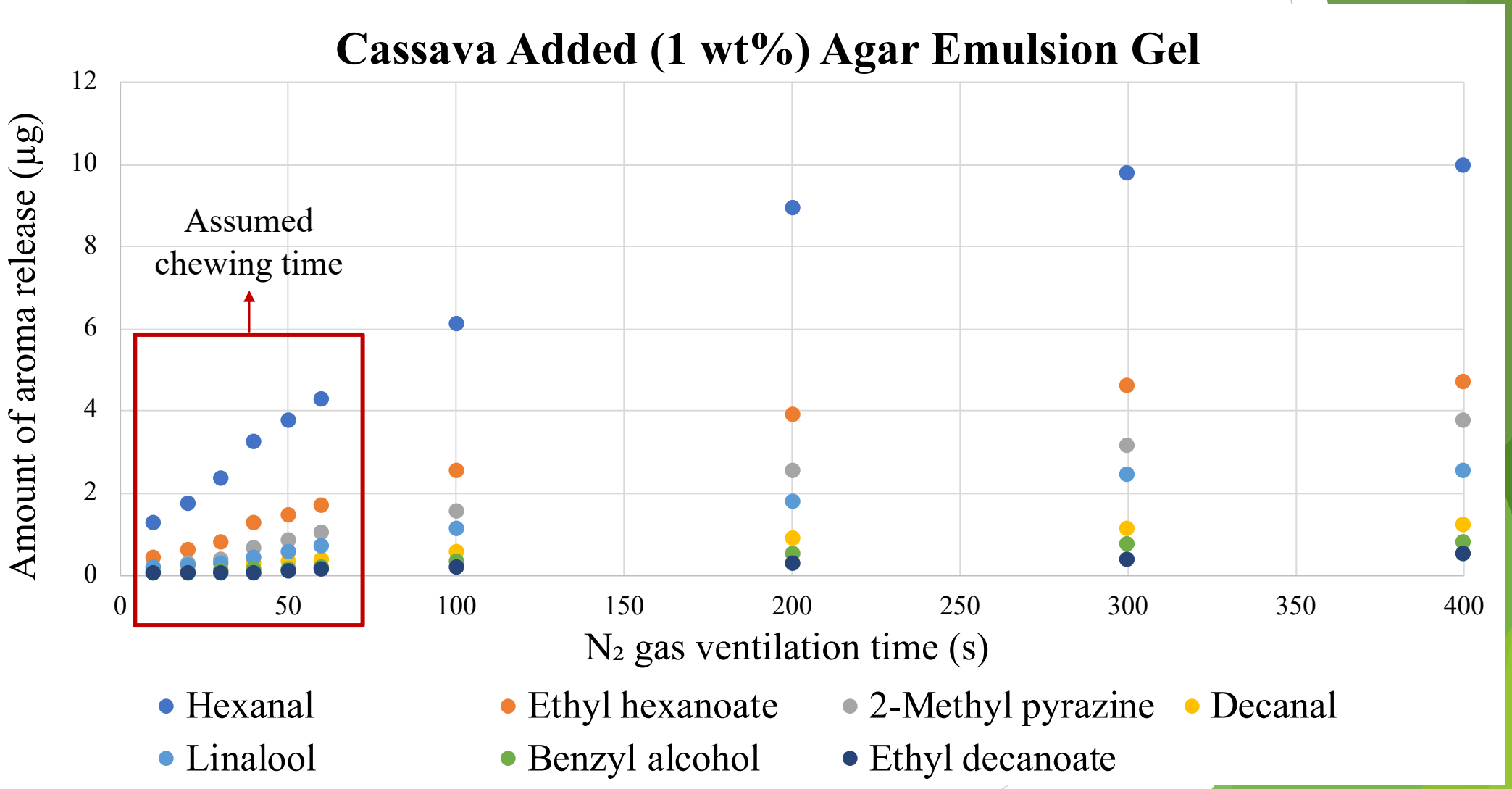

Aroma compounds release rate from **potato** added AEG during 60s

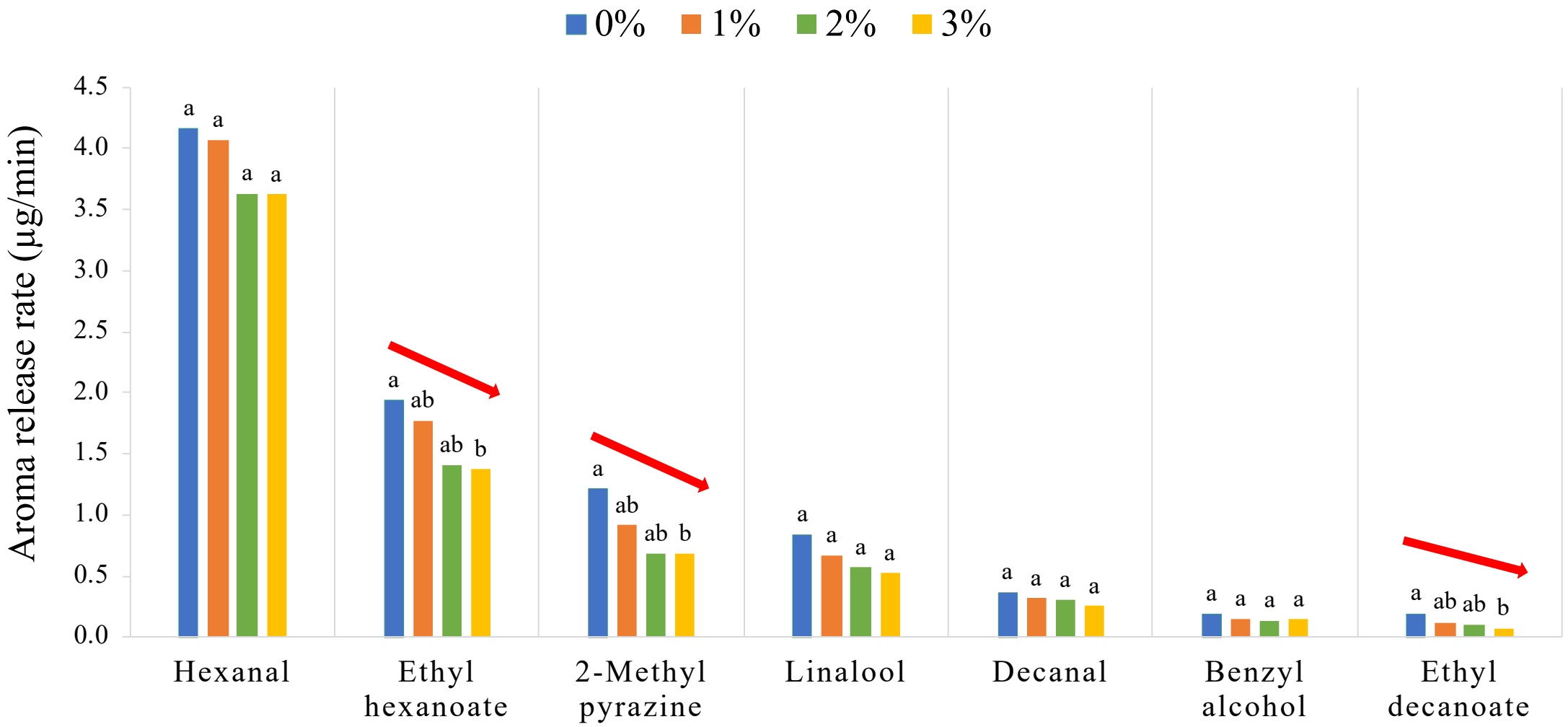

Statistical analysis according to Tukey-Kramer, different letters indicate significant differences at $p < 0.05$, $n = 3$

Aroma compounds release rate from **sweet potato** added AEG during 60s

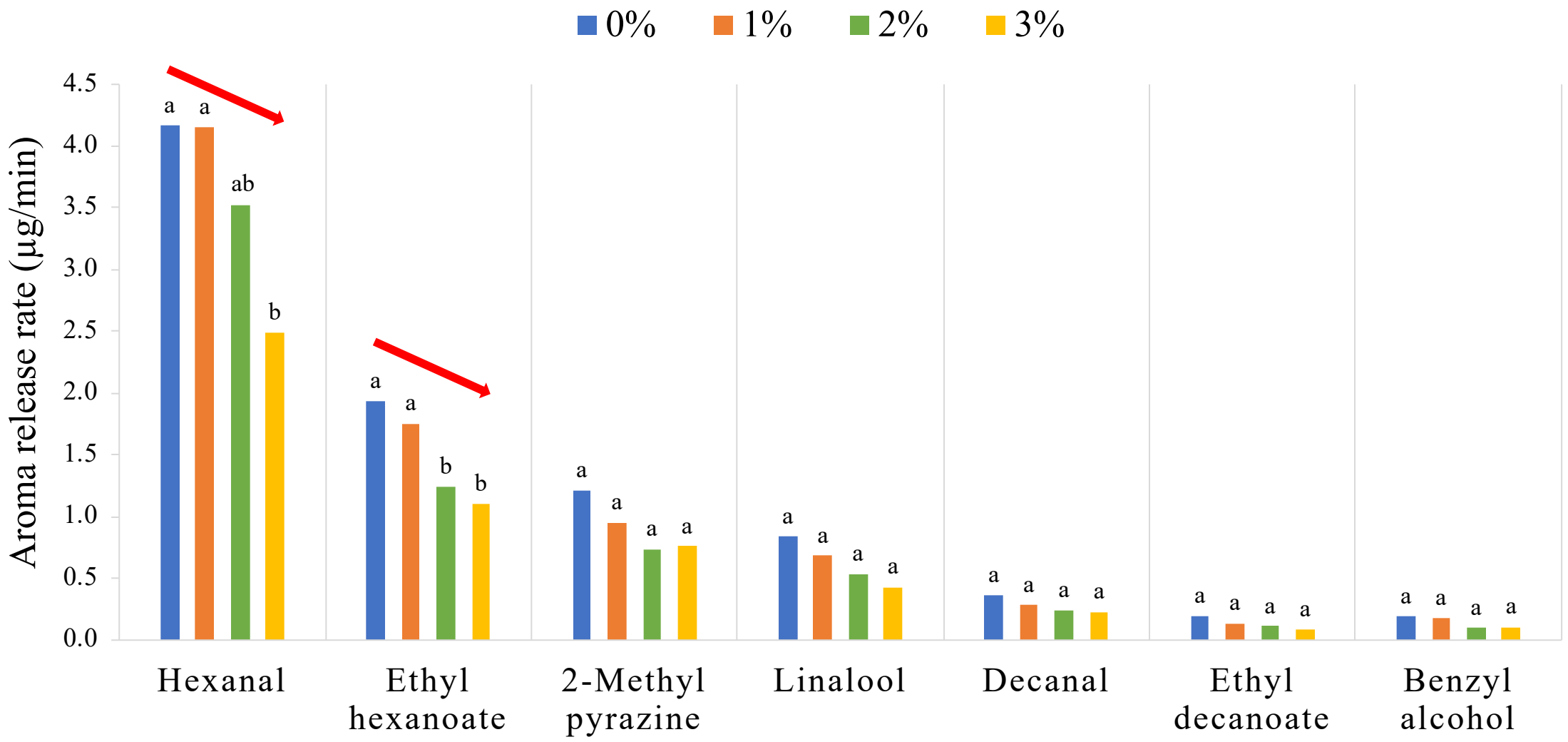

Statistical analysis according to Tukey-Kramer, different letters indicate significant differences at $p < 0.05$, $n = 3$

Aroma component release rate from **cassava** added AEG during 60s

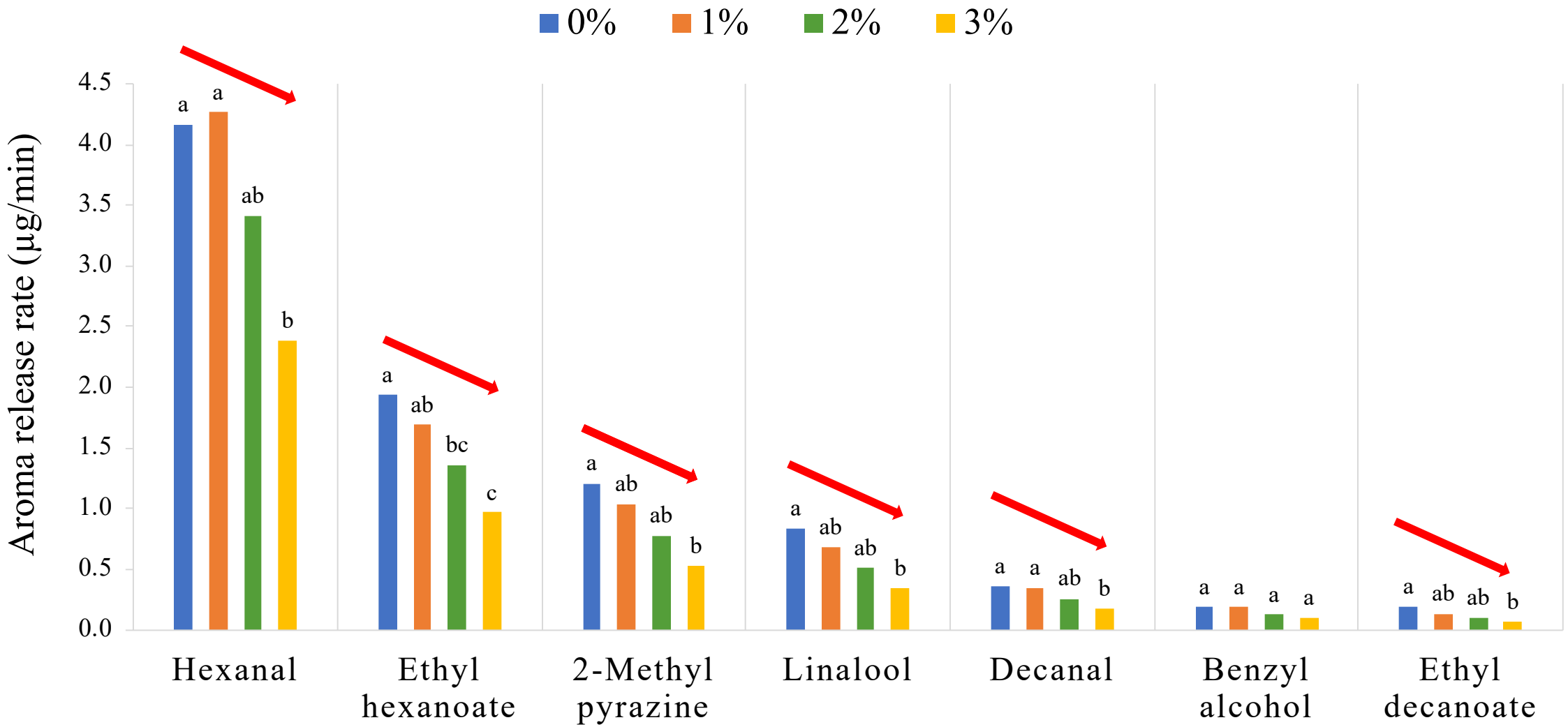

Statistical analysis according to Tukey-Kramer, different letters indicate significant differences at $p < 0.05$, $n = 3$

The relationship between aroma release and starch concentration

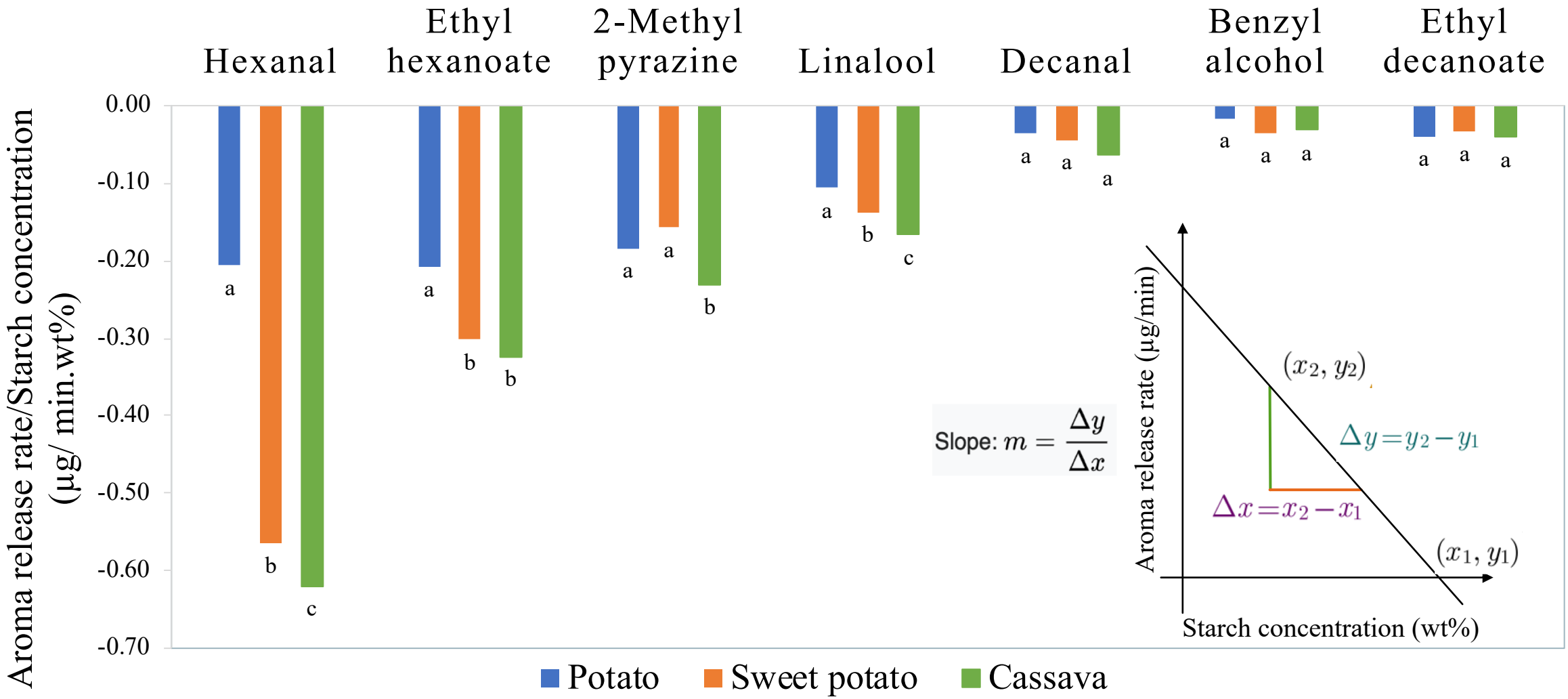

Statistical analysis according to Tukey-Kramer, different letters indicate significant differences at $p < 0.05$, $n = 3$

CONCLUSION

The amount of aroma release in AEG were decreased by adding starch. The more content of added starch, the lower aroma release.

Among three types of starch, the amount and the rate of aroma release from potato starch was more than sweet potato and cassava.

→ The texture and aroma release behavior of the AEG with the addition of potato starch was preferable to other starch-added gels.

THANK YOU FOR YOUR ATTENTION

Aroma compounds characteristics

Name	Structure	log P_{ow}	Boilling point
Hexanal	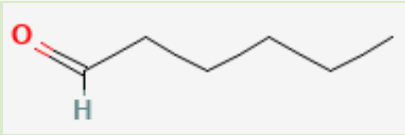	1.78	129°C
Ethyl hexanoate	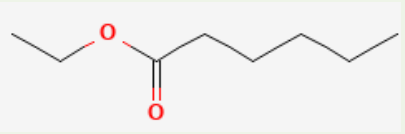	2.83	168°C
2-methyl pyrazine	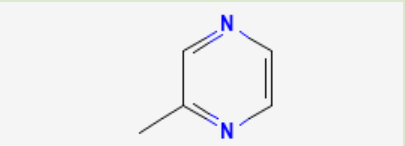	0.21	135°C
Linalool	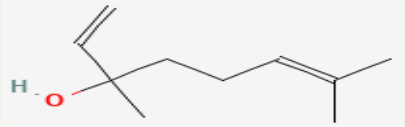	2.97	198°C
Decanal	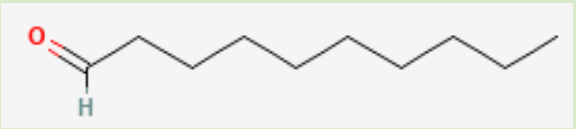	3.76	207°C
Benzyl alcohol	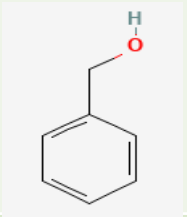	1.10	205°C
Ethyl decanoate	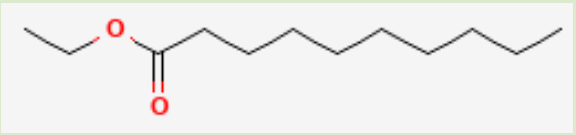	4.79	241 - 245°C

CONTENT 1 - MATERIALS AND METHODS

Sample Preparation

- Deionized water
- Agar 0.65 wt%
- Starch (0 – 3%)

Stirring (95°C, 60 min)

Stirring (65°C, 30 min)

Agar - starch solution

- Canola oil (20%)
- ML750 (1.0 g/L)

Homogenize (6000 rpm, 3 min)

Shirasu Porous Glass (Pore size 10 μm)

Emulsion

Stirring (65°C, 5 min)

Fill in the tube

Ice water (10 min)

Agar emulsion gel

Maintaining (25°C, 15 min)

Cutting (10 mm)

Maintaining (25°C, 10 min) → Sample measurement

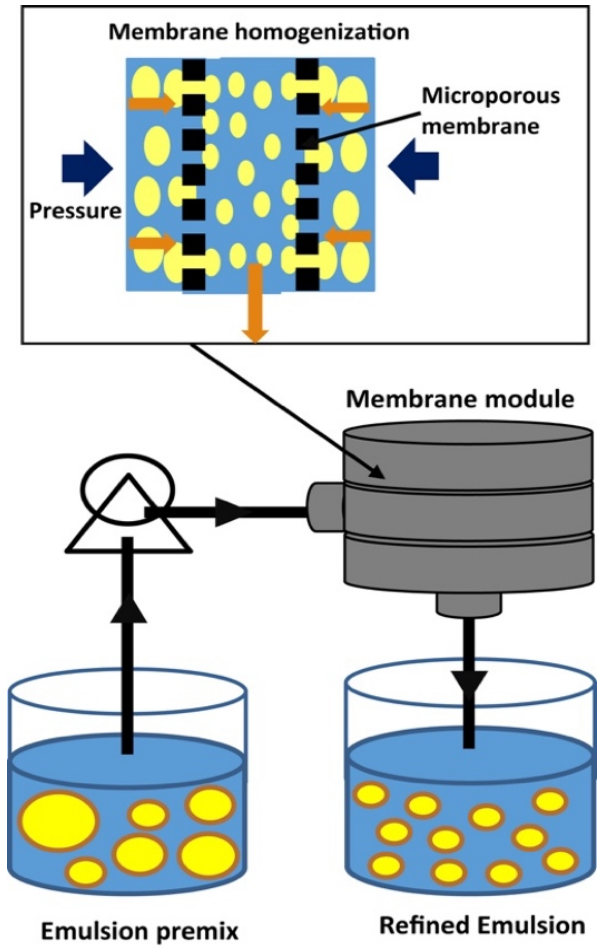

(Mugabi, Jophous, et al., Colloids and Surfaces A: Physicochemical and Engineering Aspects, 2021)

CONTENT 1 – RESULT & DISCUSSION

Hardness

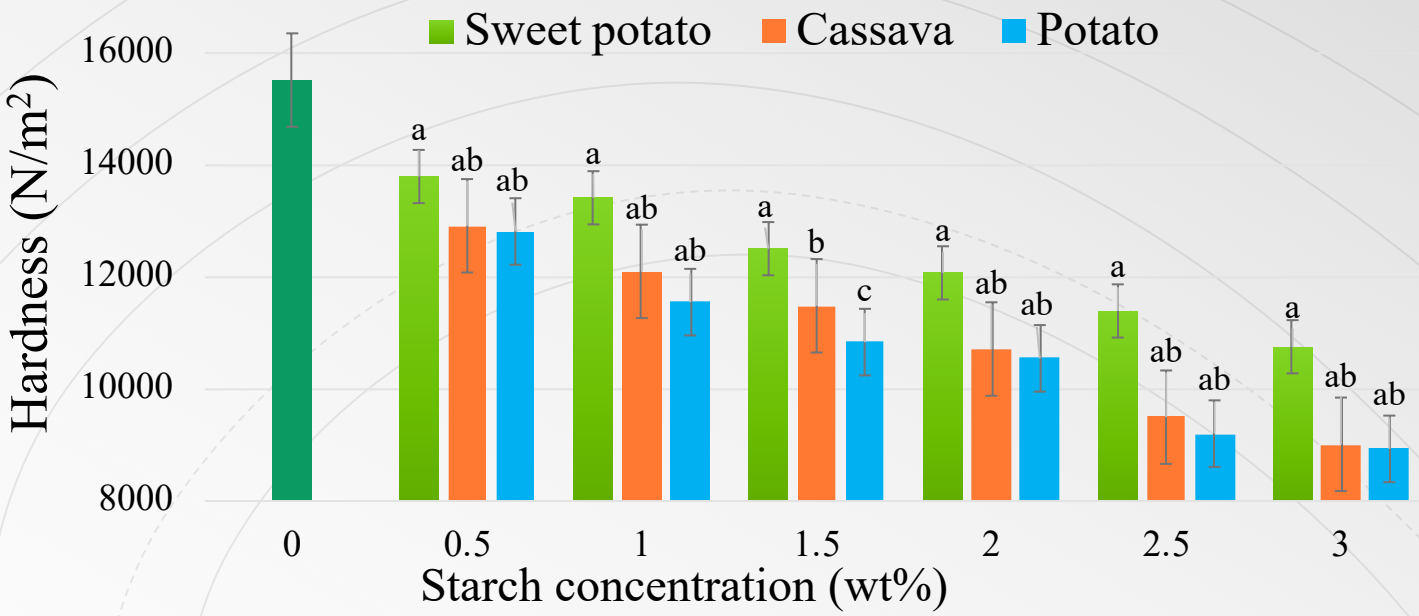

(Tukey-Kramer, different letters indicate significant differences at $p < 0.05$, $n = 3$)

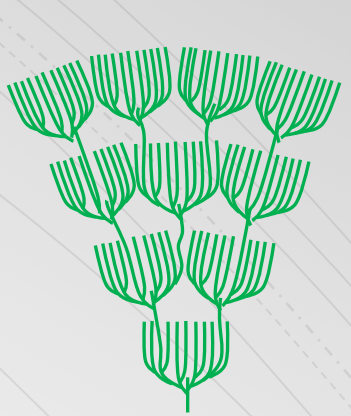

Amylopectin

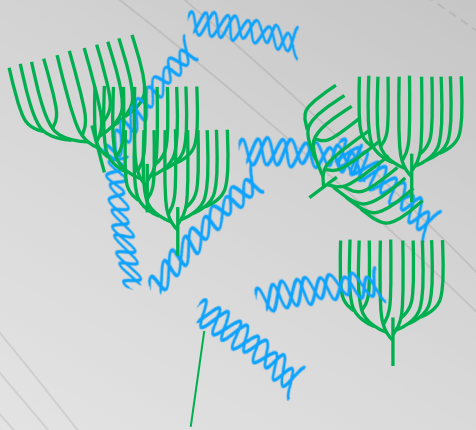

Agar molecular

- The hardness went down
- Cassava and potato samples had lower hardness compared to sweet potato AEG
- The hardness fitted the dysphagia diet's standard

Starches	Amylose	Amylopectin	Crystallinity
Potato	20-30%	70-80%	23 – 25%
Cassava	10.3-25%	75-89%	35 – 38%
Sweet potato	17.2-19%	81-82.8%	38 – 45%

(S J Tian et al., Journal of Food & Agriculture, 1991)

CONTENT 1 - MATERIALS AND METHODS

Sample measurement & Sample evaluation

Sample measurement

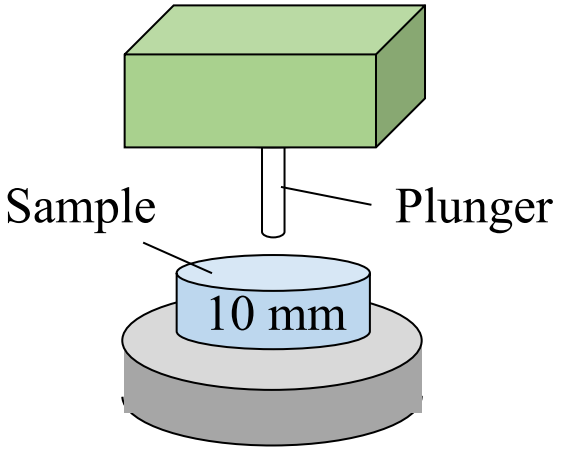

Measurement parameter	
Plunger diameter	3.0 mm
Sample thickness	10.0 mm
Measurement distortion	70%
Puncture speed	10.0 mm/sec

Sample evaluation for the dysphagia diets			
Standard	Permission Criteria I	Permission Criteria II	Permission Criteria III
Hardness (N/m^2)	2.5×10^3 –1×10^4	1×10^3 –1.5×10^4	3×10^2 –2×10^4
Adhesiveness (J/m^3)	4×10^2 or less	1.5×10^4 or less	1.5×10^3 or less
Cohesiveness (-)	0.2 – 0.6	0.2 – 0.9	–
Ministry of Health, Labour and Welfare (2009)			

13 main national agricultural products include: 1- Rice; 2- Coffee; 3- Rubber; 4- Cashew; 5- Pepper; 6- Tea; 7- Vegetables and fruits; 8- Cassava and cassava products; 9- Pork; 10. Poultry meat and eggs; 11- Pangasius; 12- Shrimp; 13- Wood and wood products.






Food Packaging and Shelf Life 45 (2024) 101331

Contents lists available at ScienceDirect

Food Packaging and Shelf Life

journal homepage: www.elsevier.com/locate/fpsl

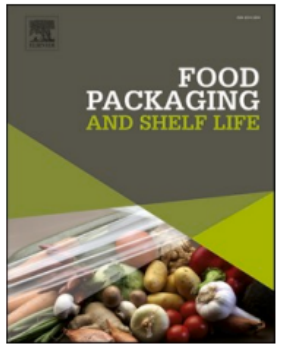

Development of a coating material composed of sodium alginate and kiwifruit seed essential oil to enhance persimmon fruit quality using a novel partial coating technique

Mohammad Hamayoon Wardak [a], Francis Ngwane Nkede [a], Tran Thi Van [a], Fanze Meng [a], Yan Xirui [a], Jakia Sultana Jothi [b,c], Fumina Tanaka [c], Fumihiko Tanaka [c,*]

[a] The Graduate School of Bioresources and Bioenvironmental Science, Kyushu University, Fukuoka 819-0395, Japan

This presentation is a part of data published in the journal of Food packaging and Shelf life and can be accessed thought following link:

Wardak, M. H., Nkede, F. N., Van, T. T., Meng, F., Xirui, Y., Jothi, J. S., ... & Tanaka, F. (2024). Development of a coating material composed of sodium alginate and kiwifruit seed essential oil to enhance persimmon fruit quality using a novel partial coating technique. *Food Packaging and Shelf Life*, *45*, 101331.

Enhancing the Shelf-life of Persimmon with a Novel Partial Coating of Sodium Alginate and Kiwifruit Seed Essential Oil

Mohammad Hamayoon Wardak
Kyushu University
The Graduate School of Bioresource and Bioenvironmental Sciences
Laboratory of Post Harvest Science
Prof. Fumihiko Tanaka
Asst. Prof. Fumina Tanaka

Food Waste

FAO

1.3 billion

tones of food is wasted globally each year

40% of food losses at post-harvest levels

Plastic Pollution

34% of Leatherback Sea Turtles

1000 years for complete degradation

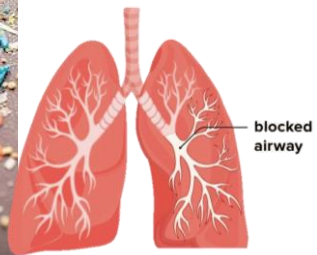

Persimmon (*Diospyros Kaki*)

- A climatic fruit
- National Fruit of Japan
- 14th most consumed fruit in the world

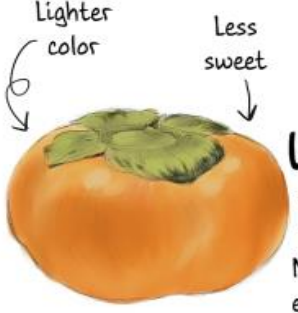

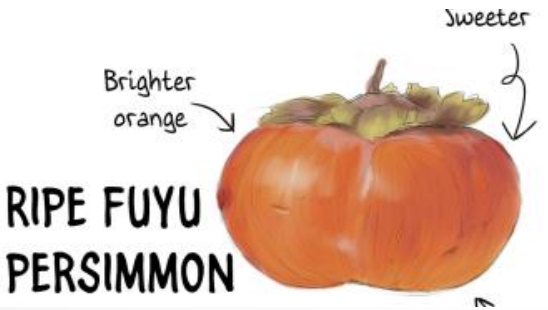

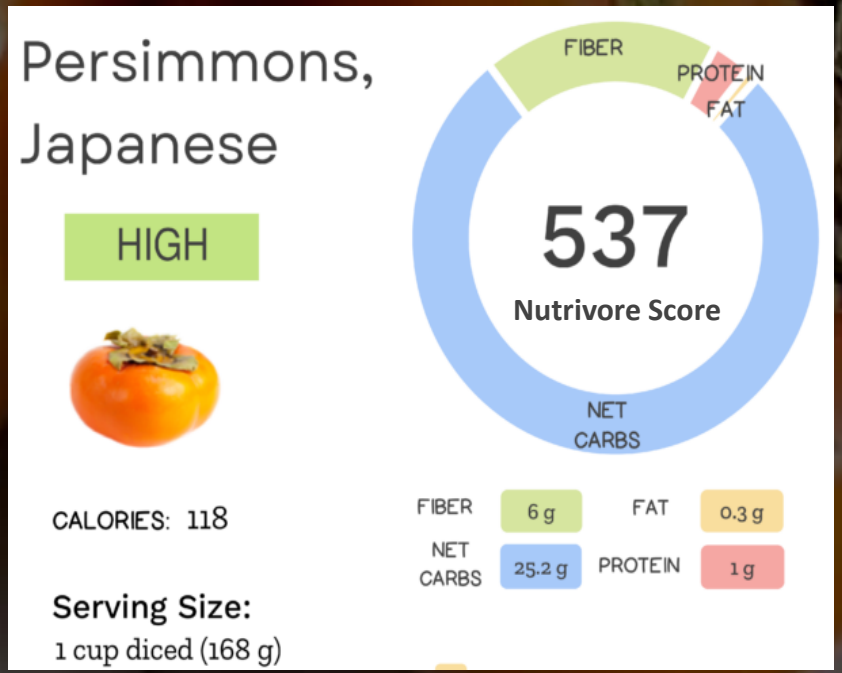

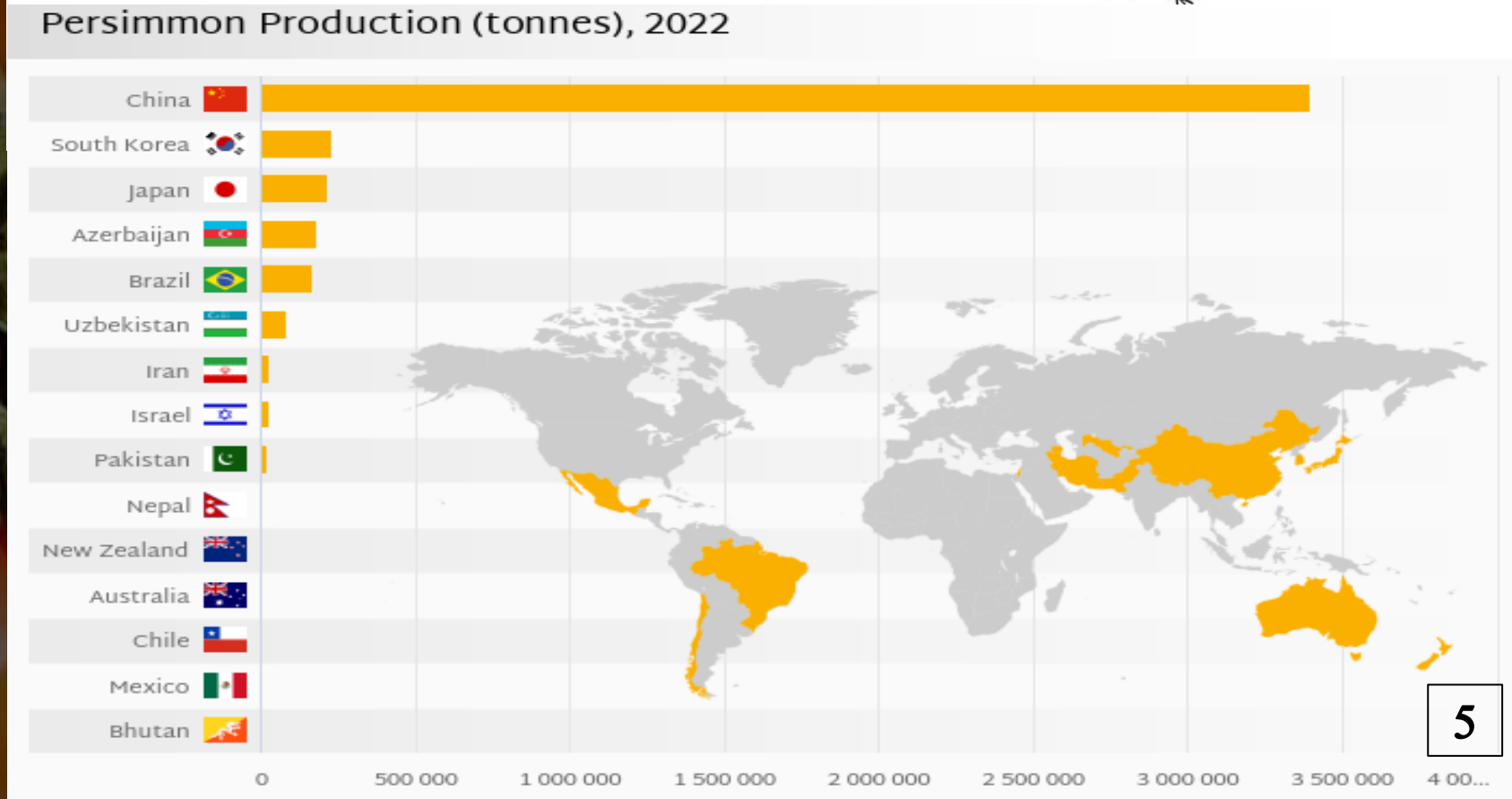

HelgiLibrary

Ripening and Deterioration

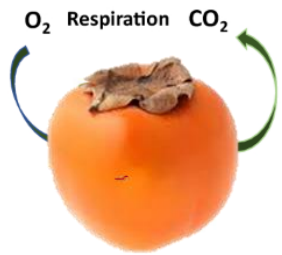

Ripening

Softening

Plays an important role in respiration

Deterioration

Main preservation methods

Low-temperature storage

Modified Atmosphere Packaging

Limitations

Costly

Chilling injury

Pollution

Edible Coating

Generally, are made from polysaccharides; like sodium alginate (SA)

- Eco-friendly
- Inexpensive
- Non-toxic
- Biodegradable

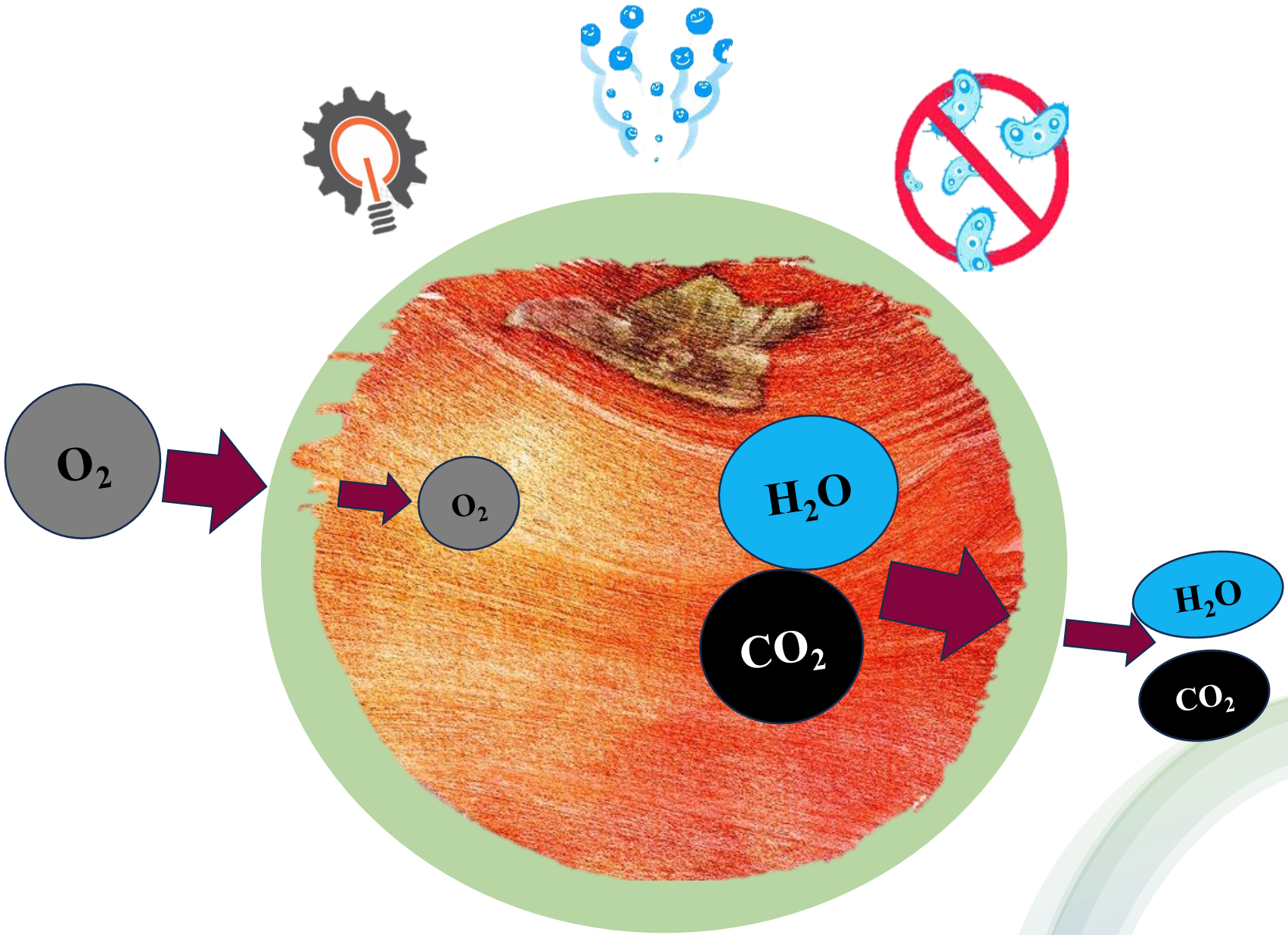

Partial coating

Less solution will be used and adhered to the product

Easy application

Dry faster

- Minimizing Waste
- Saving time and effort
- Lowering cost
- Enhancing consumers acceptability

Calyx is greatly involved in the moisture loss and respiration

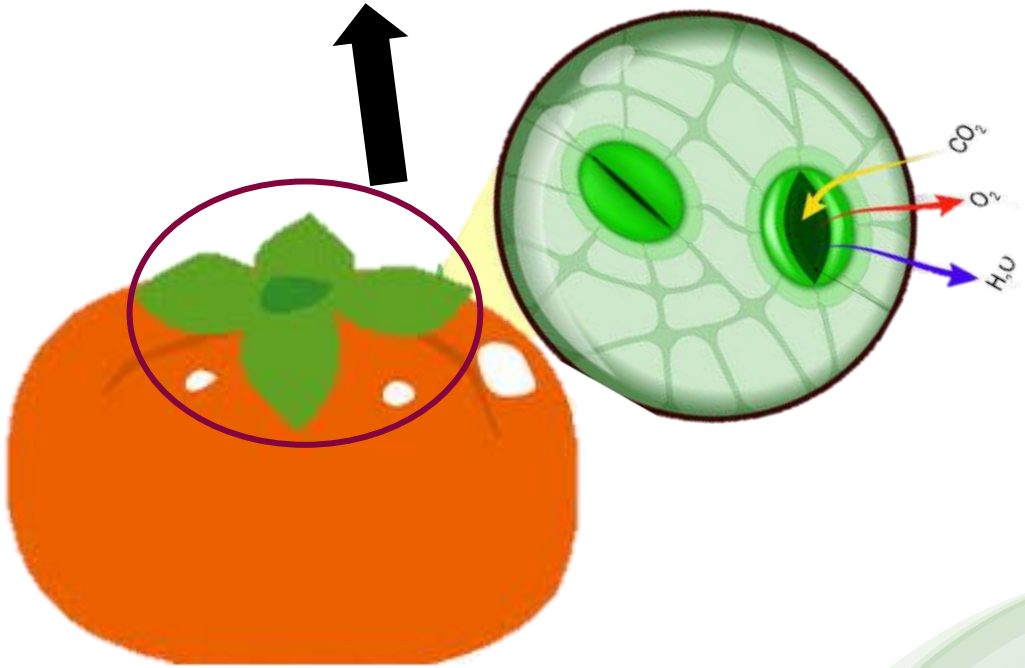

Objective

Evaluate the effectiveness of sodium alginate (SA) and kiwi-seed essential oil (KSO) coating material using the novel partial coating technique on the quality of persimmon fruits

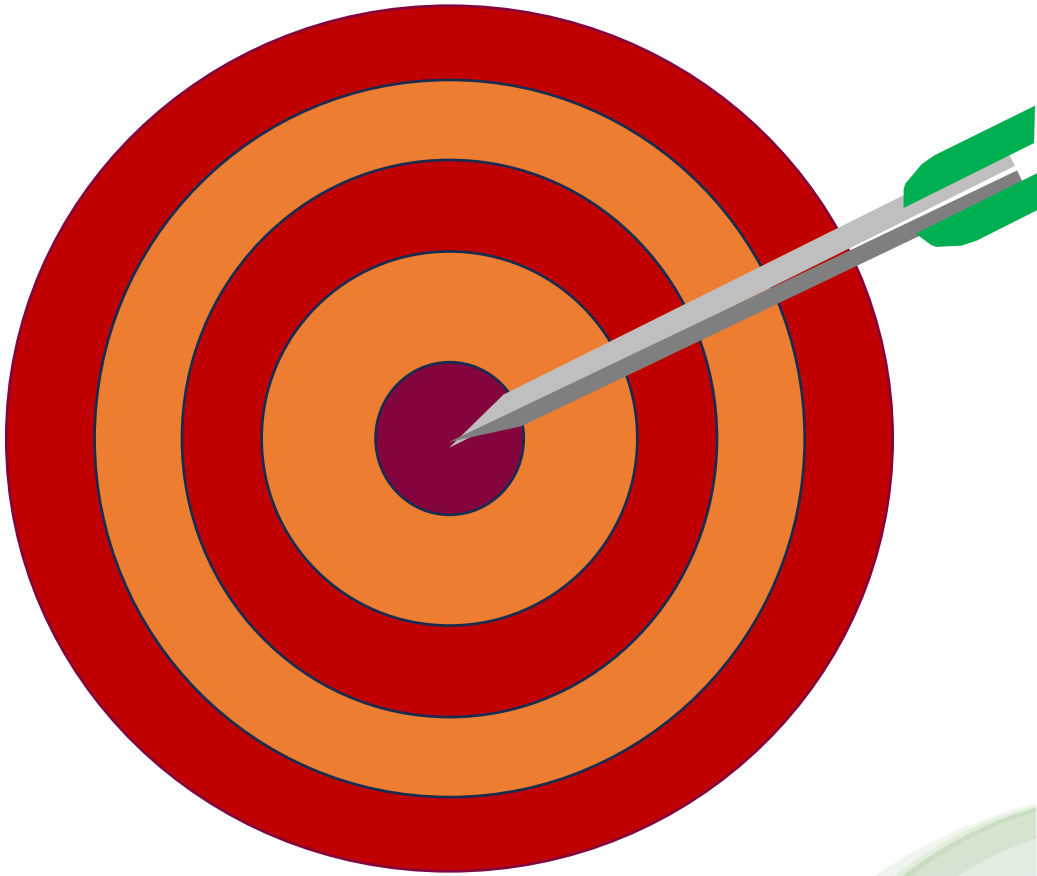

Preparation of Coating Materials

SA [1.25% (w/v)],
Glycerol [20% (v/w SA)]

Gelatinized at 55 ° C for 30 min

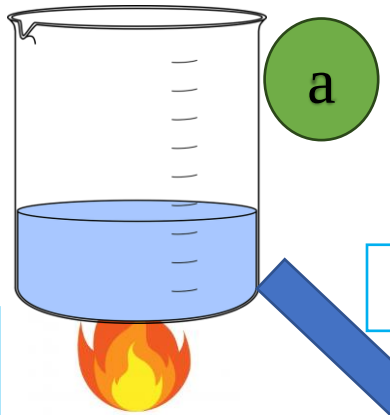

Mixed

Homogenized for 5 min

KSO [30 % (v/w, SA)]
Tween 80 [25% (v/v EO)]

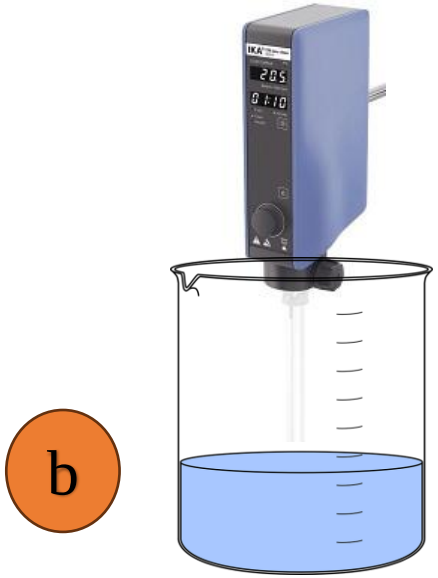

Homogenize for 3 min

Coating application

Coating application (Dipped 2 min)

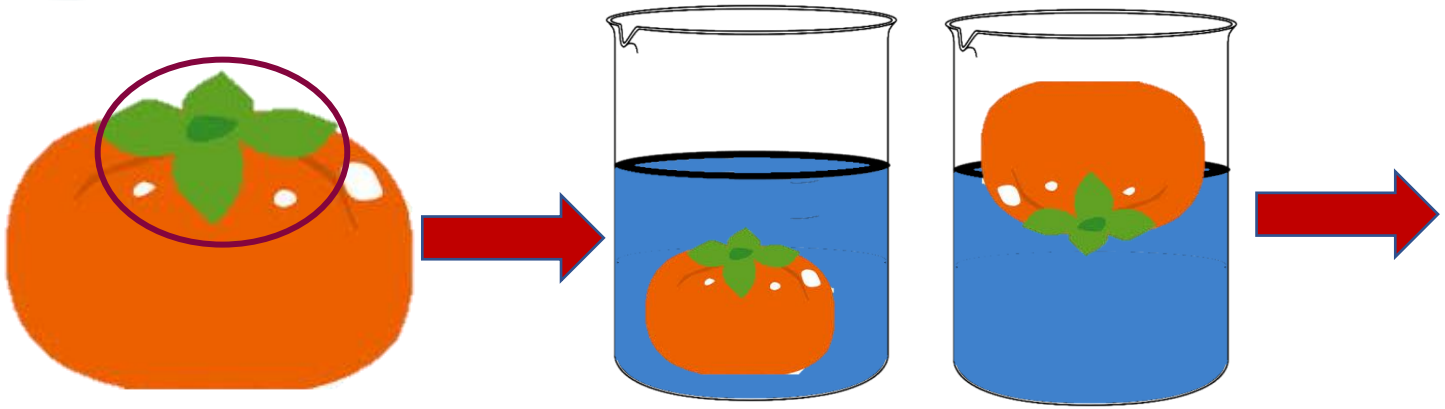

Dry the sample using fan

Stored in an incubator at **20 ± 2 ° C** and **80% RH**.

Qualitative measurements were performed every was performed at 4-d intervals for **20 d**.

The treatments were called **PSA, PKSO30, FSA, and FKSO30**, where **P** stands for **partial coating**, **F** for **full coating**, **SA** for **sodium alginate**, **KSO30** for **30% (v/w of SA) KSO, and control** persimmons **without coating**.

Quality parameters of Persimmon fruits

- Weight loss
- Respiration
- Firmness
- pH and TSS
- Skin and calyx Color

Balance

Firmness machine

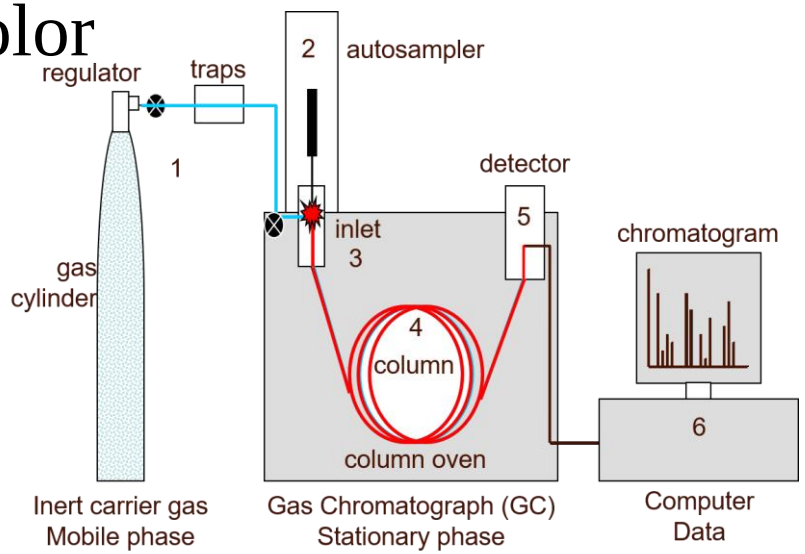

Gas Chromatography

Weight loss

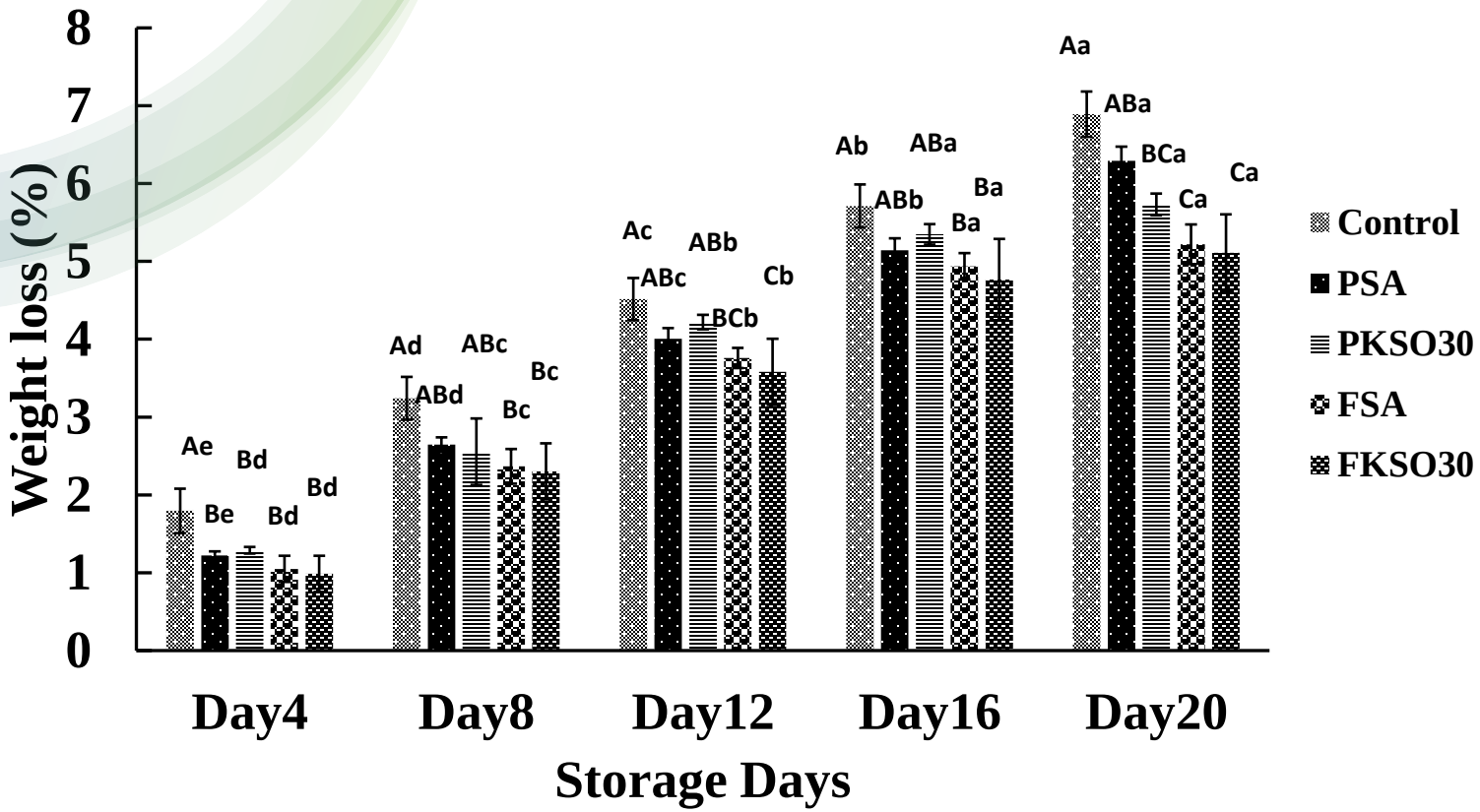

Fig. 1 Weight loss of uncoated and coated persimmon stored at 20 ± 2 ° C and 80% RH for 20 days.

Different uppercase letters on the bars indicate significant differences in treatments at the same storage times ($P < 0.05$). Different lowercase letters on the bars indicate significant differences in same treatment at different storage times ($P < 0.05$). Each bars represent the standard deviation.

Quality parameters of Persimmon fruits

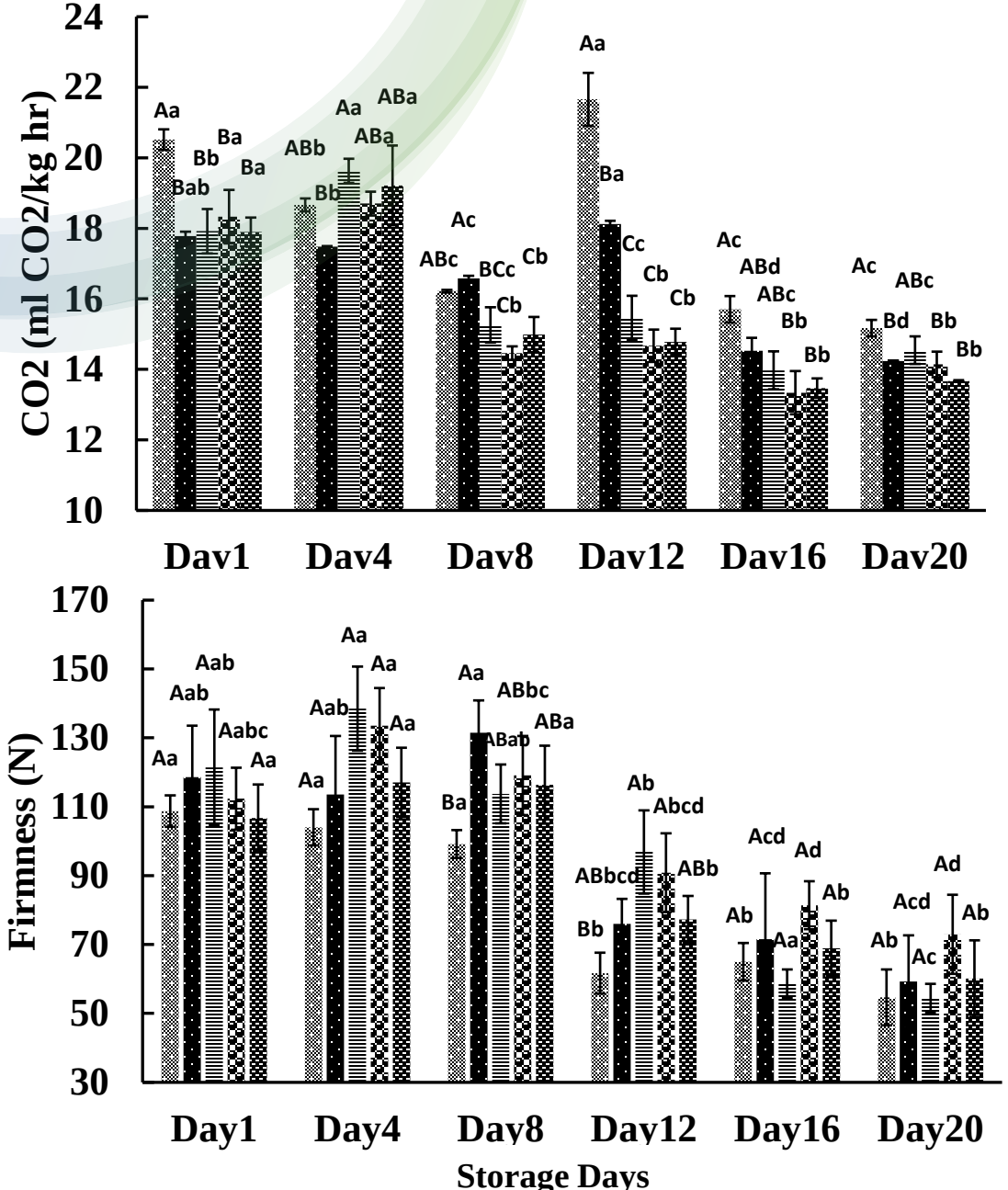

Fig. 2 (a) Respiration **(b)** Firmness of uncoated and coated persimmon stored at 20± 2° C and 80% RH for 20 days.

Different uppercase letters on the bars indicate significant differences in treatments at the same storage times ($P < 0.05$). Different lowercase letters on the bars indicate significant differences in same treatment at different storage times ($P < 0.05$). Each bars represent the standard deviation.

Quality parameters of Persimmon fruits

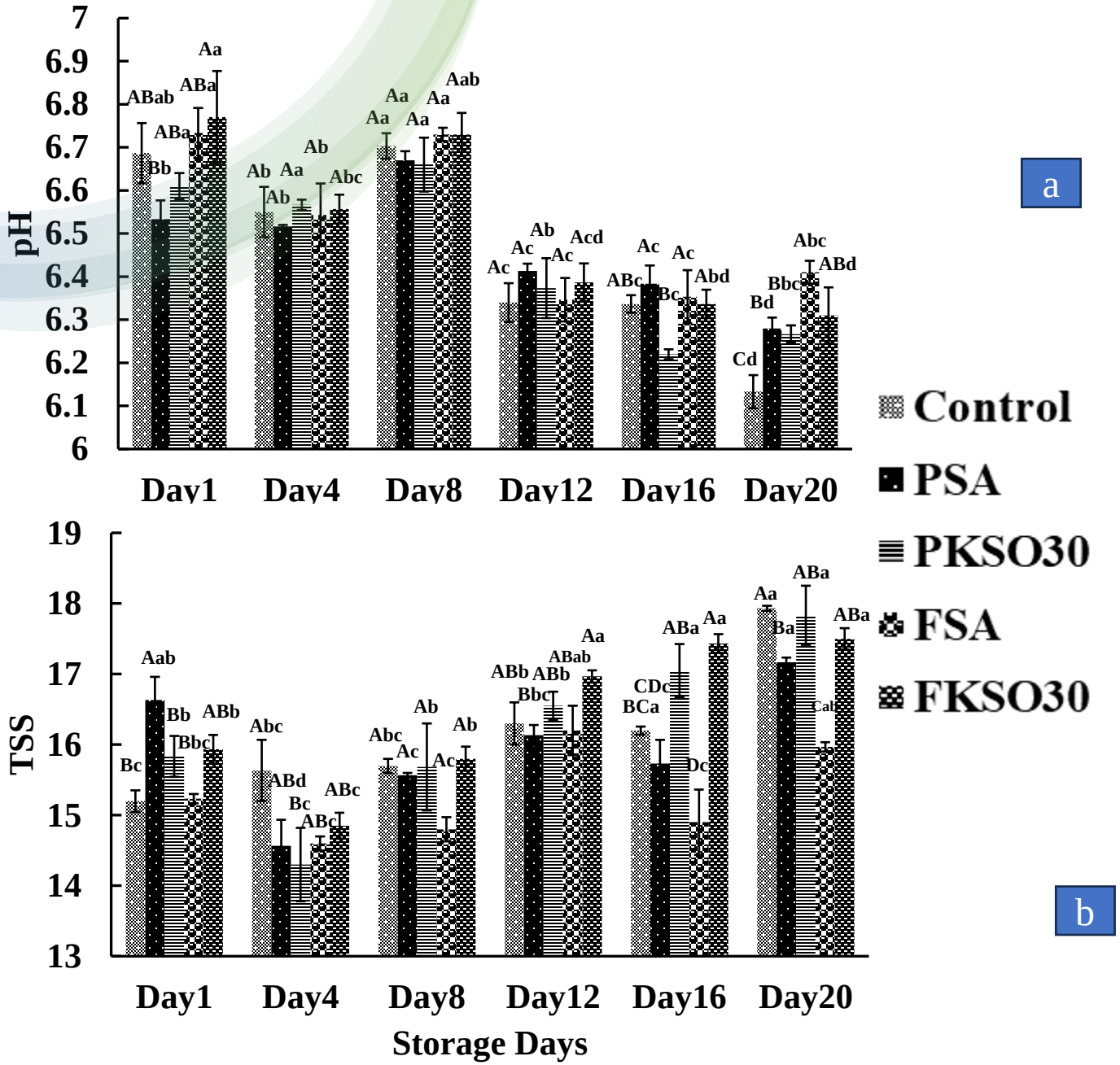

Fig. 3 (a) pH **(b)** TSS of uncoated and coated persimmon stored at 20 ± 2 ° C and 80% RH for 20 days. Different uppercase letters on the bars indicate significant differences in treatments at the same storage times ($P < 0.05$). Different lowercase letters on the bars indicate significant differences in same treatment at different storage times ($P < 0.05$). Each bars represent the standard deviation.

Skin color

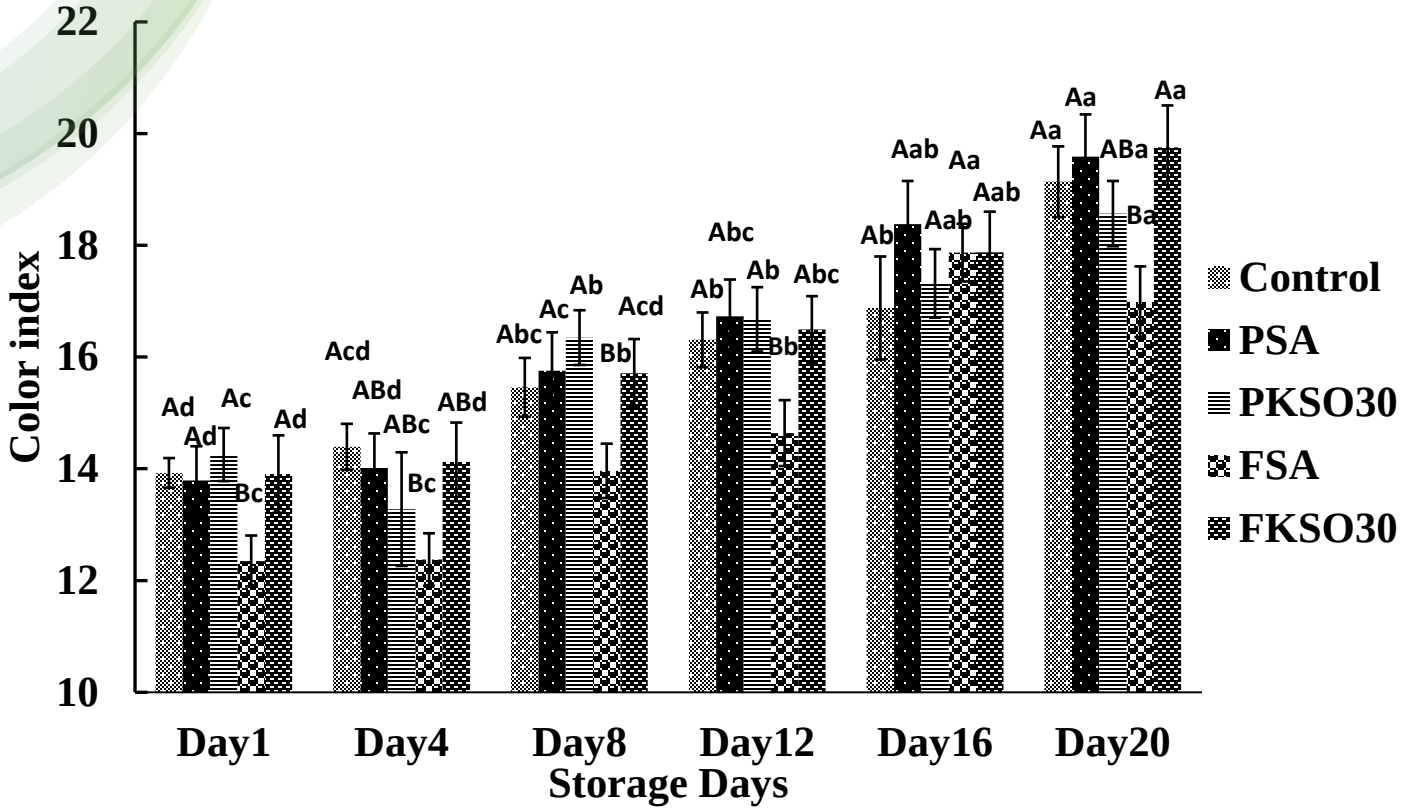

Fig. 4 Color index of uncoated and coated persimmon stored at 20 ± 2 ° C and 80% RH for 20 days.

Different uppercase letters on the bars indicate significant differences in treatments at the same storage times ($P < 0.05$). Different lowercase letters on the bars indicate significant differences in same treatment at different storage times ($P < 0.05$). Each bars represent the standard deviation.

Calyx Color

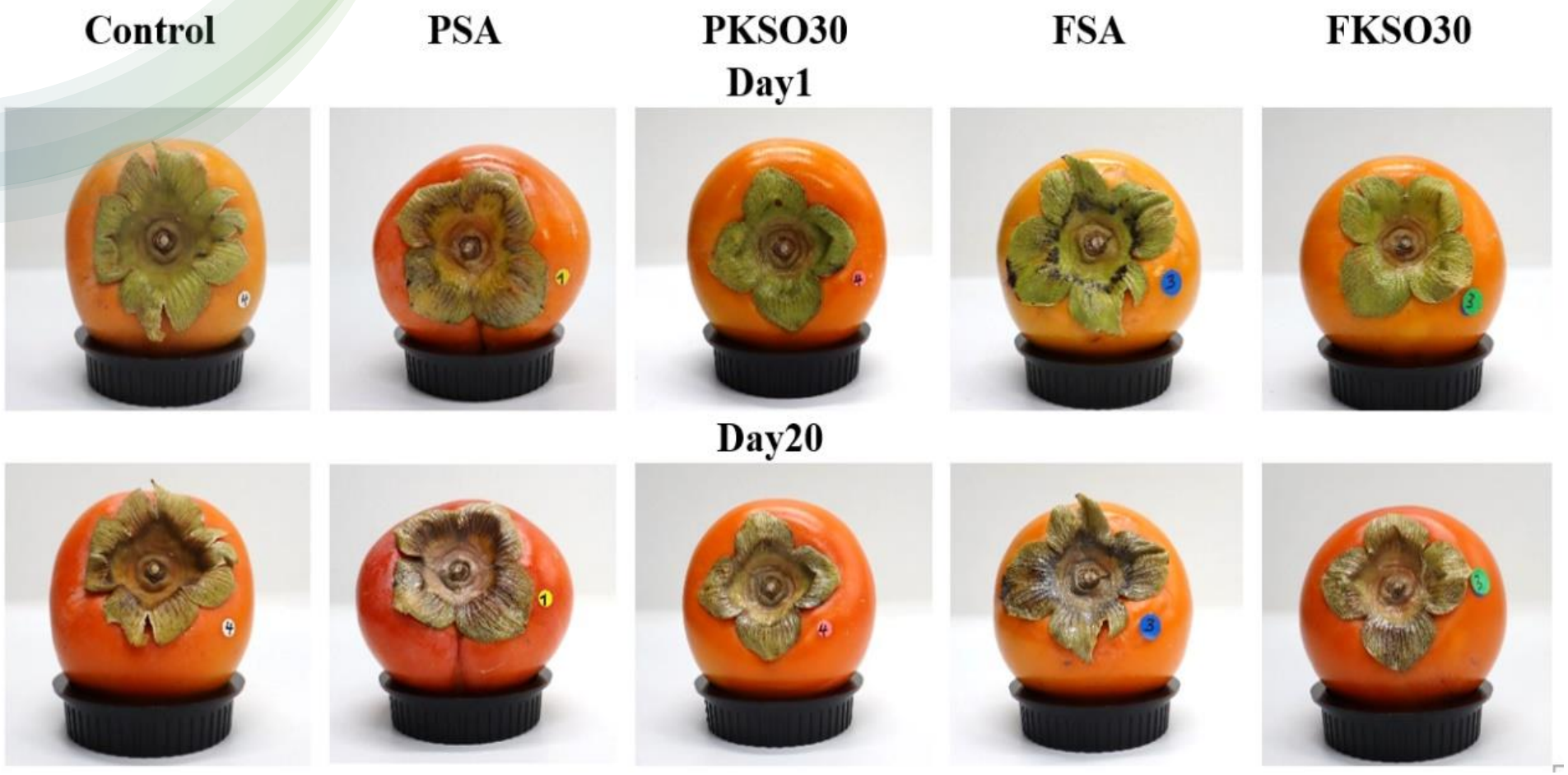

Fig. 8 Visual appearance of calyx of uncoated and coated persimmon stored at 20± 2° C and 80% RH for 20 days

Conclusion

- The developed **coating material** effectively **reduced the weight loss, maintained the firmness and respiration** rate of persimmon fruits. Although the full coating technique was more effective in reducing weight loss**, no significant changes was noticed between the partial and full coating methods was observed when evaluating the respiration rate and firmness**.
- These findings underscore the potential of the innovative approach of **partial coating with SA and KSO** coating materials to preserve the quality of **persimmon fruits** during storage and suggest that it can **extend** the **shelf-life and marketability of this product**.

THANK YOU!

九州大学
KYUSHU UNIVERSITY

The 6th Workshop on Interdisciplinary Sciences (WIS 2024)
Kyushu University, Fukuoka Japan

The influence of coating components on the metabolic profiles of cold stored strawberries

Tran Thi Van

Supervisor: Prof. Fumihiko TANAKA

Asist. Prof. Fumina TANAKA

Laboratory of Postharvest Science

Graduate School of Bioresources and Bioenvironmental Sciences

九州大学
KYUSHU UNIVERSITY

Introduction

Presentation contents

- Part 1. Introduction
- Part 2. Methodology
- Part 3. Results and Discussion
- Part 4. Conclusion

Introduction

➢ Strawberry (*Fragaria* × *ananassa*)

❖High level of vitamins, antioxidants and other important nutritional ingredients

❖Sensitive fruits with a short shelf life

❖Easily damaged after harvesting because of their soft texture and thin peel

Harvest condition

Post harvest condition

Picture source: https://www.bing.com/images

九州大学
KYUSHU UNIVERSITY

Introduction

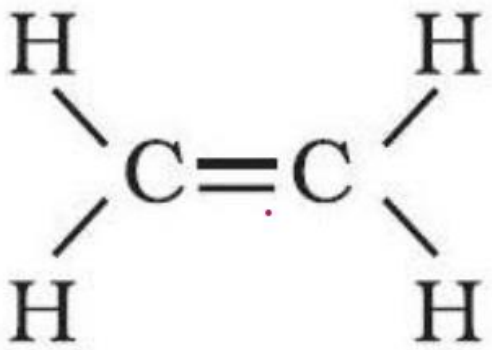

Ethylene

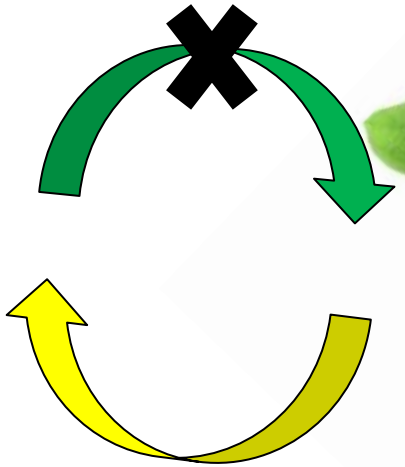

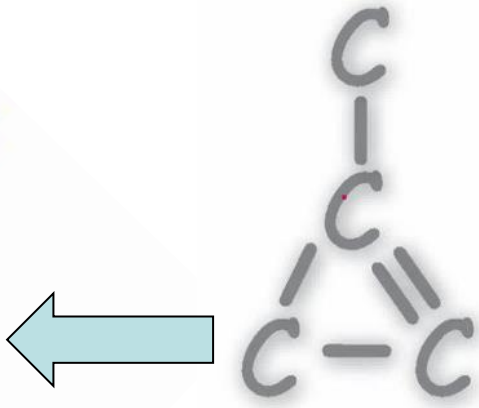

1-MCP

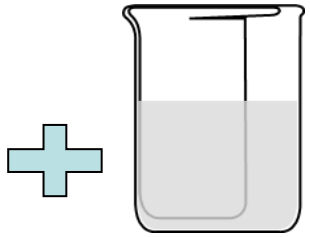

Coatings

- Positives of coatings with 1-MCP:

1-MCP (1- methycyclopropene) interacts with internal ethylene by binding to ethylene receptors and blocking their receptors, thereby preventing the absorption of external ethylene, delays quality decay in non-climacteric fruits such as strawberries.

九州大学
KYUSHU UNIVERSITY

Introduction

Coating:

- Prevent fruits with external influences
- Limit the inner processes
- Antifungal ability

⇒ Prolong the shelf-life of agriculture products

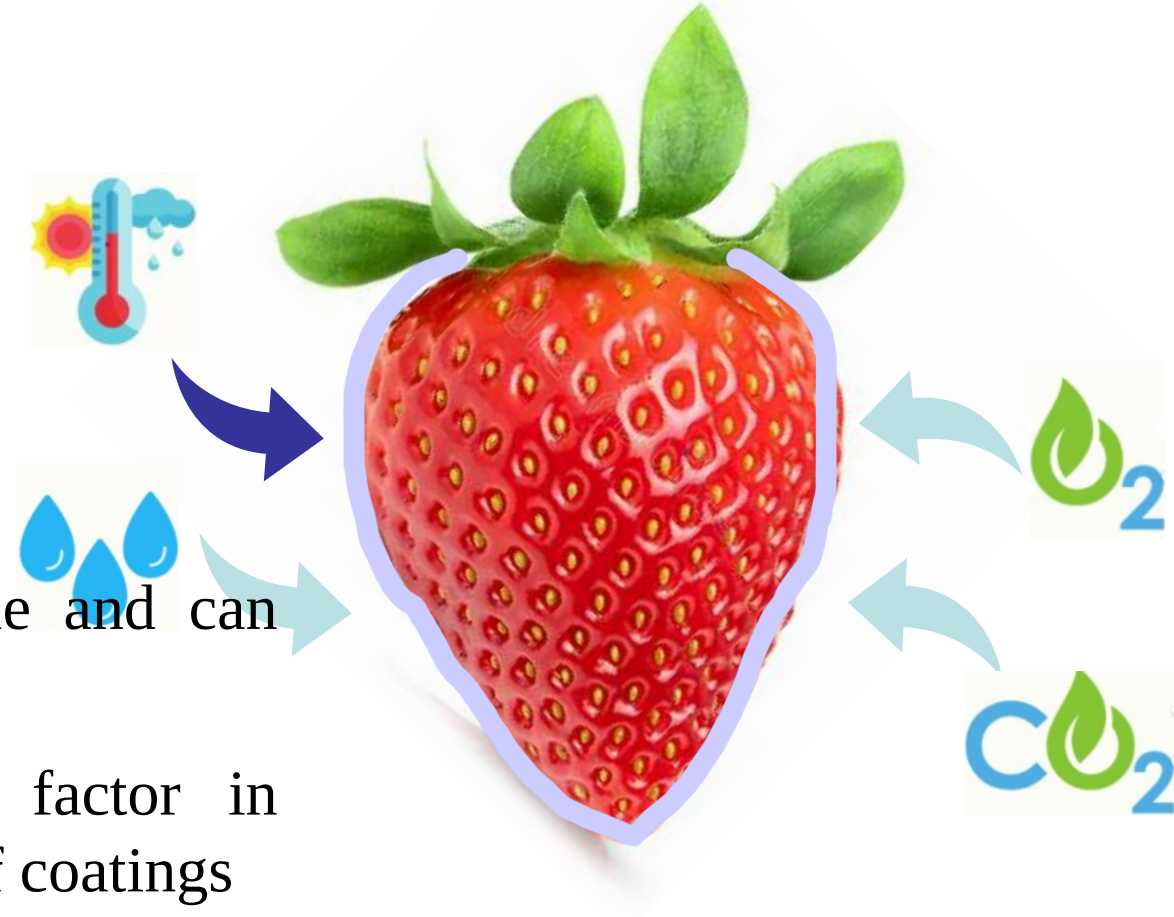

This study

- CMC (Carboxymethyl cellulose) is water-soluble and can form films that are moderately air-permeable.
- Nanoparticles such as cellulose is a critical factor in improving the mechanical and barrier properties of coatings
- ME was extract from the mandarin peel, These extracted compounds have demonstrated antifungal and antibacterial properties in fruits.

Introduction

Objective:

- This study aimed to determine the effects of dissolving 1-MCP/ME into CMC/CNF-based coatings to store fresh strawberry, and metabolic profiles during cold storage

Methods

Film making

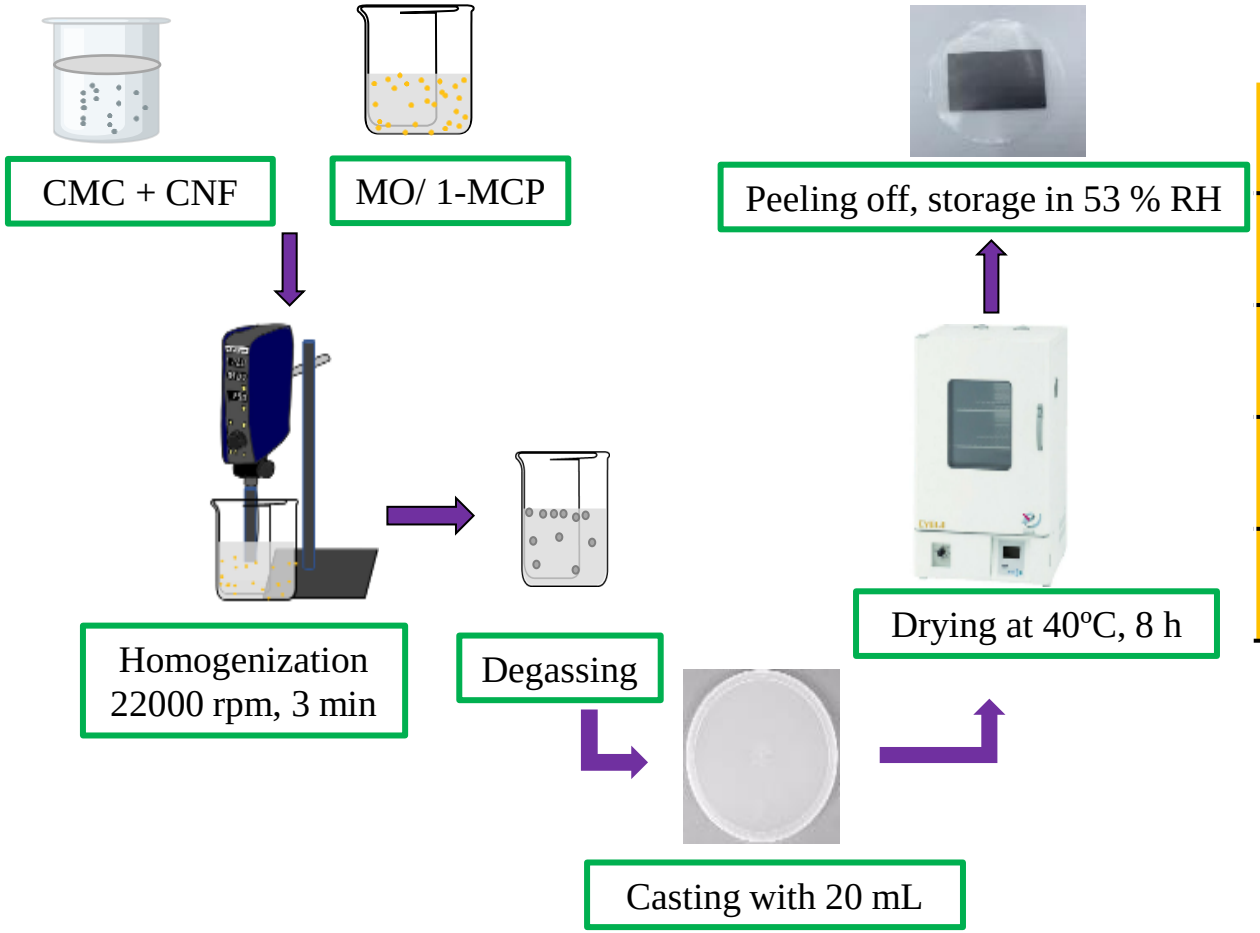

Fig. 1 Coating making procedure (Tran, 2024)

Table 1. Coating components

% (w/v)	CMC	CNF	Glycerol	Tween 80	Oleic acid	MO	1-MCP
CCM1-1	1	0.5	0.35	0	0	0	0
CCM1-2	1	0.5	0.35	0	0	0	0.1
CCM2-1	1	0.5	0.35	0.03	0.05	0.05	0
CCM2-2	1	0.5	0.35	0.03	0.05	0.05	0.1

九州大学 KYUSHU UNIVERSITY

Methods

Fruit application

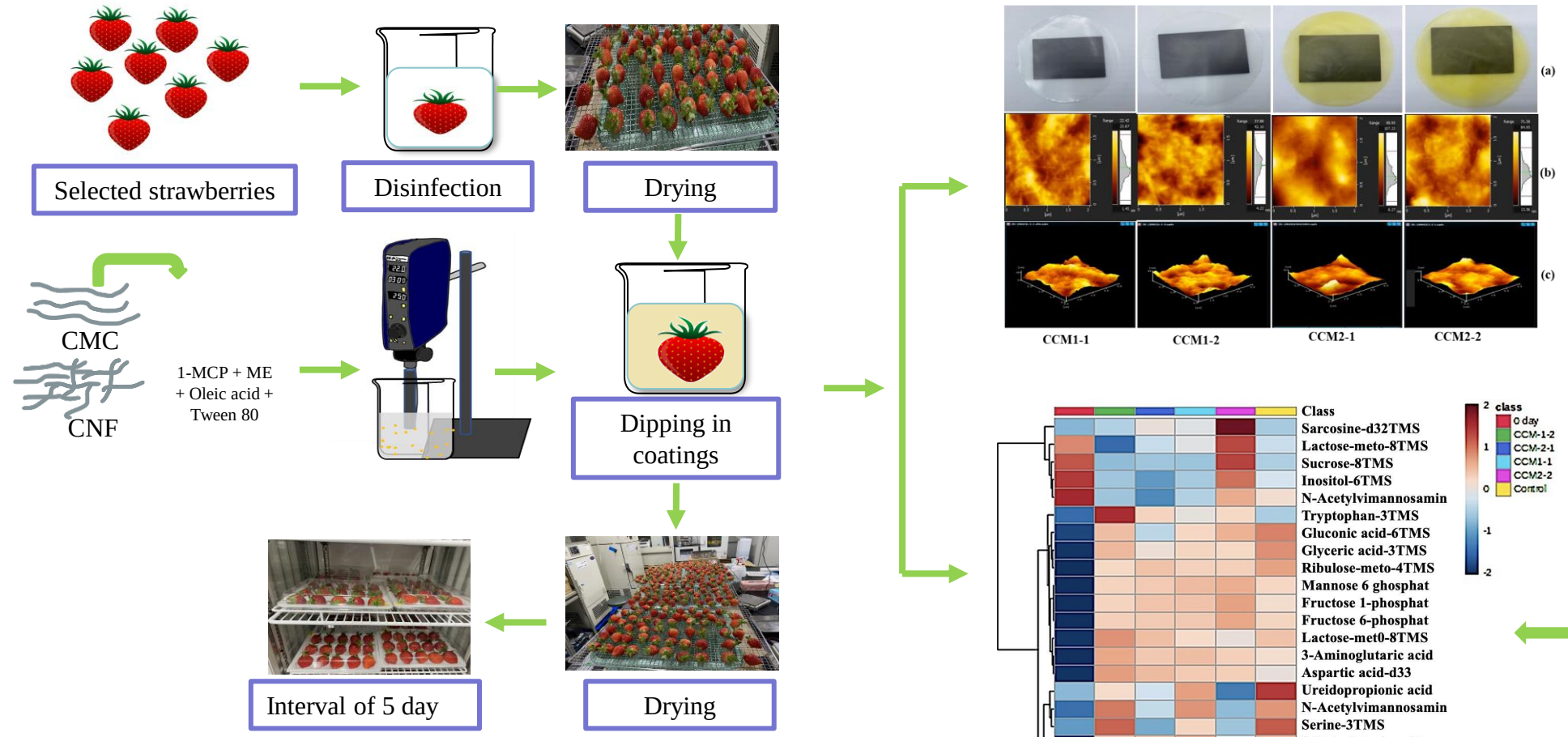

AFM 5000II

GCMS/MS 2030

Fig. 2 Fruit application (Tran, 2024)

九州大学
KYUSHU UNIVERSITY

Results

Film characteristics

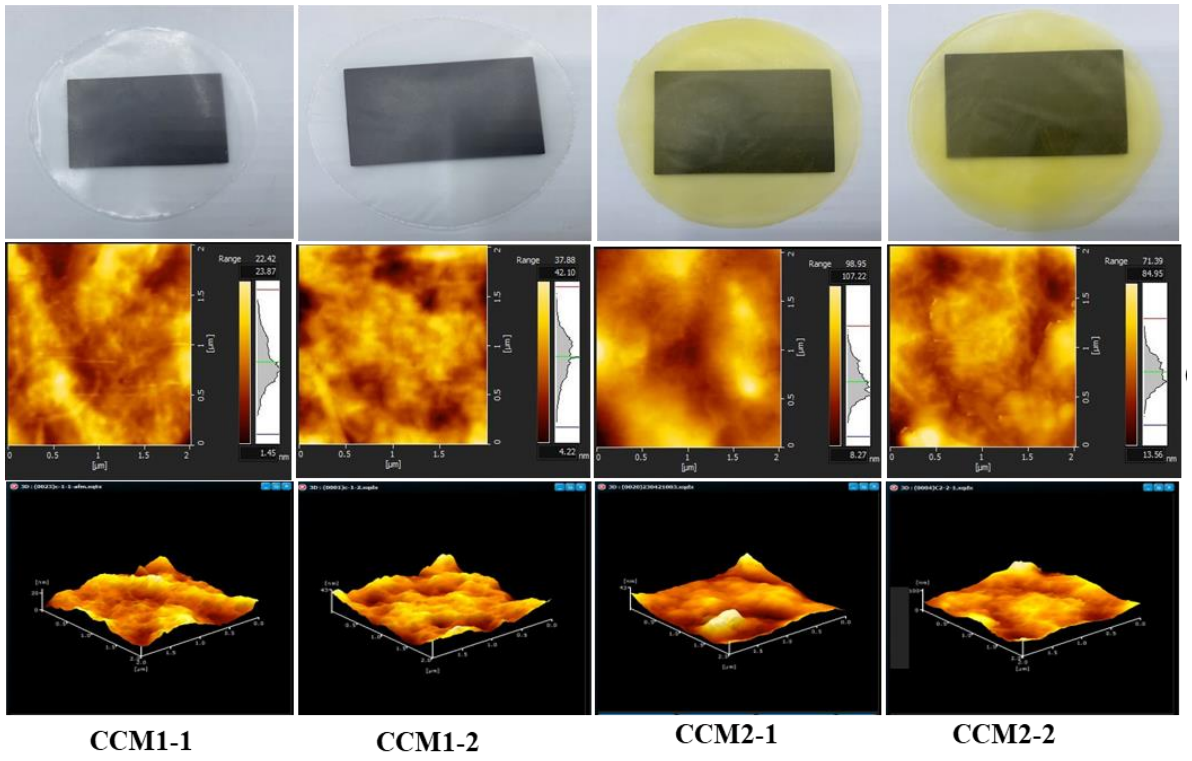

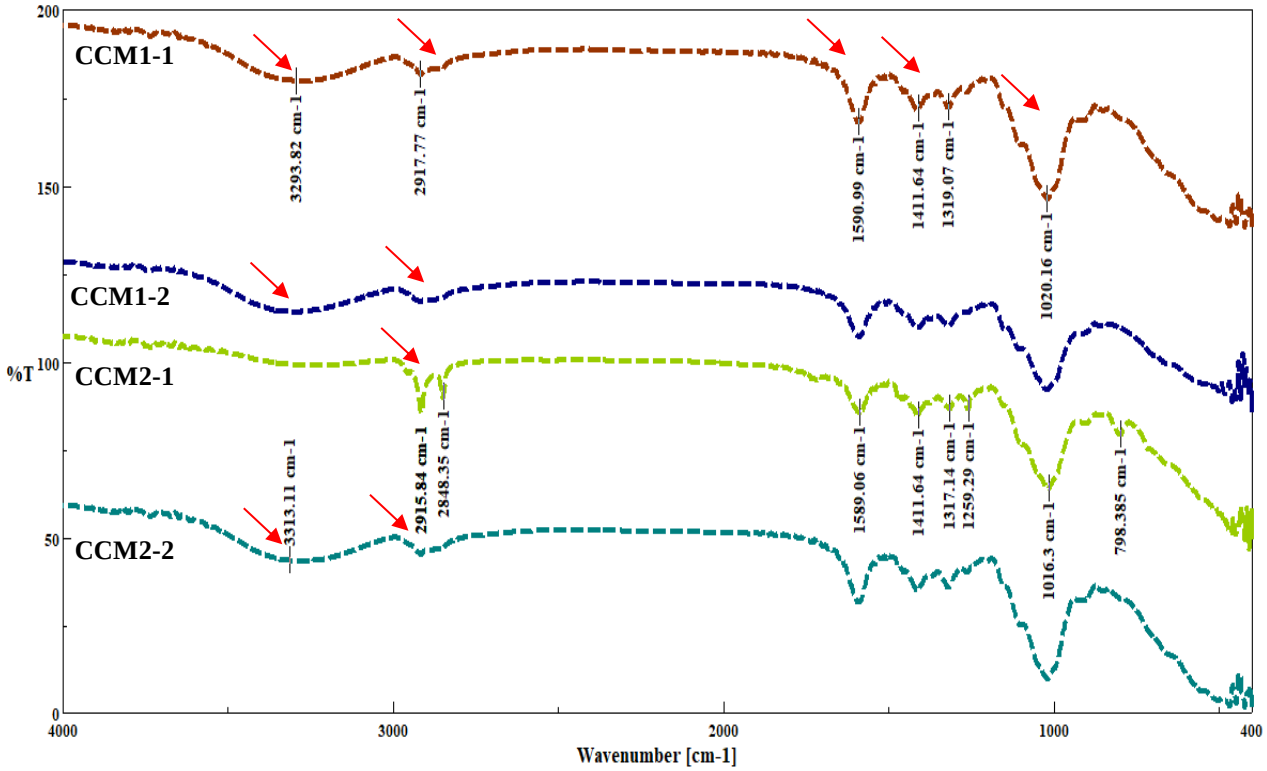

Fig. 3. Physical appearance (a); AFM images of surface roughness in 2D (b) and in 3D (c) of films, and FTIR analysis

Results

Weight loss and firmness of strawberry

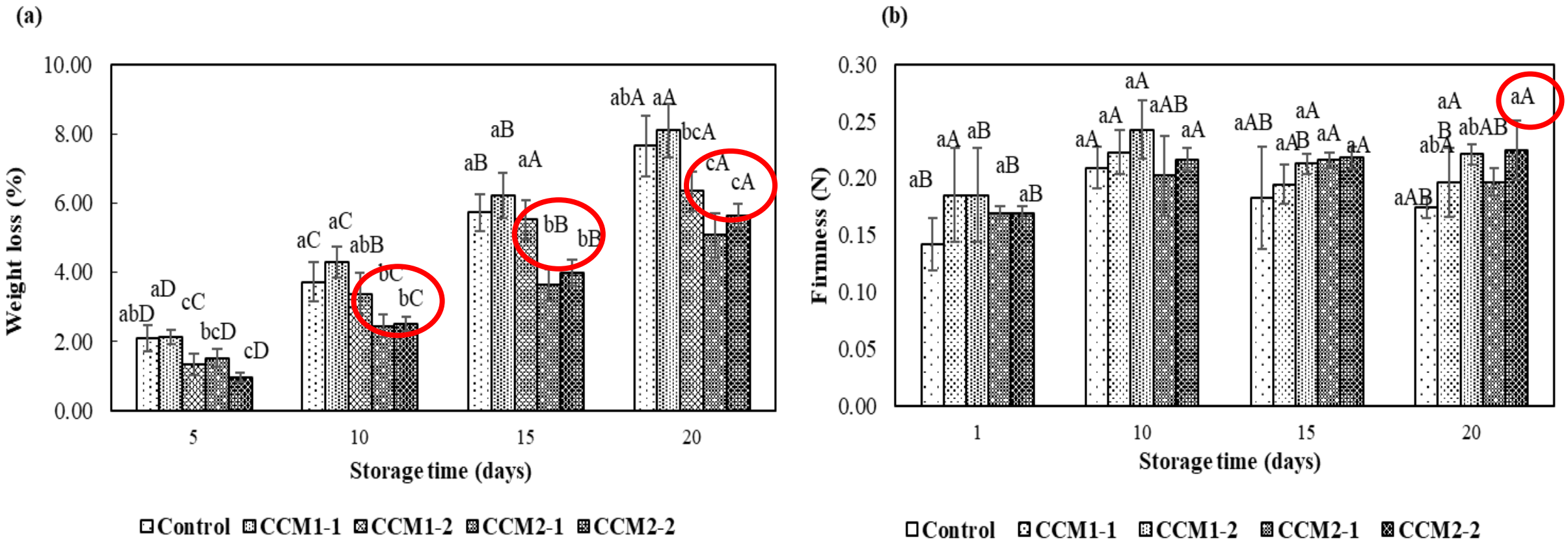

Fig. 4. Weight loss and firmness of uncoated (control) and coated strawberry stored at 5 °C, 85 ± 5 % RH (n = 5)

Results

Heat map of strawberry

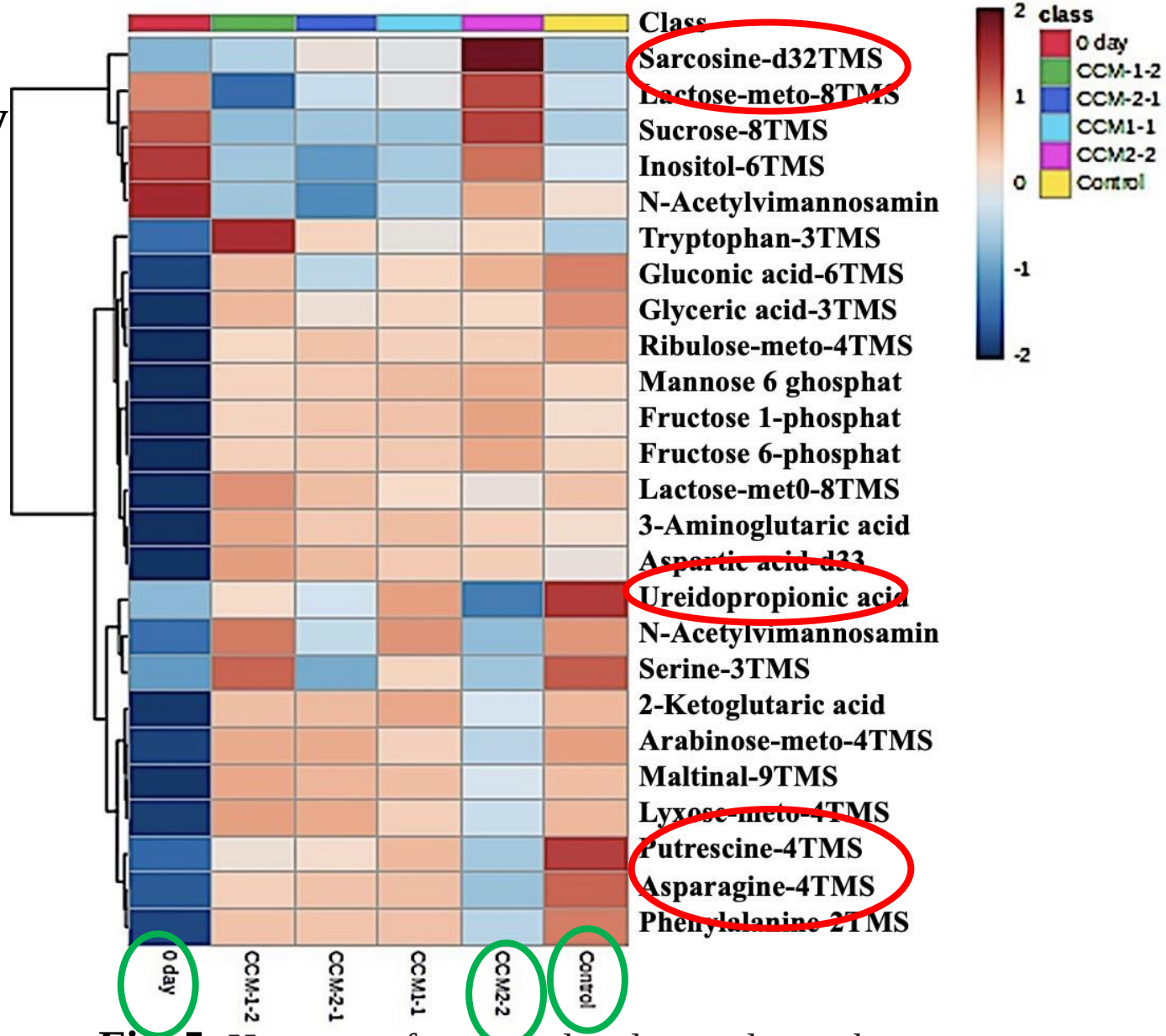

Fig. 5. Heatmap of uncoated and coated strawberry

九州大学 KYUSHU UNIVERSITY

Results

PCA score plot and biplot of strawberry

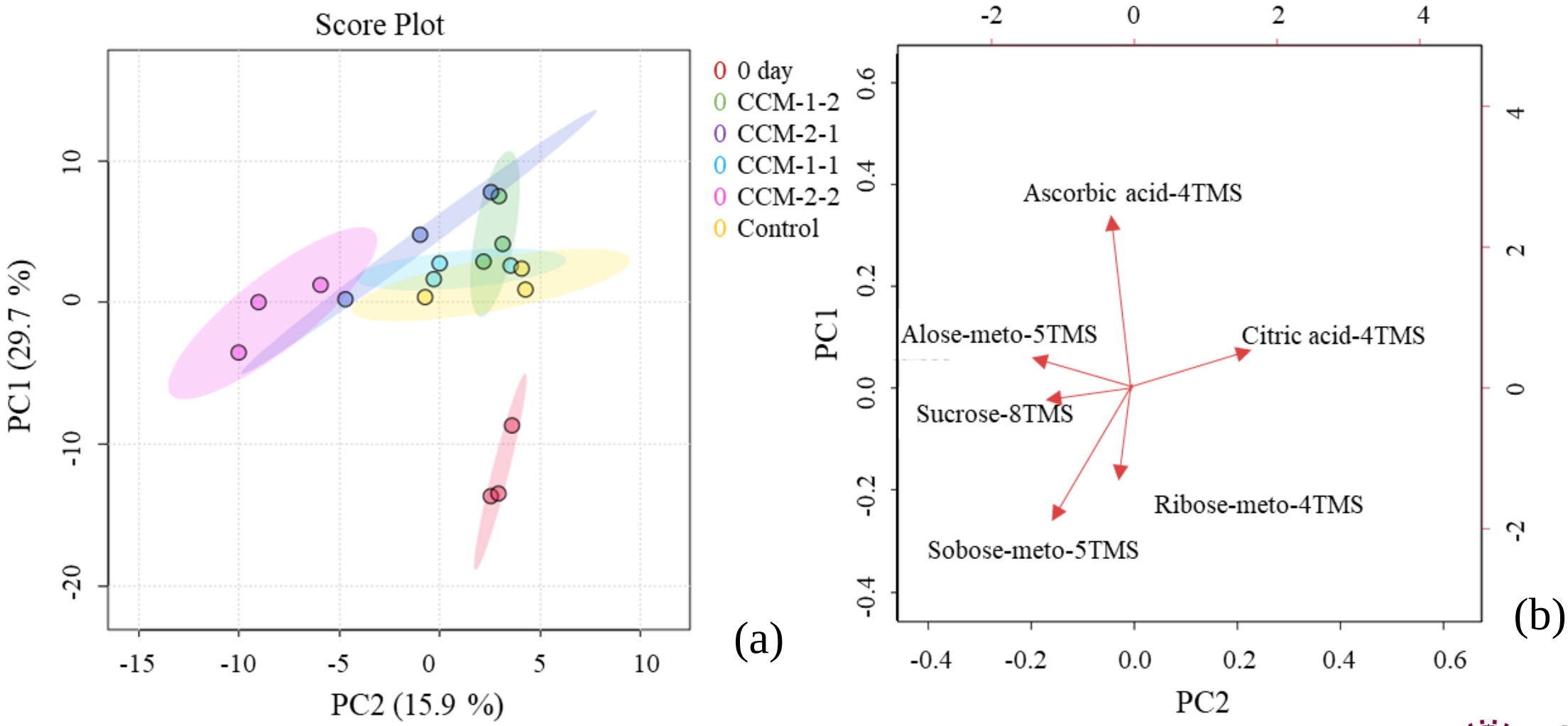

Fig. 6. PCA score plot (a), biplot (b) of uncoated and coated strawberry

Results

PLS-DA score plot (a) and important features of strawberry

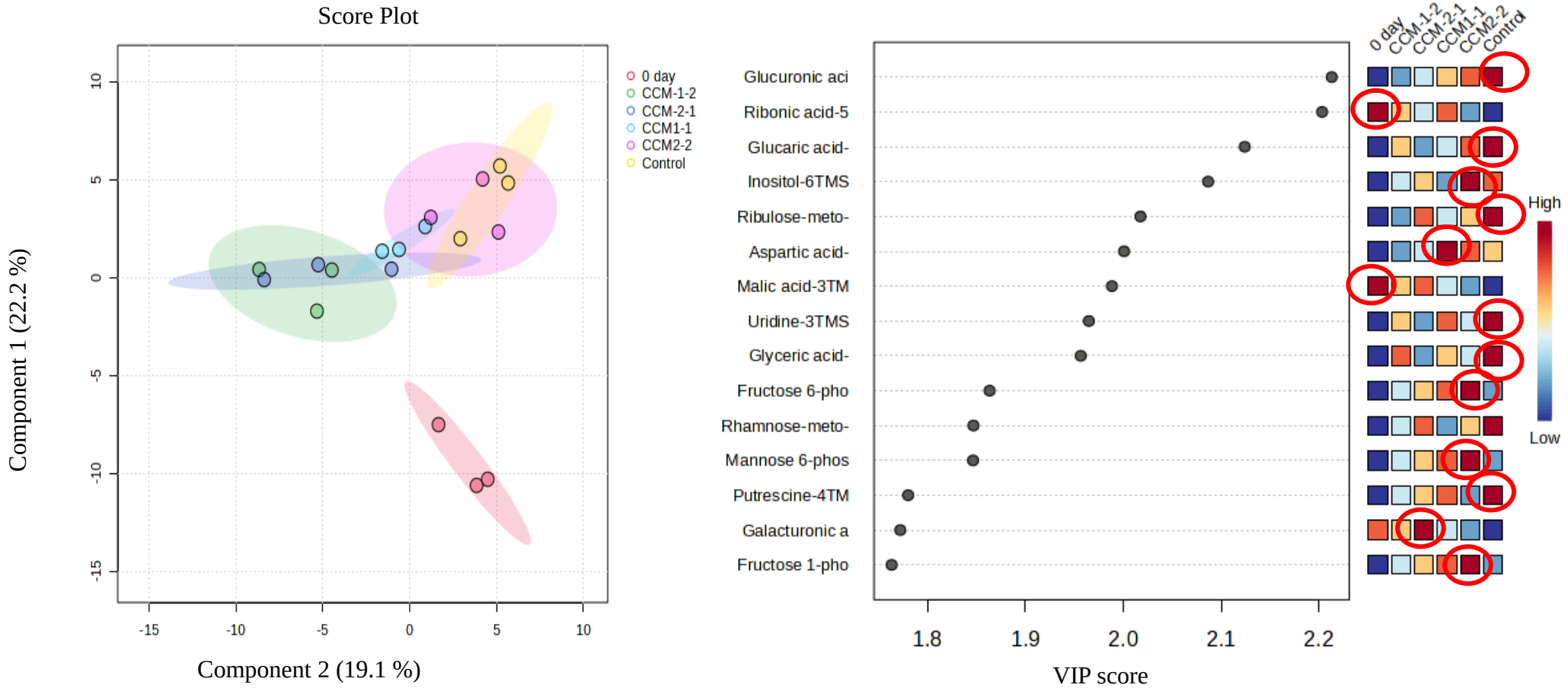

Fig. 7. PLS-DA score plot (a) and important features (b) of uncoated and coated strawberry

九州大学 KYUSHU UNIVERSITY

ELSEVIER

Food Chemistry
Volume 461, 15 December 2024, 140819

Effect of coatings containing 1-methylcyclopropane or mandarin peel extract on the freshness and metabolic profiles of cold stored strawberry

Tran Thi Van [a b], Fumina Tanaka [c], Mohammad Hamayoon Wardak [a], Jakia Sultana Jothi [a d], Nguyen Thi Hang Phuong [e], Xirui Yan [a], Artur Zdunek [f], Fumihiko Tanaka [c]

Show more

+ Add to Mendeley Share Cite

https://doi.org/10.1016/j.foodchem.2024.140819 Get rights and content

Highlights

- Diluting of 1-MCP in coatings helped to maintain the coating colour up to 50days
- Coatings containing 1-MCP showed significant absorption values in spectra peaks

Q1, IF 8.5

Conclusion

- ✓ The application of 1-MCP contributed to the preservation of the coating colour for up to 50 d.
- ✓ The addition of ME increased the Ra and Rq values, indicating that the films had a significantly rougher surface.
- ✓ Coatings enhanced with ME and/or 1-MCP maintained the post harvest freshness of strawberries by reducing weight loss and maintaining firmness, TSS, citric acid content, colour, and TPC
- ✓ Strawberries coated with CCM2-2 exhibited superior quality and metabolic outcomes

Acknowledgments

- Prof. Fumihiko Tanaka
- Asst. Prof. Fumina Tanaka
- All lab members
- Family members and friends
- The Project for Human Resource Development Scholarship (JDS)

References

1. Tran et al., (2021). Effect of edible coatings developed from chitosan incorporated with tea seed oil on Japanese pear. *Scientia Horticulturae.*
2. Van, T. T et al., (2023). Effect of edible coating incorporating sodium carboxymethyl cellulose / cellulose nanofibers and self-produced mandarin oil on strawberries. *Food Packaging and Shelf Life*.
3. Van, T. T et al., (2023). Characterization of an edible chitosan film incorporating tea seed oil/montmorillonite and antifungal activity against Botrytis cinerea. *International Journal of Food Science and Technology*.


THANK YOU
FOR YOUR ATTENTION

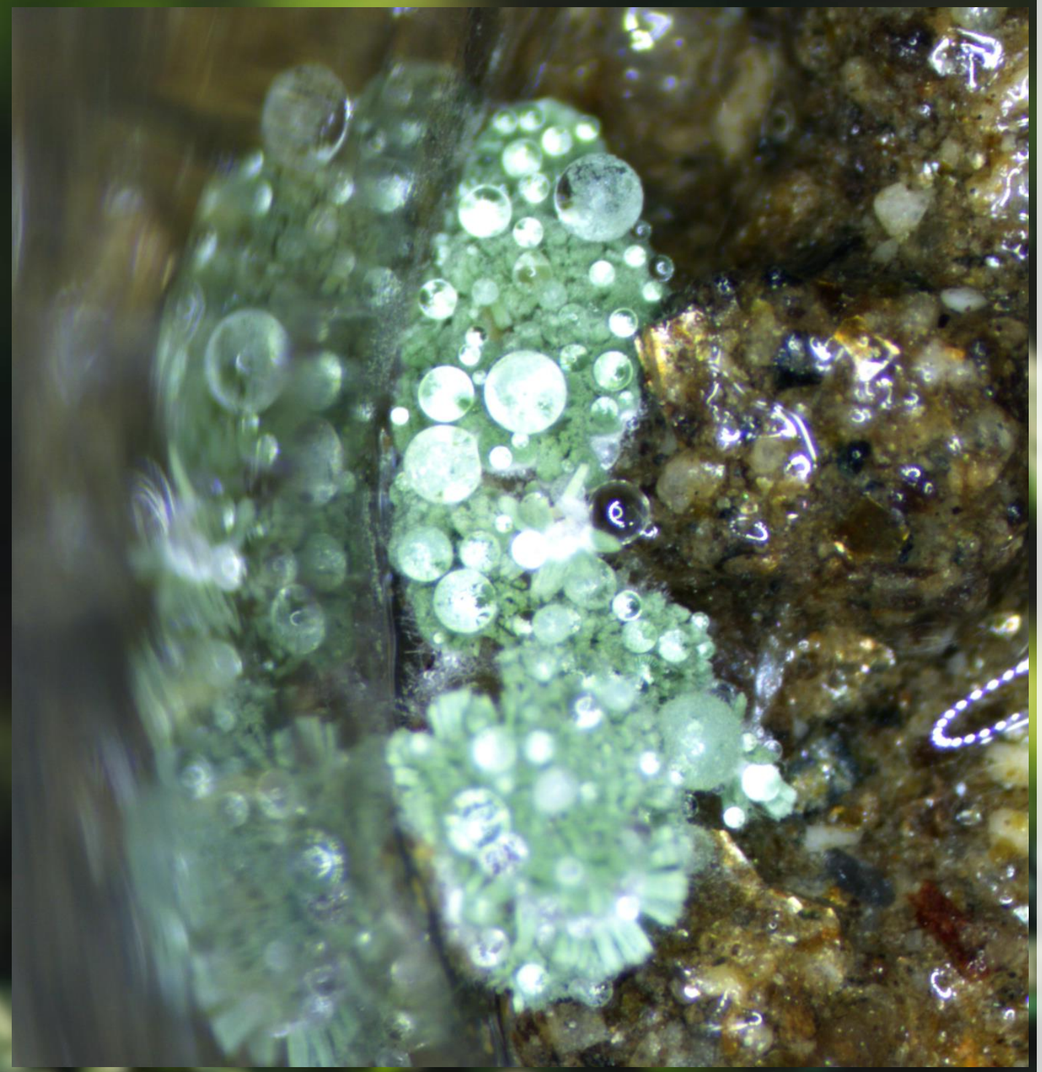

Kyushu University

DEVELOPMENT AND IMPROVEMENT OF ISOLATION METHODS FROM SOIL FOR ENTOMOPATHOGENIC FUNGI EFFECTIVE FOR THE CONTROL OF COMMON CUTWORM, SPODOPTERA LITURA

Duong Danh Thanh

Insect Pathology and Microbial control

29th November, 2024

I. Introduction

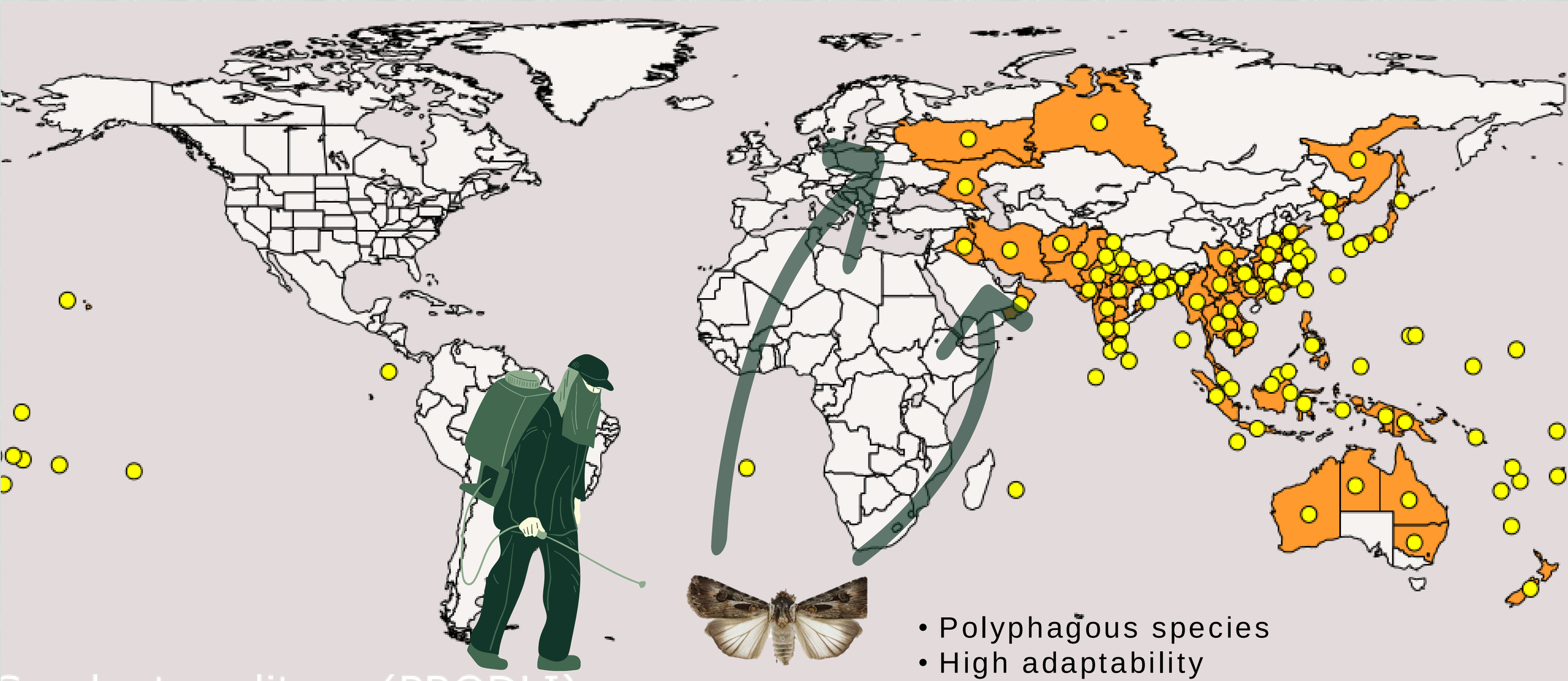

- Polyphagous species
- High adaptability

Spodoptera litura (PRODLI)

Present

2022-07-19

(c) EPPO https://gd.eppo.int

- *Metarhizium rileyi*: An entomopathogenic fungus specific to Lepidoptera (especially family Noctuids), including *Spodoptera litura*. (Fronza et al., 2017).

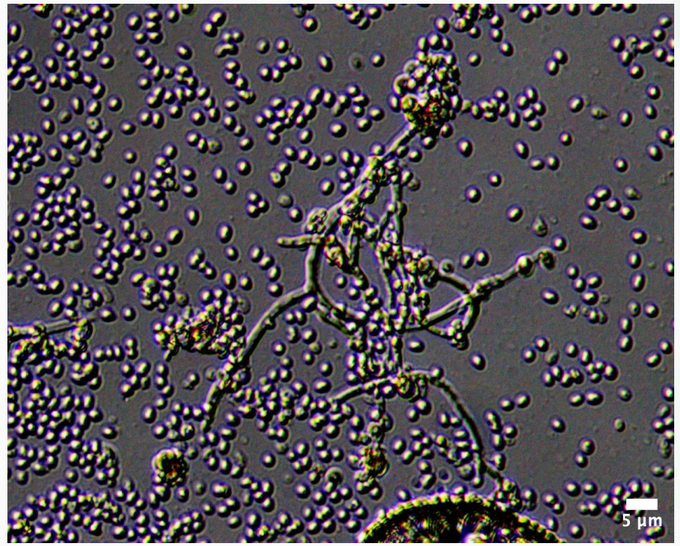

- Development and improvement of isolation methods from soil for entomopathogenic fungi.

II. OBJECTIVES

Plating method

Insect bait method

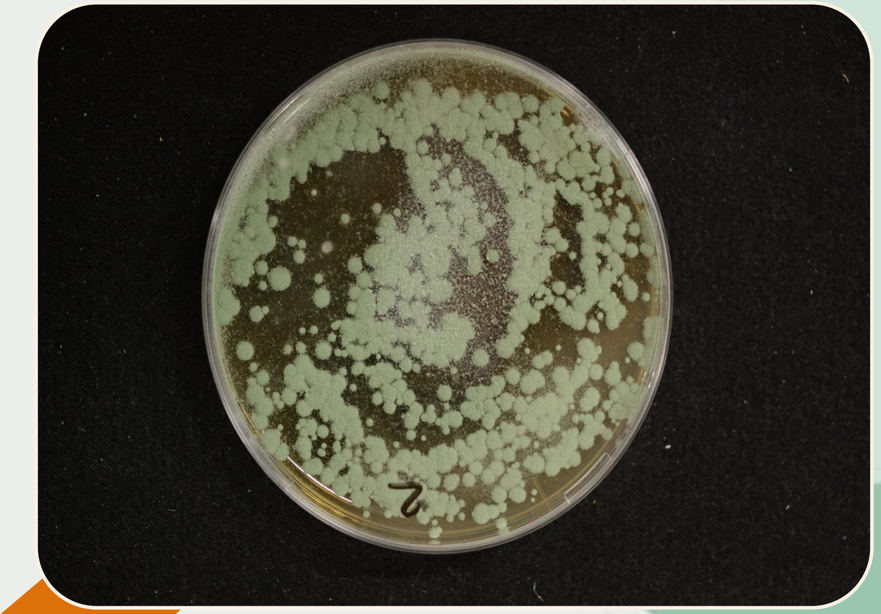

Plating method

The optimized method to isolate *M. rileyi* from natural soil

III. METHODOLOGIES

Plating method

- 5 – 9

Potential of Hydrogen (pH)

- Glucose
- Sucrose
- Maltose
- Trehalose

Carbon sources (Sugar)

Concentration of fungicides

- Cycloheximides
- Copper chlorides
- Dodine
- Validacin
- Sumilex

Insect-associated additives

- Insect hemolymph
- Insect cuticule
- Grace’s insect media

➤ Calculate the detection limit of the optimized agar media by using the artificially contaminated soil.

III. METHODOLOGIES

Plating method

Fungal suspension solution or artificially contaminated soil with a suitable concentration

- 1 x 10^6
- 1 x 10^7 - 1 x 10^1
- 1 x 10^1

The selective medium

- Potential of Hydrogen (pH)
- Carbon sources (Sugar)
- Fungicides
- Insect-associated additives

- The diameter of the colonies.
- The number of conidia per cm^2.

- The diameter of the colony
- The number of colonies (Natural soil and artificially contaminated soil).
- Colony formation rate

IV. RESULTS

Potential of Hydrogen (pH)

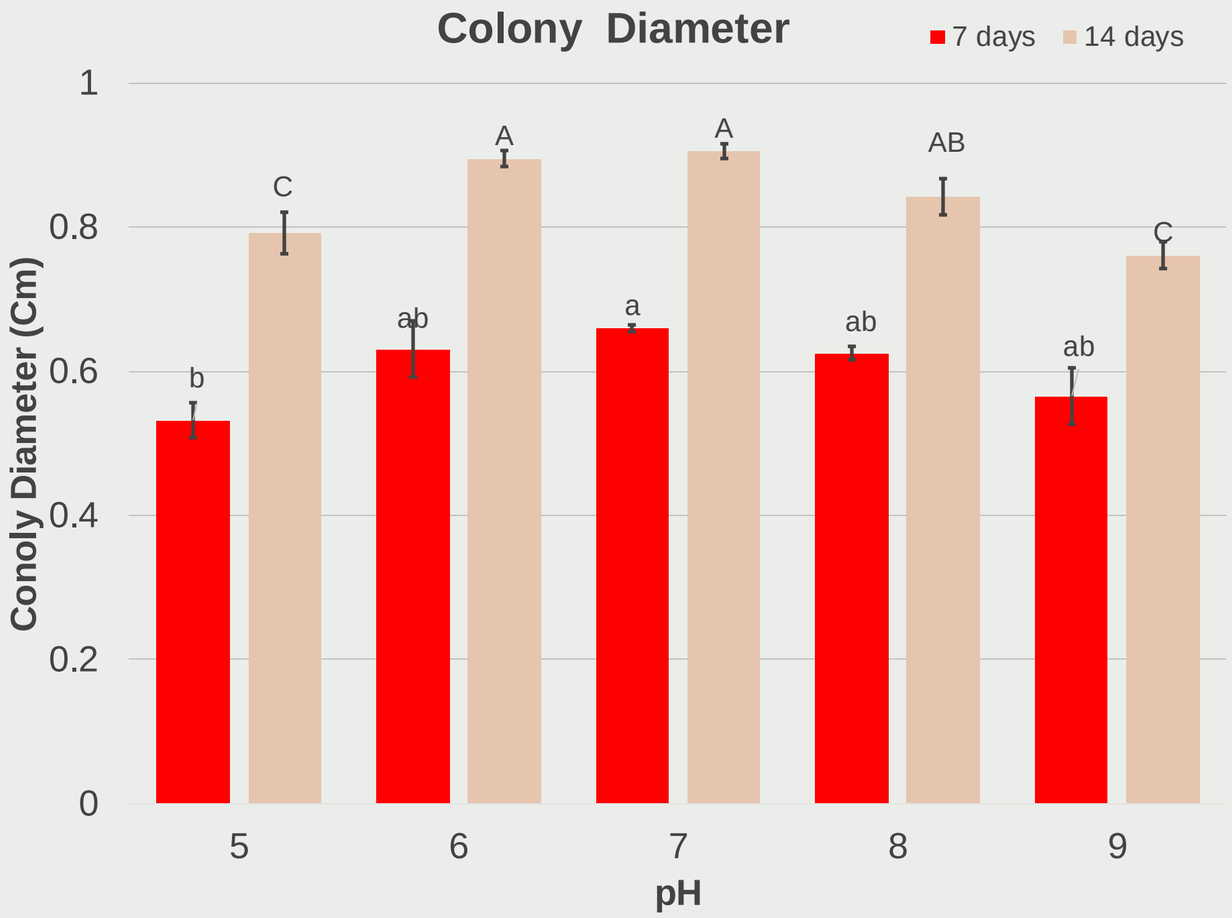

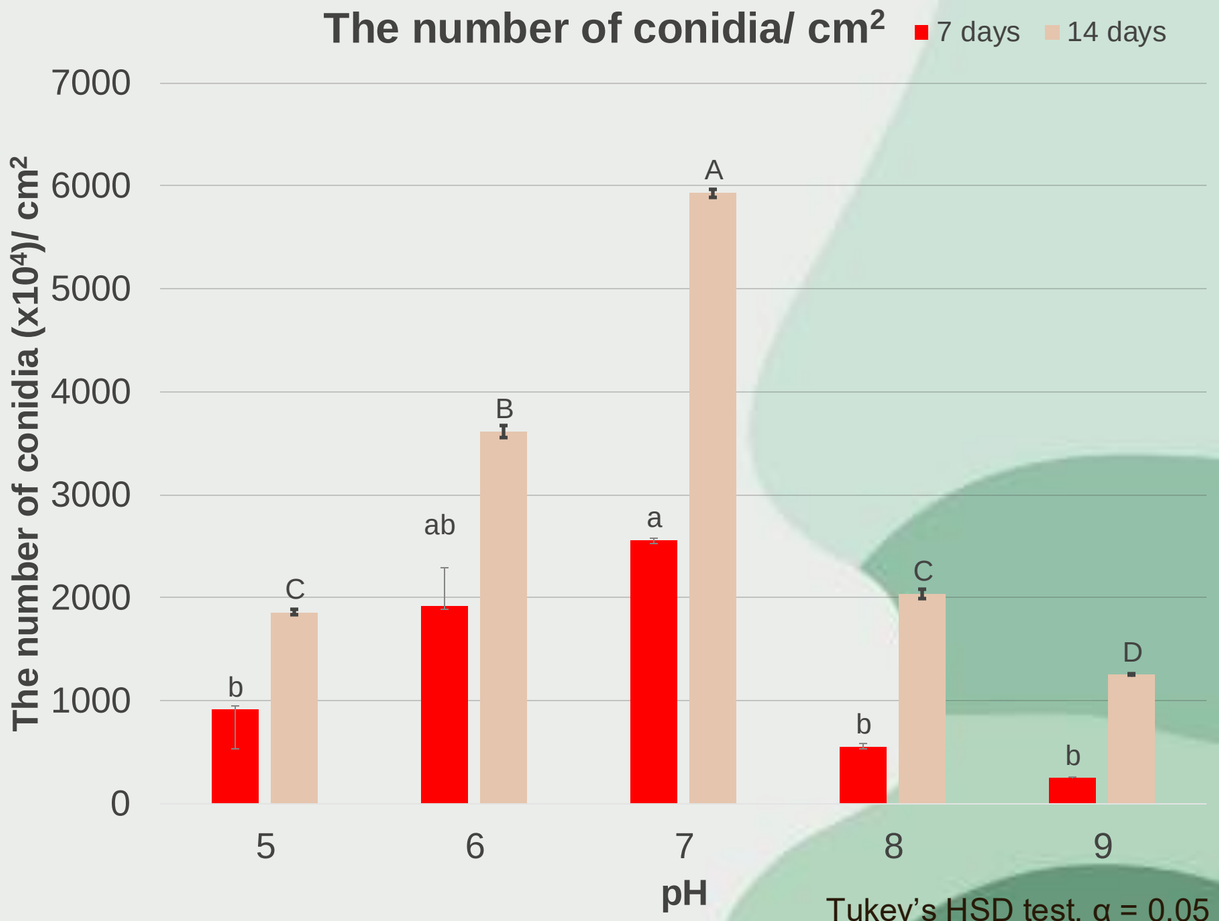

Tukey's HSD test, α = 0.05

pH7 is the best for both colony growth and conidial production

IV. RESULTS

Type of Carbon sources (Sugar)

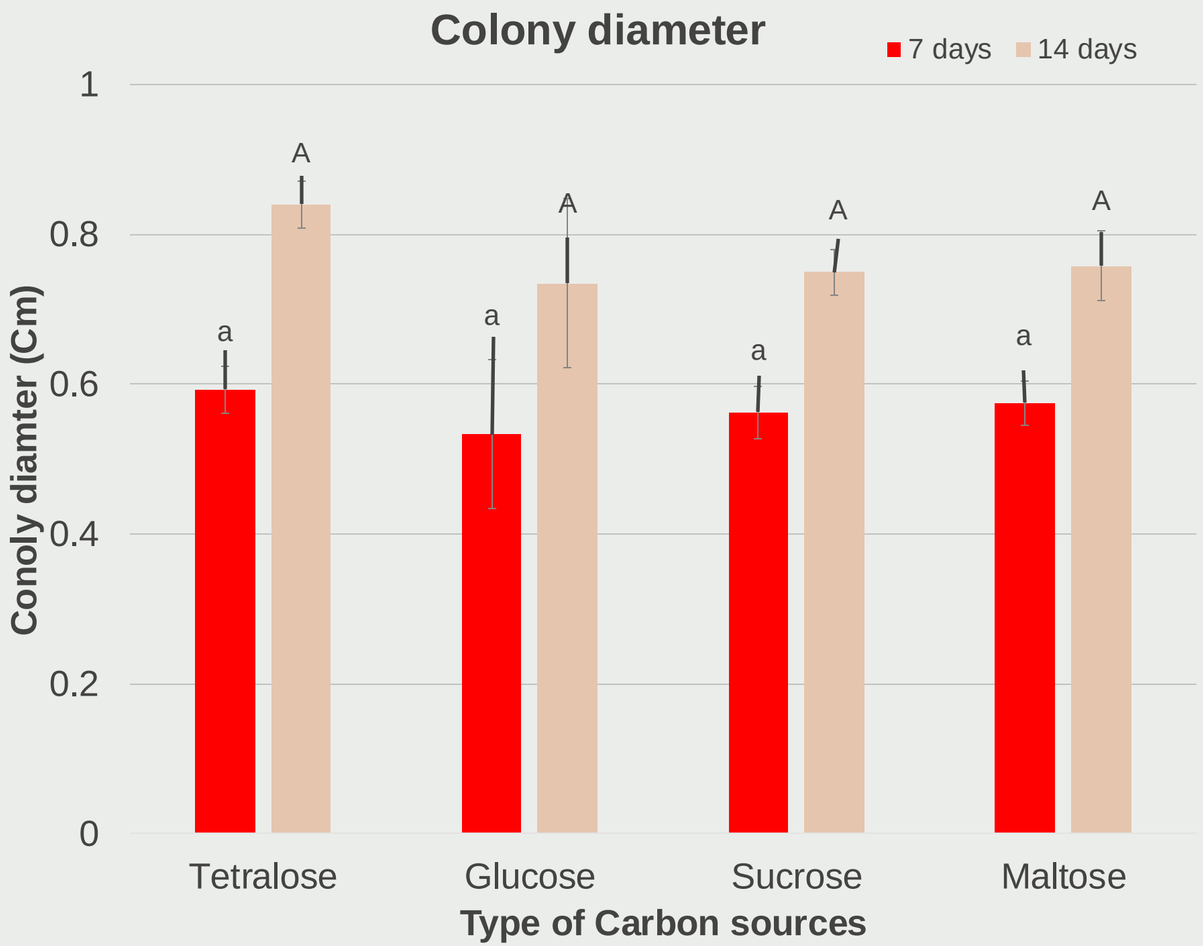

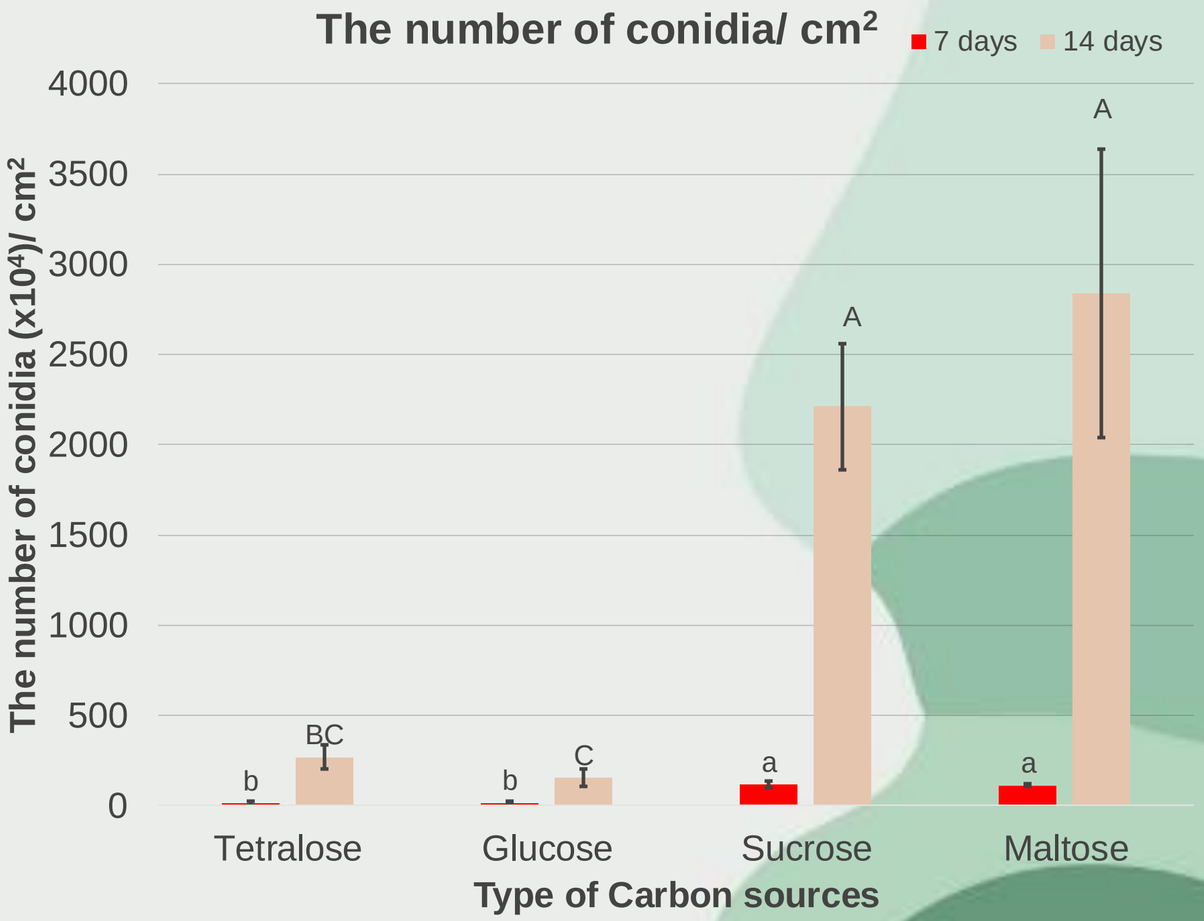

Tukey's HSD test, α = 0.05

Maltose is the best for conidial production

IV. RESULTS

Concentration of Carbon sources (Sugar)

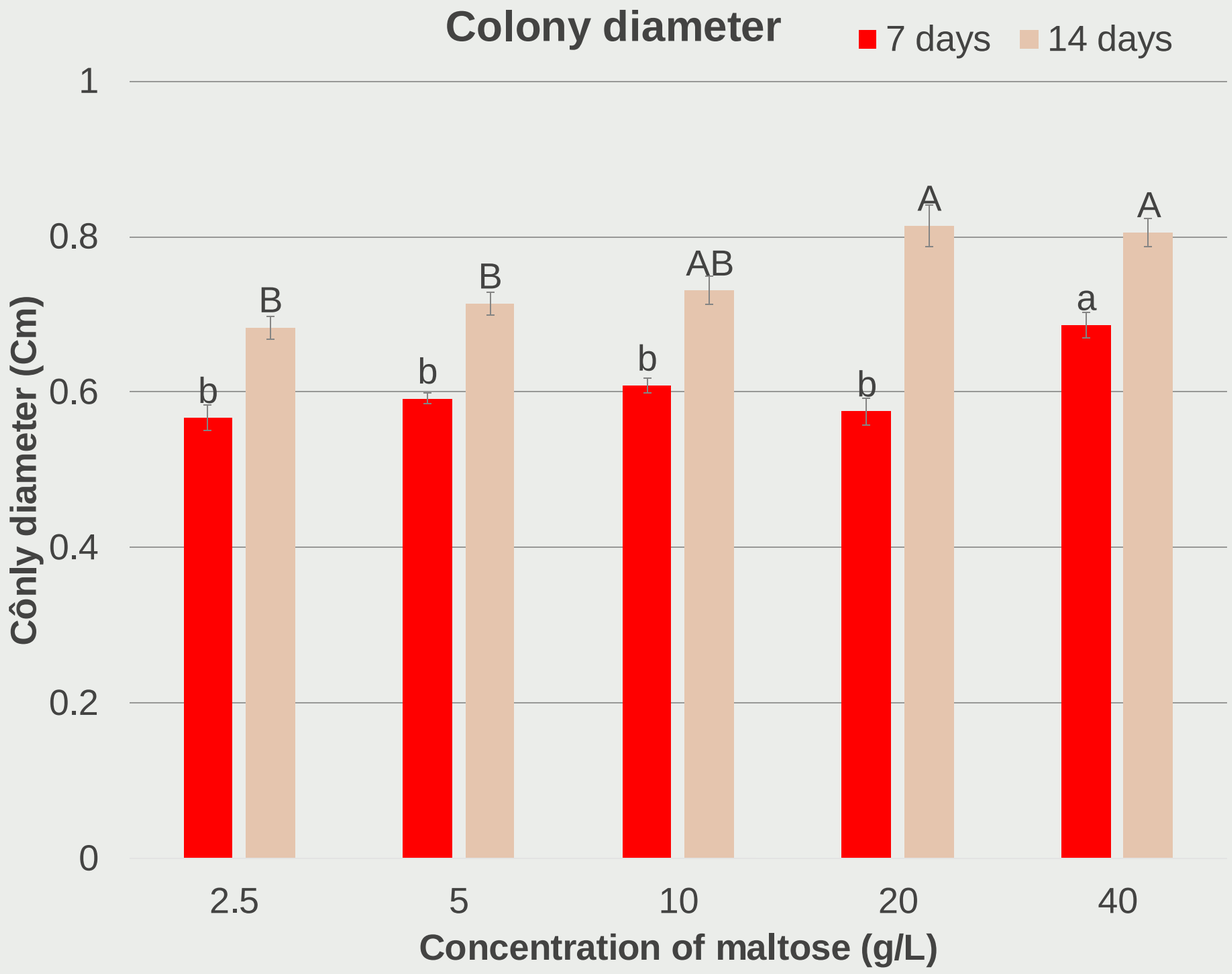

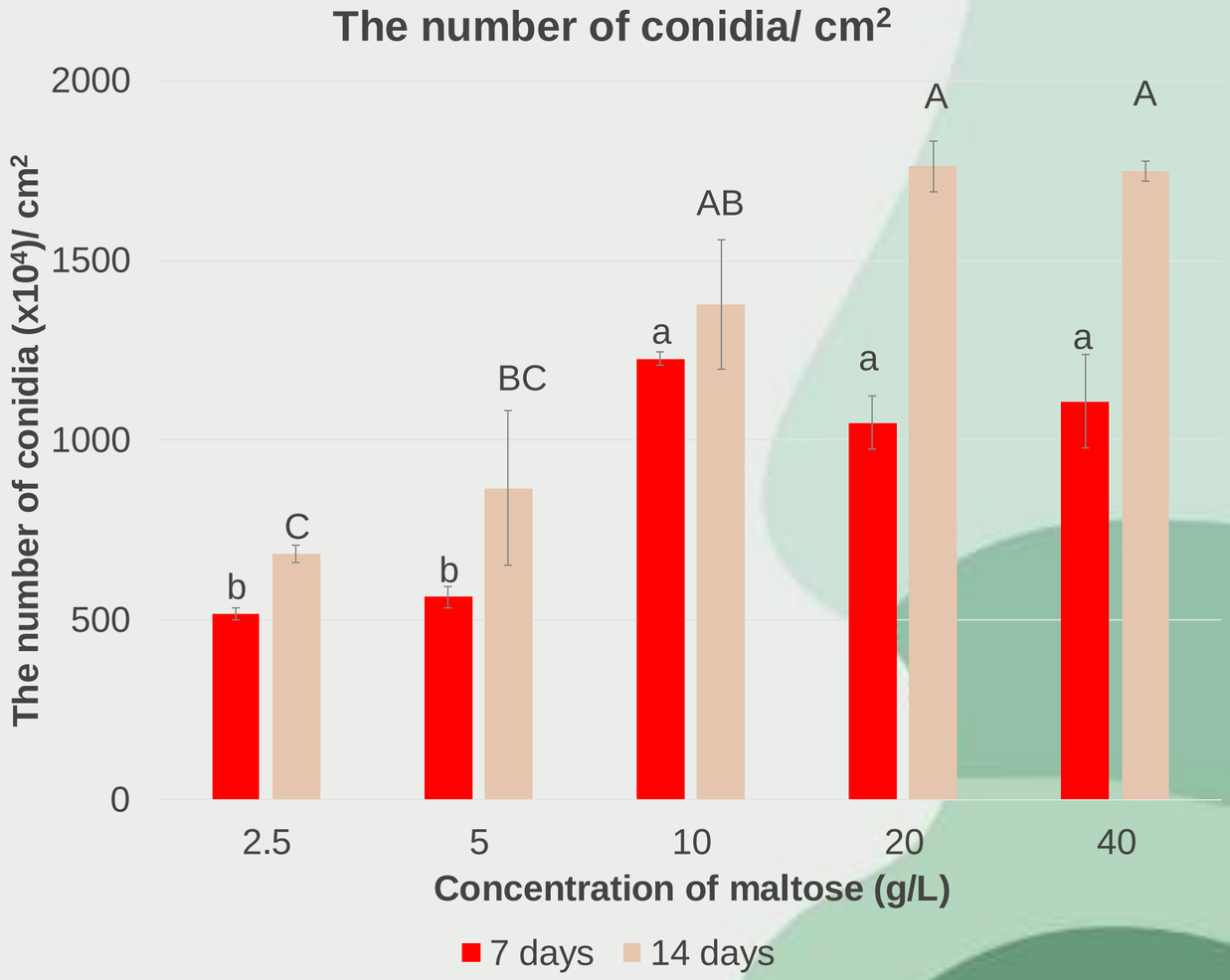

Tukey's HSD test, α = 0.05

20 g/L of Maltose is the best for both colony growth and conidial production

IV. RESULTS

Effect of fungicides on colony growth of *M. rileyi*

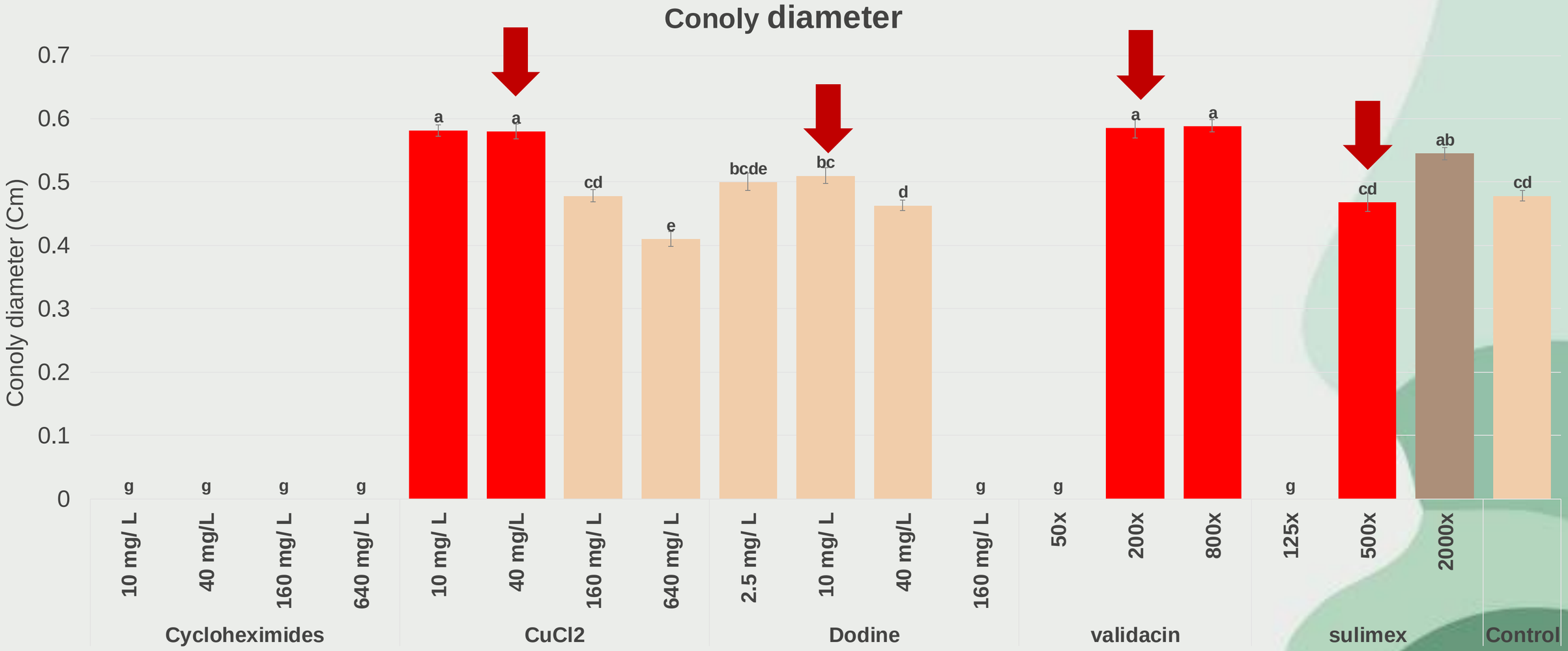

Tukey's HSD test, α = 0.05

$CuCl_2$ (40 mg/L), Dodine (10 mg/L), Validacin (200 times dilution), Sumilex (500 times dilution) could be used in selective media

IV. RESULTS

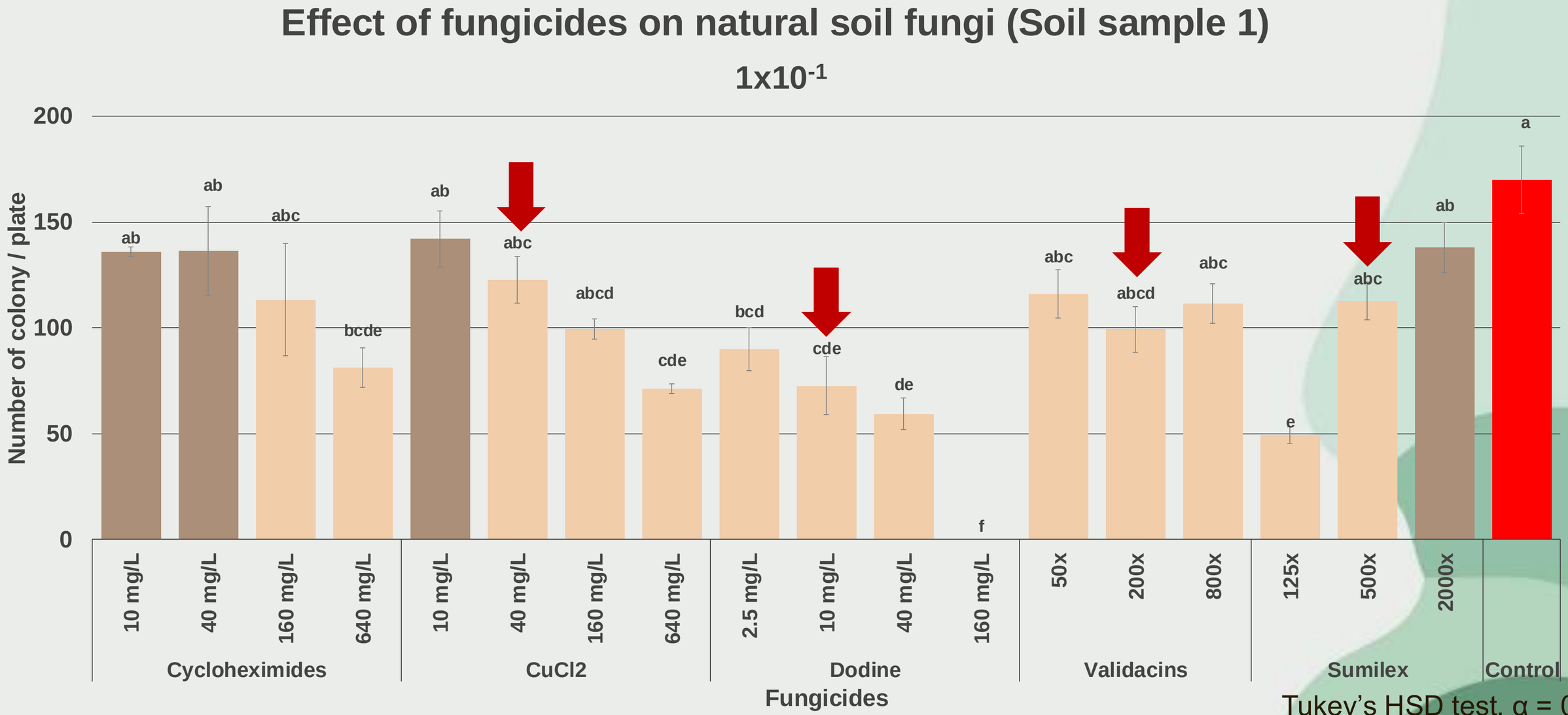

Tukey's HSD test, α = 0.05

$CuCl_2$, Dodine, Validacin, Sumilex at concentrations that did not inhibit *M. rileyi* colony growth inhibited colony formation of natural soil fungus

IV. RESULTS

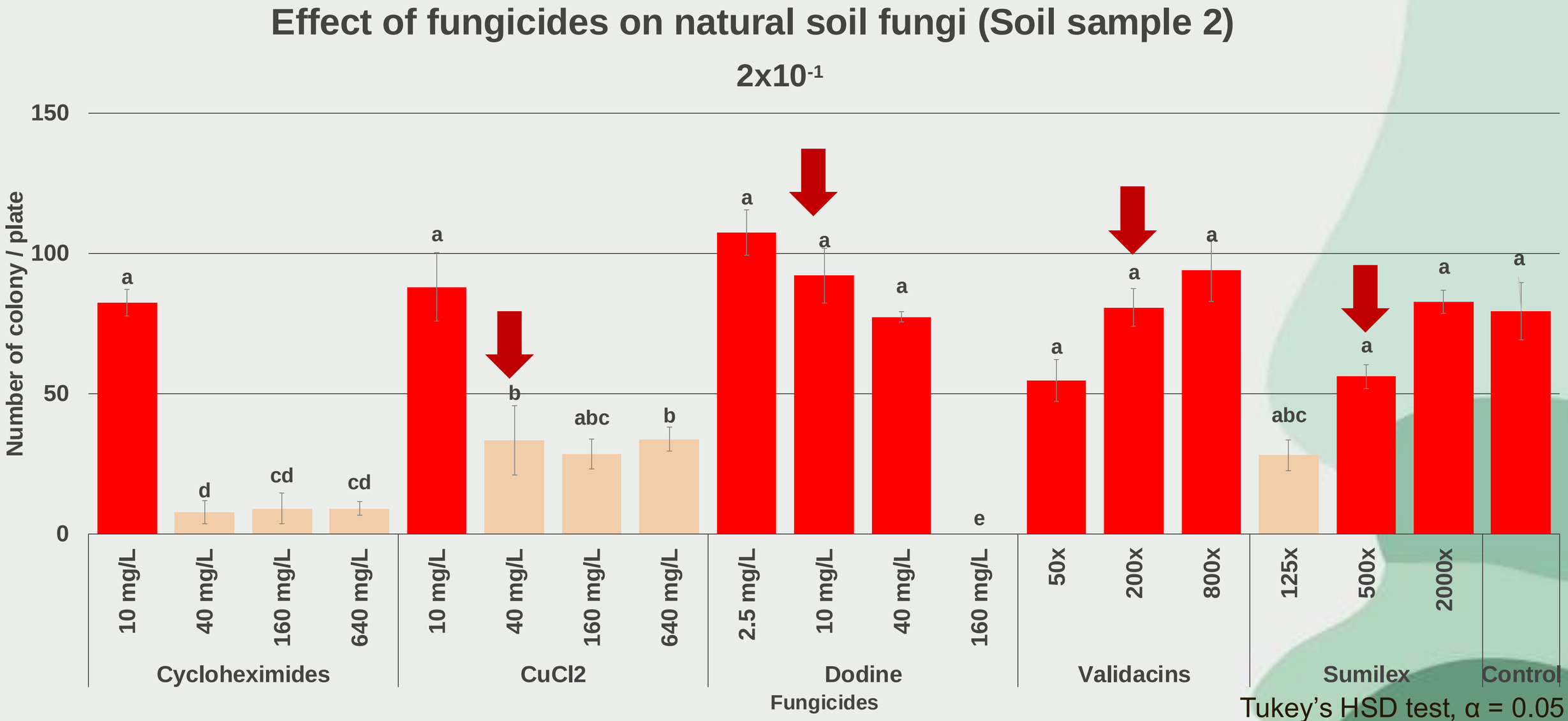

Tukey's HSD test, α = 0.05

$CuCl_2$, Dodine, Validacin, Sumilex at concentrations that did not inhibit *M. rileyi* colony growth inhibited colony formation of natural soil fungus

IV. RESULTS

Effect of fungicides on natural soil fungi (Soil sample 3)

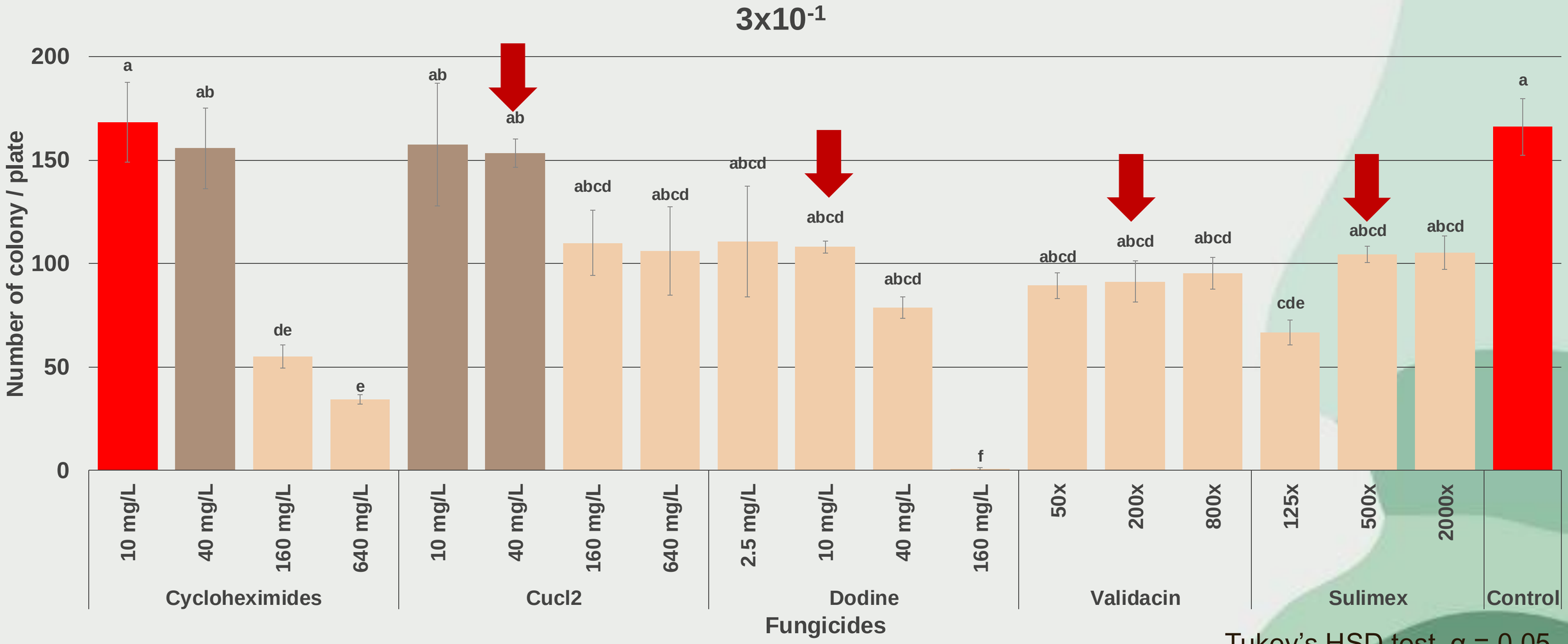

Tukey's HSD test, α = 0.05

$CuCl_2$, Dodine, Validacin, Sumilex at concentrations that did not inhibit *M. rileyi* colony growth inhibited colony formation of natural soil fungus

IV. RESULTS

Effect of fungicides on colony formation rate of *M. rileyi*

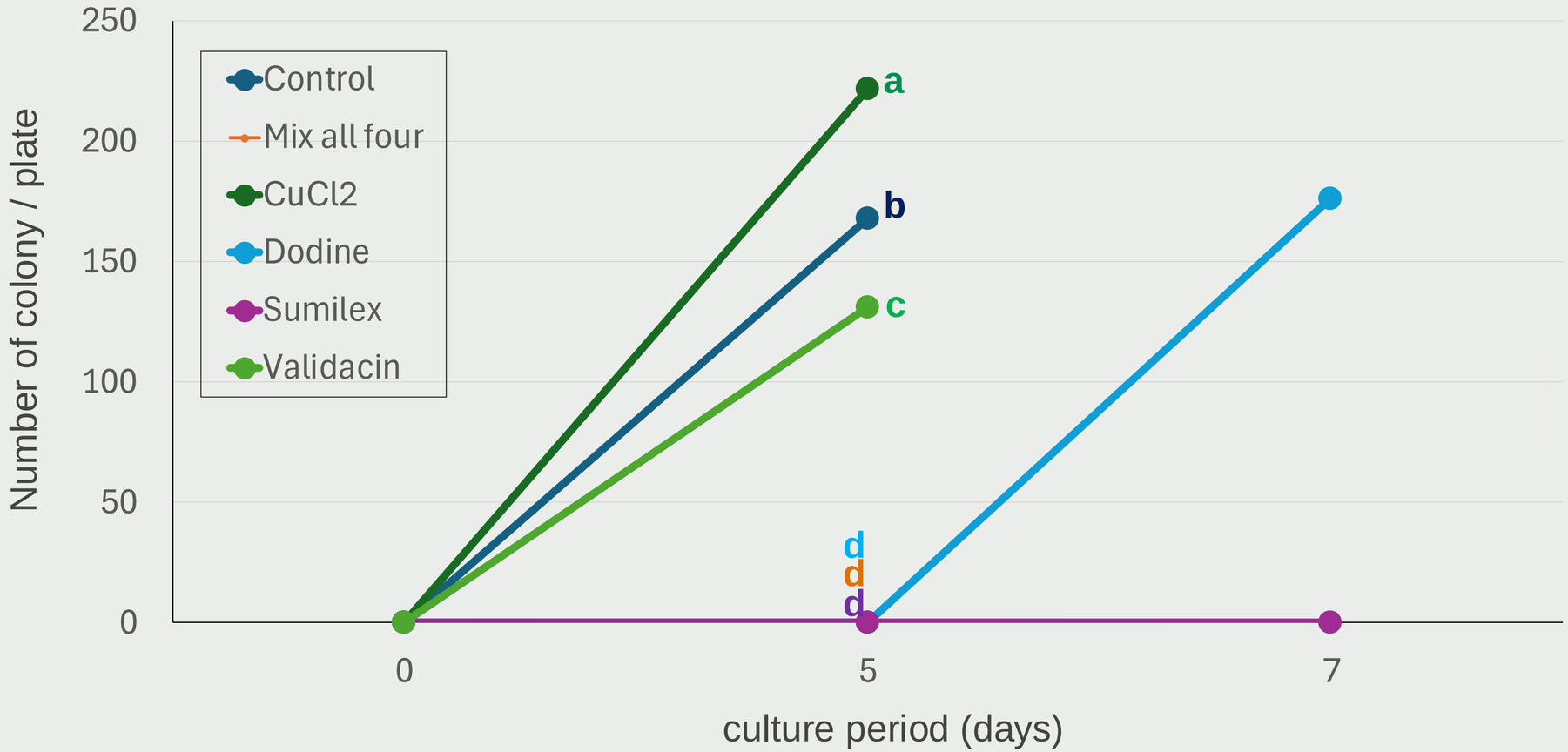

Tukey's HSD test, α = 0.05

$CuCl_2$ and Validacin at concentrations that did not inhibit *M. rileyi* colony growth had relatively small negative effects on colony formation rates

IV. RESULTS

Effect of fungicides mix on colony formation rate of *M. rileyi*

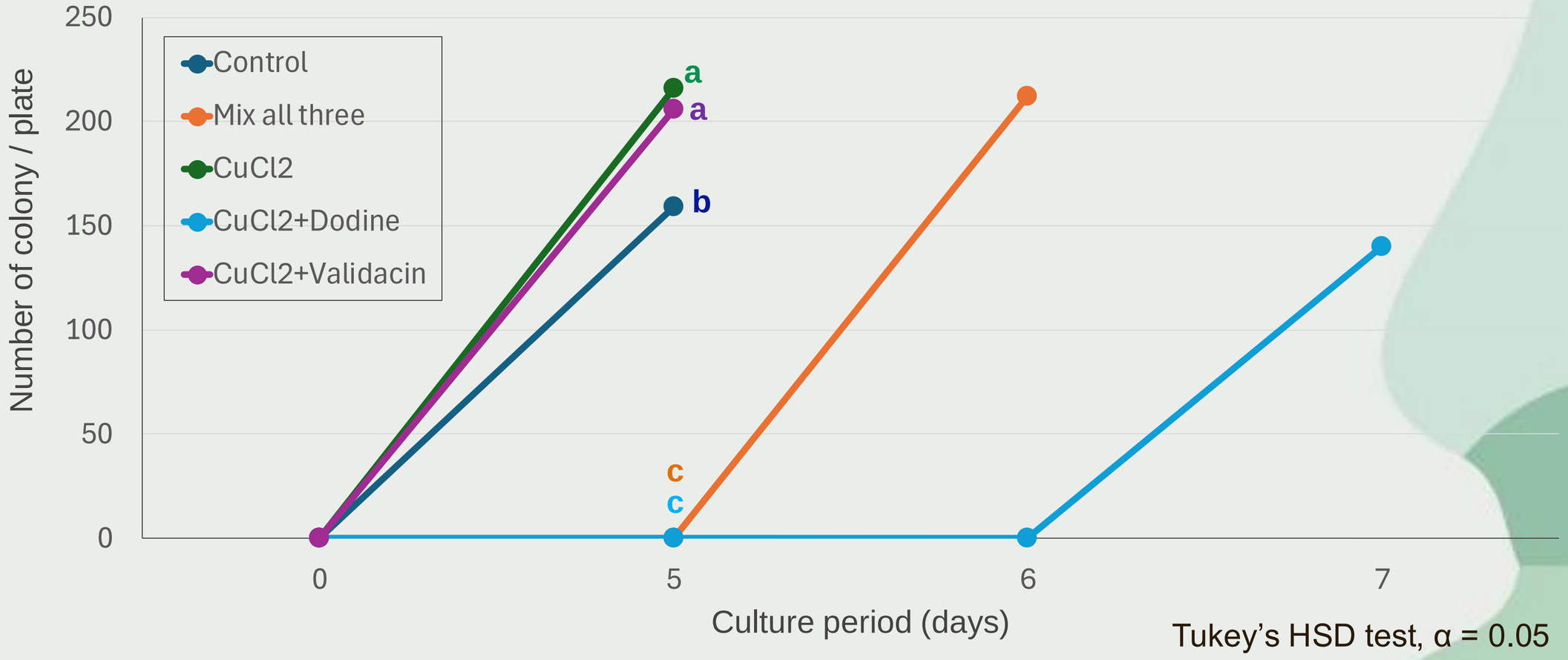

Mix of $CuCl_2$ and Validacin at concentrations that did not inhibit *M. rileyi* colony growth had relatively small negative effects on colony formation rates

IV. RESULTS

Effect of insect-associated additives (pupa powder) on colony formation of *M. rileyi*

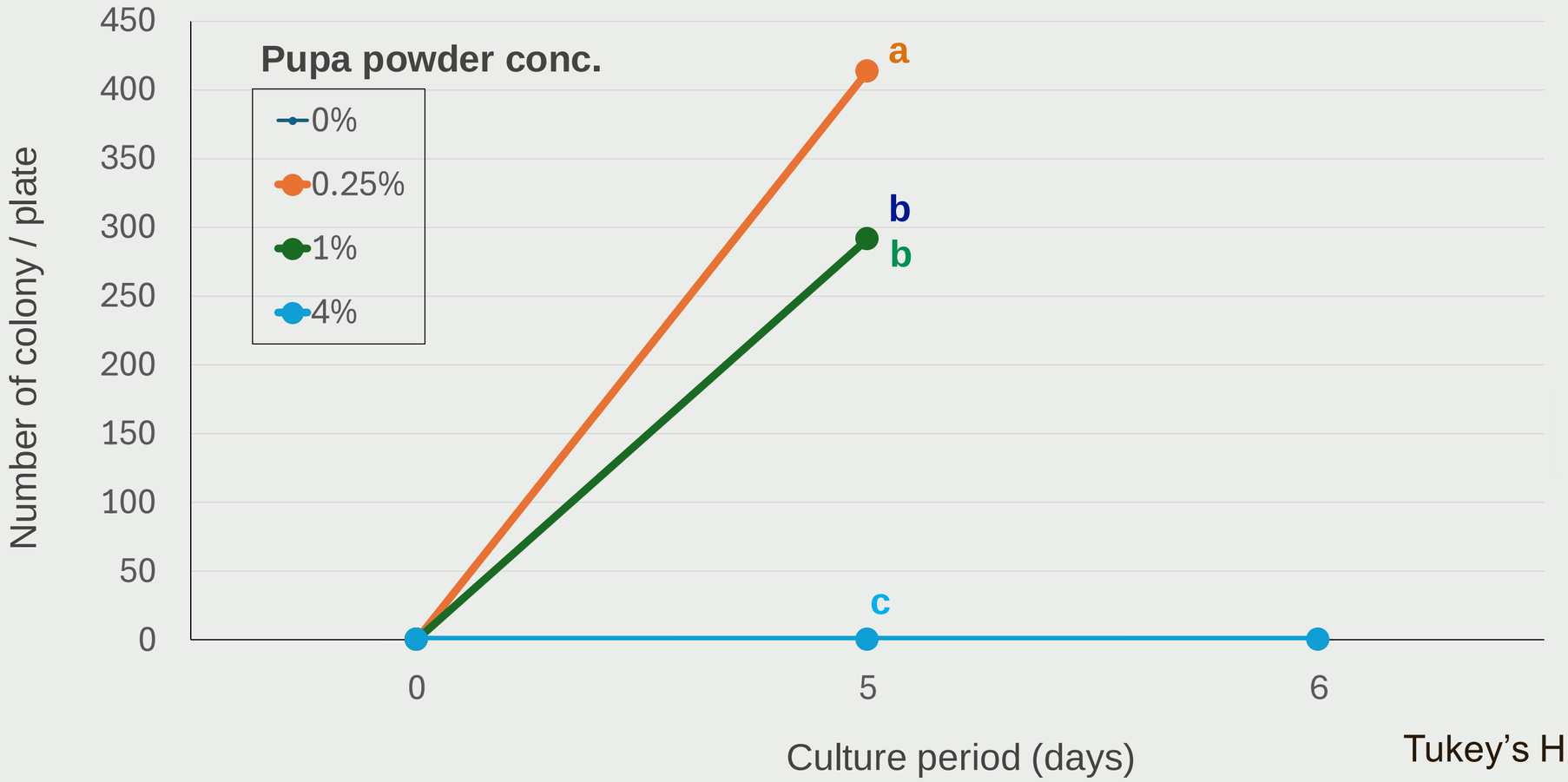

Tukey's HSD test, α = 0.05

<u>0.25% cuticle powder</u> significantly increased the colony formation number

Further concentration optimization is needed

IV. RESULTS

Effect of insect-associated additives (Grace's medium) on colony formation rate of *M. rileyi*

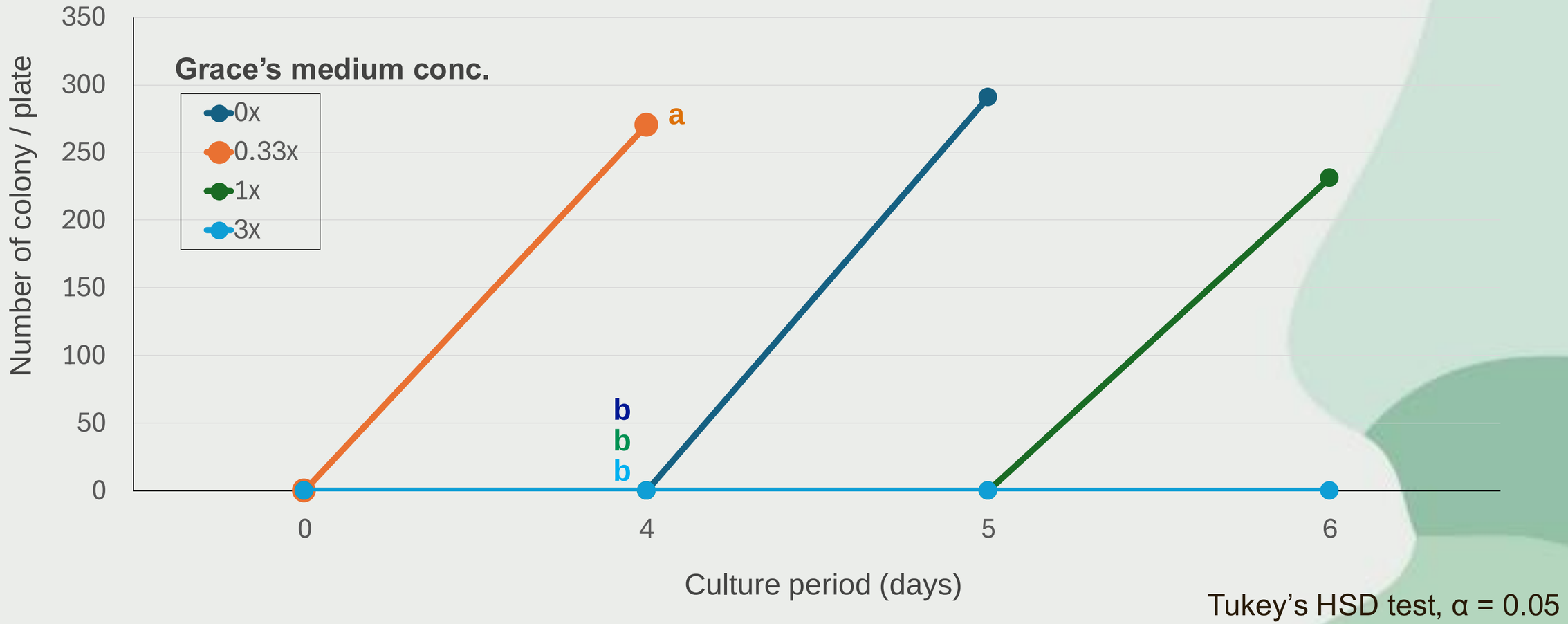

Tukey's HSD test, α = 0.05

0.33x Grace's medium promoted the colony formation rate

Further concentration optimization is needed

IV. Result

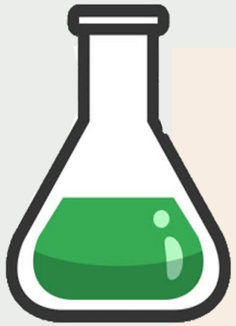

SSYA media:

- 20g Sucrose
- 10g Pepton
- 10g Dried yeast extract
- 15g Agar
- 0.1g Chloramphenicol

Optimized SSYA media:

- pH: 7
- 20g Maltose
- 10g Pepton
- 10g Dried yeast extract
- 15g Agar
- 0.1g Chloramphenicol
- Copper chlorides: 40mg/ L + Validacin: 200 times dilution (Copper chlorides: 40mg/ L + Validacin: 200 times dilution + Dodine: 10g/ L)
- Insect cuticle 0.25% (Grace’s Insect 0.33X).

Thank you for your attention

HOW DO WE MOVE FORWARD REGARDING THE FOREST AND BIODIVERSITY CRISES IN ASIA? VIETNAM AND BEYOND.

Thorkil Casse, Roskilde University (Denmark) and Kyushu University

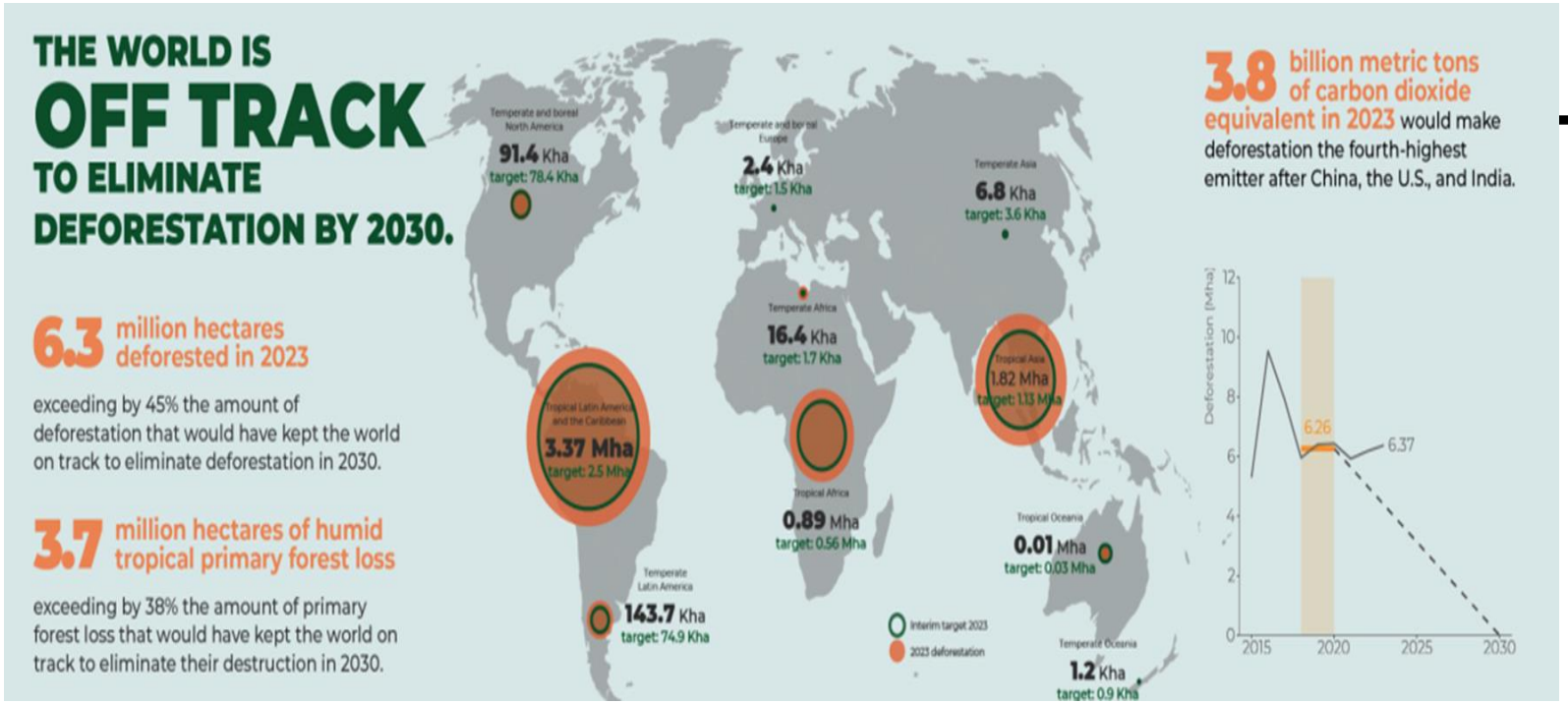

Nearly 96% of all deforestation in 2023 took place in tropical countries. Worse in Latin America, second in south-east Asia, Forest Declaration Assessment Partners. (2024). Forests under fire: Tracking progress on 2030 forest goals.

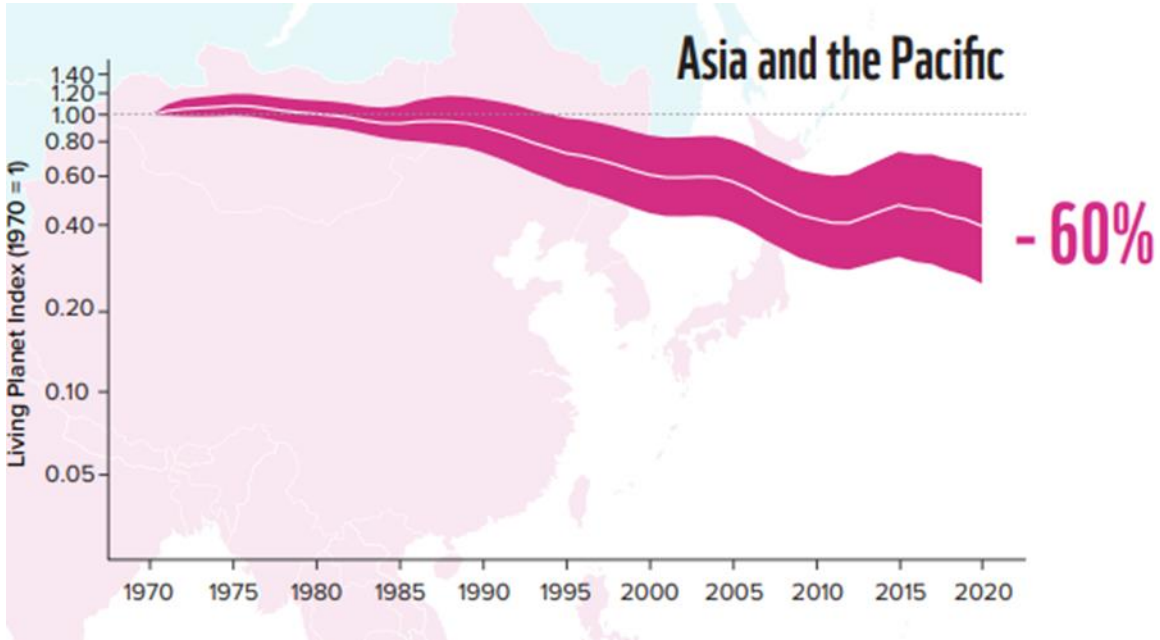

The living planet monitors 35,000 populations of 5,500 vertebrate species, WWF (2024 Living Planet Report). Asia comes second again in aggregated accumulation of biodiversity loss. Only pushed down the negative ranking list by Latin America.

A basic question is why after 50 years of discussion on how to halt global deforestation, we have not yet been able to move on. In the first article, we zoom in on Vietnam and in the second article we zoom out to the global level.

In a draft article, we (Do Thi Nhinh, Ton Ta Viet and myself) with the aim to assess the management of national parks claim that establishment of national parks at two locations in Vietnam marked a turning point in the relationship between park managers and local people. State officials seem to have gained momentum through ensuring the exclusive control of natural resources.

Under certain conditions, the creation of national parks, can backfire , resulting in less income for local people, increasing deforestation and loss of biodiversity. Lack of time series of data at a disaggregated level required a different approach. The only solution is to trace down changes over time by use of local perceptions, storytelling and photos. A- showing a house of one of the households, B- showing the house of a forest manager's parents using timber from an illegal forest species (pơ mu).

Analysing biodiversity trends over time is even more challenging. We adopted an approach to pretend to appear as potential clients of wild meat collected in the national park.

Figure 7 : Wild meat product and a caged wild boar, Yok Đôn National Park

In a second article, not yet written, we ask the question at the global scale whether there are barriers to effective creation and use of research in policy and practice. Possible explanations:

1) Researchers have formulated ideas or policy advice, but internal power struggles in government circles often prevent translation of ideas into practical policies.
2) Researchers tend to formulate very general ideas that are not likely to translate into concrete actions.
3) Research ideas are often pure technical and fail to include substantial socio-economic concerns.

In other words, forest policies are meant to demonstrate Support but ultimately set up to fail, or forest policies are not set up to fail but often fail because of weak enforcement or lack of institutional capacity and funding.

A comparative study of forest policies in Vietnam, Indonesia Argentina, Brazil and the US.

The potential of AI application in agricultural economics research-revenue and labor employment optimization with simulation

○Hisako Nomura, Junyi Qi, Tianyu SONG, Tadashige Iwao
hnomura@agr.Kyushu-u.ac.jp

KYUSHU UNIVERSITY

Contents

1. AI x Economics

The number of publications is increasing.

Keyword: machine learning & economic analysis

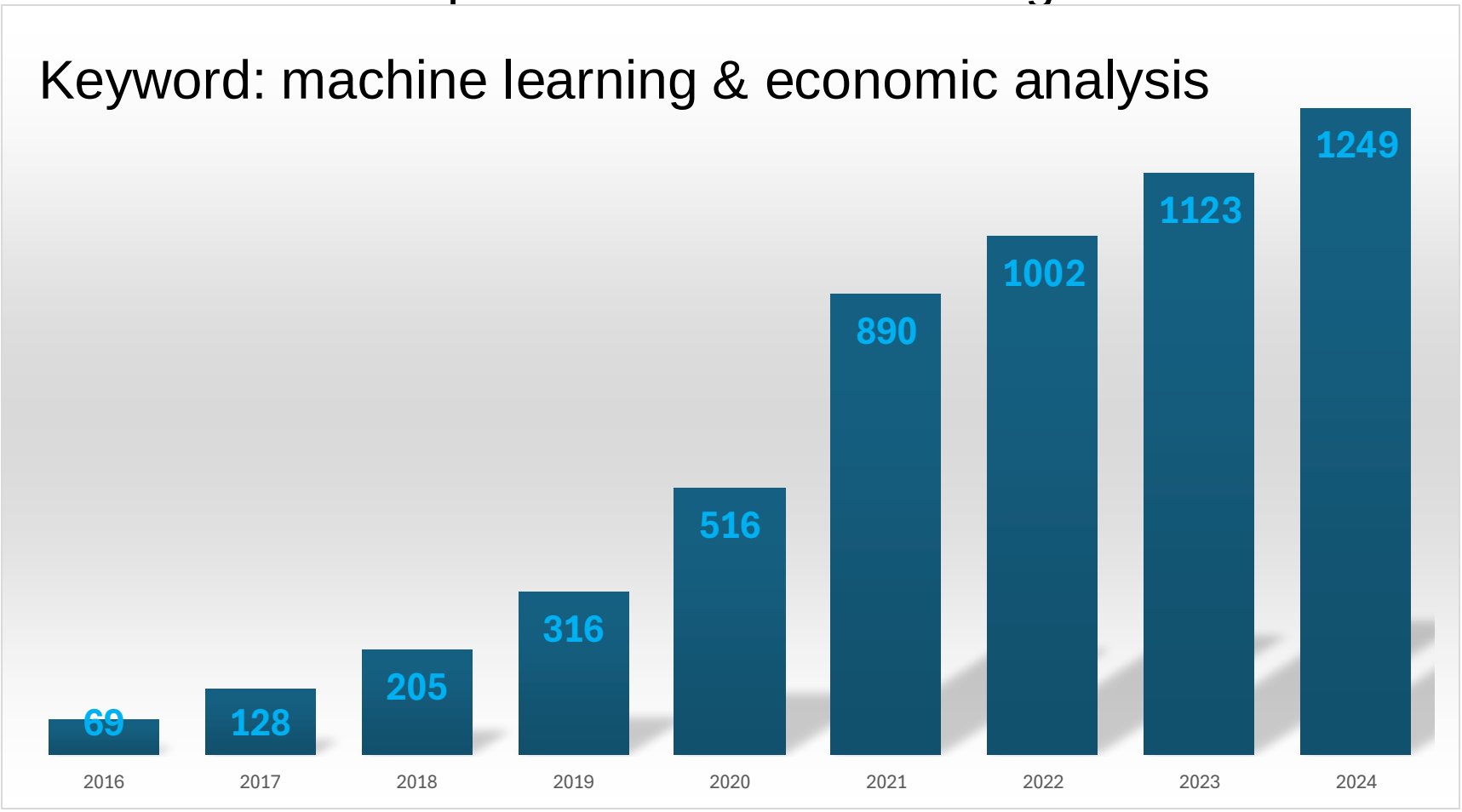

Web of Science (20024)

1. AI x Agricultural Economics

This research area has the potential to increase.

Keyword: machine learning & economic analysis & agriculture

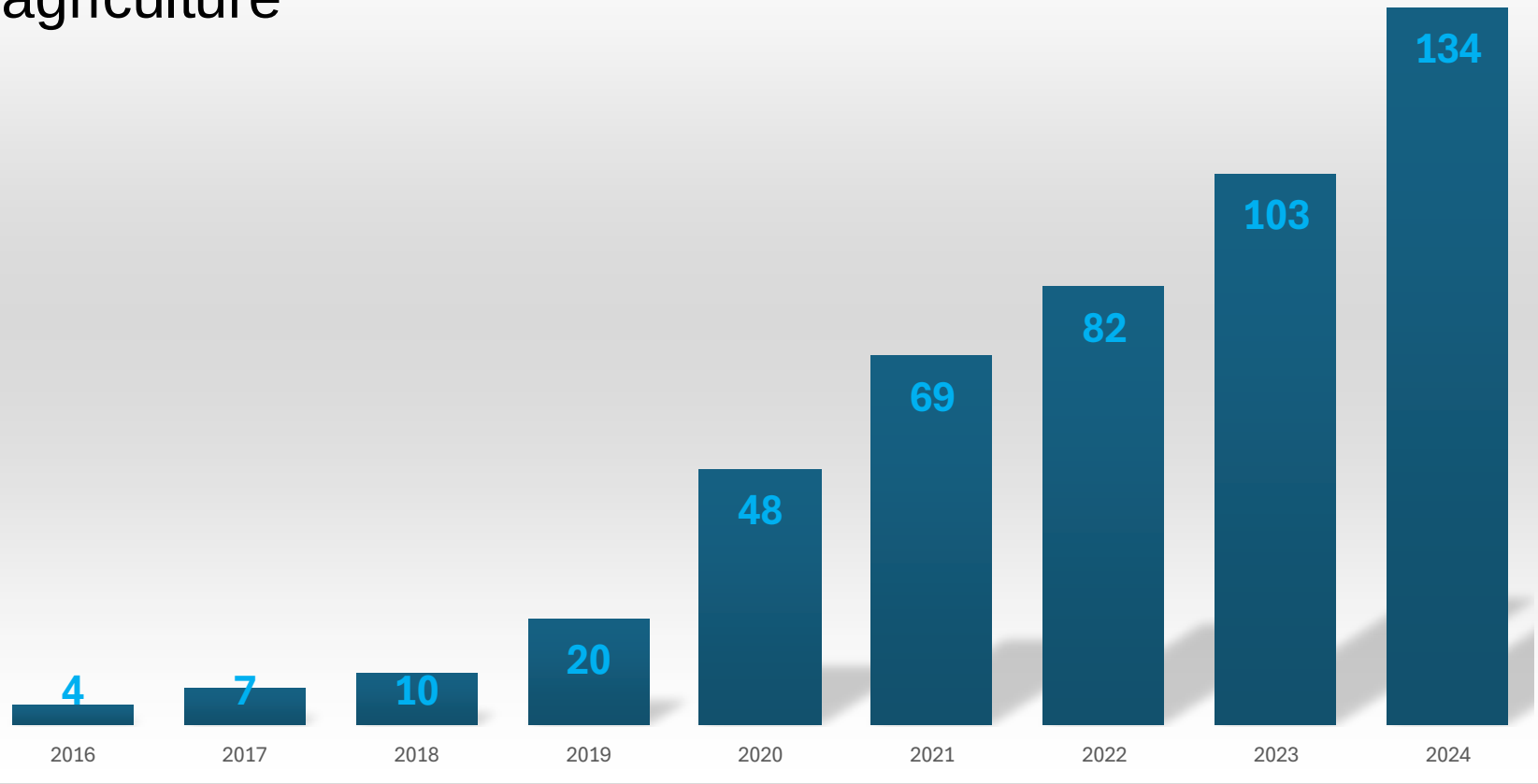

Web of Science (20024)

2. Introduction

Smart Agriculture does not only refer to the use of advanced technologies but also data analytics and innovative practices to optimize agricultural production, improve efficiency, and minimize environmental impact.

Studying smart agriculture under the Sustainable Development Goals (SDGs) is crucial because it aligns directly with several key global objectives to foster sustainability, improve food security, and address environmental challenges.

2. IoP project in Kochi prefecture 2020-2030 SAWACHI Application

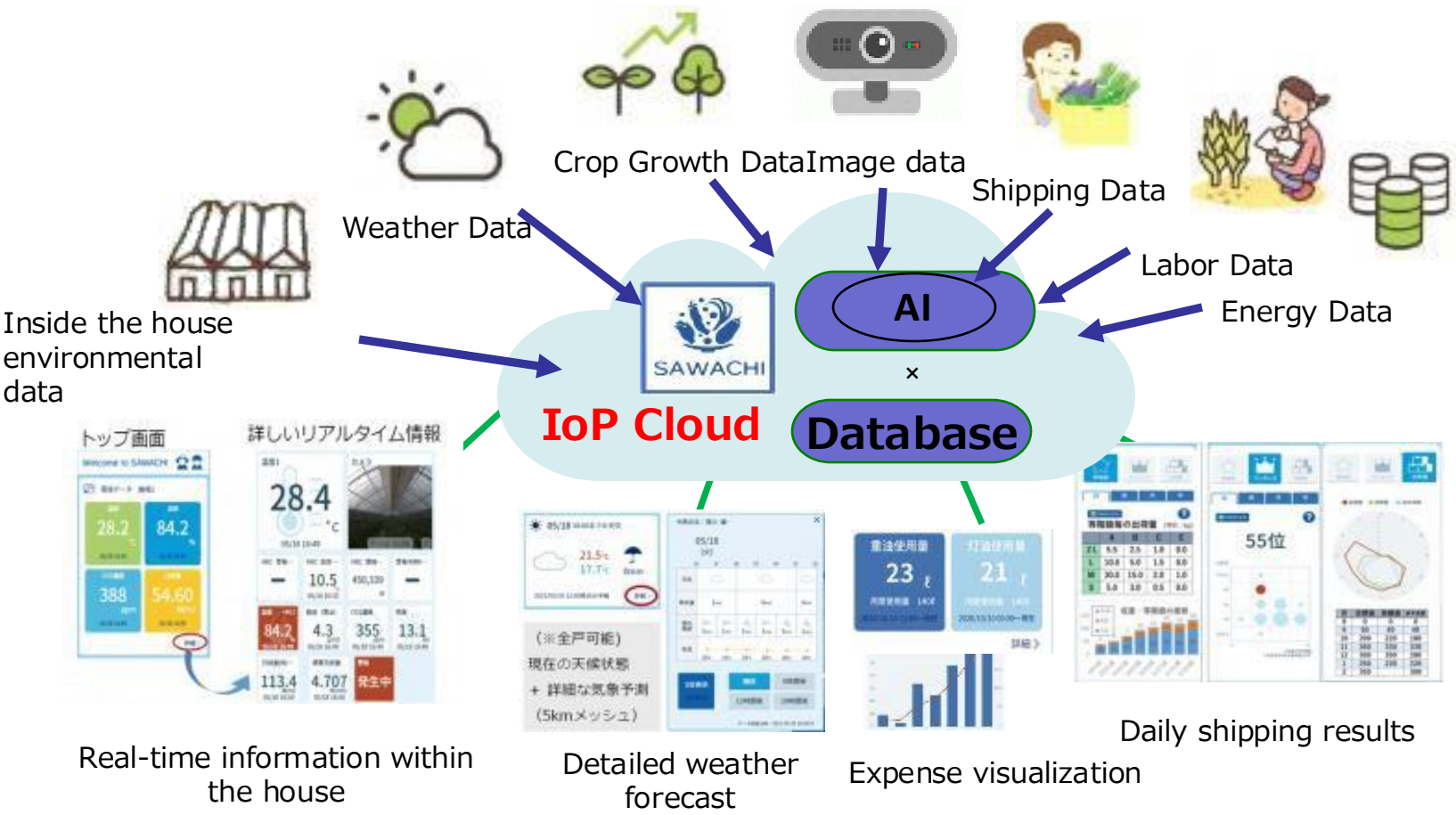

3. Case study 1 profit maximization

In Japan, agricultural produce has a standard.

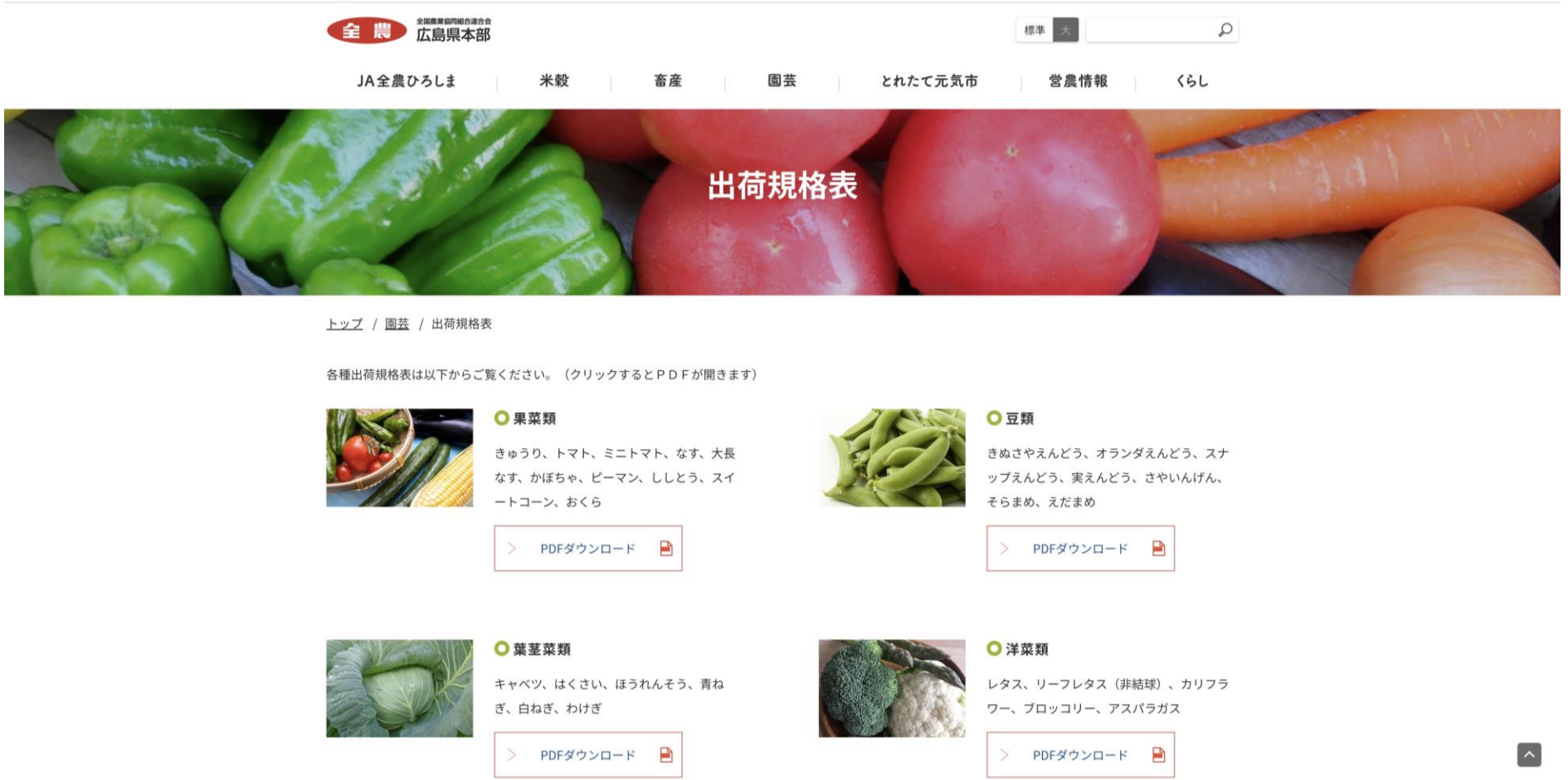

https://www.zennoh.or.jp/hr/syukkakikaku/img/kikaku08.pdf

https://www.zennoh.or.jp/hr/syukkakikaku/

4. Background

Ex. Standard based on size, color, and straightness

A/B B is more bent than A

C/D

4. Background

Ex. Standard based on size, color, and shape

A/B

C/D

The definition of outside standard quality regards its size and shape rather than the taste and flavor.

5. Problem Statement

Due to the CD quality products (outside standard quality but no problem with safety, taste, and flavor), their selling price in the central market is only half the price of A/B quality products. Hence, transferring part of the CD products to the farmer's market (such as Ito Sai Sai) run by JA, where prices are higher than that of the central market, is crucial for improving overall profitability. However, the farmer's market has a capacity limit and incurs a management fee. On the other hand, the central market charges a transaction fee while it does not have capacity limit.

6. Research Question and Hypothesis

Therefore, the optimization objective is to determine the optimal farmer's market price P_f, central price P_{AB}, and the quantity allocated to the farmer's market $Q_{s,CD}$ in order to maximize total revenue R_{total} while satisfying demand and market constraints.

Research hypothesis is farmers can maximize profit by diversifying their products' sale venues for the given market price.

7. Methodology – Grid Search

Grid Search is a systematic optimization technique used in machine learning and statistical modeling to find the **best hyperparameters** for a given model. In this study, grid search is applied to determine the optimal combination of:

Central market price (P_{AB})

Farmer's market price (P_f)

Quantity allocated to the farmer's market ($Q_{s,CD}$)

to maximize the total revenue (R_{total}) while satisfying all relevant constraints.

7. Methodology - Functions

- Weighted Average Prediction of Farmers

The weighted average number of farmers is calculated using recent data $N_{recent,i}$ and weights w_i

$$N_{farmer} = \frac{\sum_{i=1}^{n} w_i \cdot N_{recent,i}}{\sum_{i=1}^{n} w_i}$$

Where N_{farmer} is mean number of farmers,

$Q_{per\ farmer}$ is quantity of CD products allocated per farmer (kg)

- Farmer's Market Demand Function

$$Q_{ITO}(P_f) = Q_{max} \cdot e^{-k(P_f - P_0)}$$

7. Methodology - Revenue Calculations

Actual Quantity Sold in the farmer's Market

The actual quantity of CD products sold in the farmer's market is constrained by both demand and market capacity:

$$Q_{s,CD} = \min\left(Q_{ITO,cap} \cdot Q_{farmer's\ market}(P_f)\right)$$

Ito Market Revenue

$$R_{farmer's\ market} = \alpha \cdot P_f \cdot Q_{s,CD}$$

Central Market AB Product Revenue

$$R_{central,AB} = \beta \cdot P_{AB} \cdot (Q_{max} - Q_{s,CD})$$

Central Market CD Product Revenue

$$R_{central,CD} = \beta \cdot \left(\frac{P_{AB}}{2}\right) \cdot (Q_{max} - Q_{s,CD})$$

7. Methodology - Total Revenue and Price constraints

The total revenue $R_{total} = R_{farmer's\ market} + R_{central,AB} + R_{central,CD}$

To ensure competitive pricing in the farmer's market, the following constraints must be satisfied:

$$\alpha \cdot P_f < \beta \cdot P_{AB}, \qquad \alpha \cdot P_f > \frac{\beta}{2} \cdot P_{AB}$$

7. Optimization Objective and

Objective The optimization goal is to maximize the total revenue R_{total}:

$$\max_{P_{AB}.P_f \cdot Q_{s,CD}} R_{total}$$

By systematically varying the central market price P_{AB} within the specified range, the algorithm provides a comprehensive set of results, showing the optimal strategy for each price point. These results are crucial for decision-making, as they highlight how the interplay between market prices and distribution quantities affects revenue.

8. Result

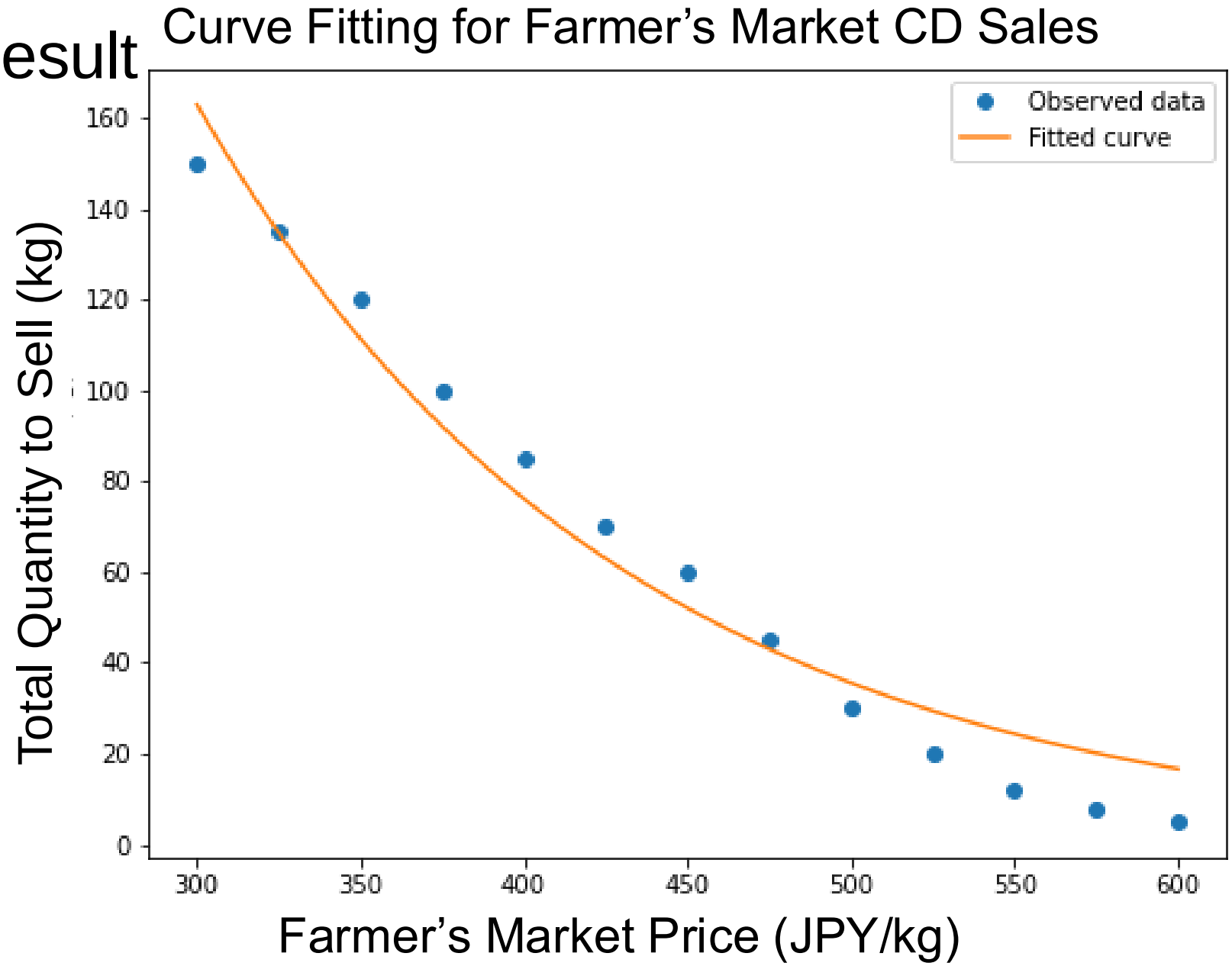
Curve Fitting for Farmer's Market CD Sales
Observed data
Fitted curve
Total Quantity to Sell (kg)
160
140
120
100
80
60
40
20
0
300
350
400
450
500
550
600
Farmer's Market Price (JPY/kg)

8. Result

Central Market Price AB (JPY/kg)	Optimal ITO Market Price CD (JPY/kg)	Optimal Total Allocation to Farmer's Market (CD) (kg)	Per Farmer Allocation to Farmer's Market (CD) (kg)	Max Profit (JPY)
600	444	55	4.07	49,368.60
650	470	45	3.33	51,878.94
700	496	40	2.96	54,586.09
750	522	35	2.59	57,454.67
800	548	25	1.85	60,455.69

9. Discussion –way forward

We could find a fitted curve by deriving the optimal farmer'smarket price P_f, central price P_{AB}, and the quantity allocated to the farmer's market $Q_{s,CD}$ in order to maximize total revenue R_{total} while satisfying demand and market constraints.

The data is based on data we created.

The next step is obtaining the real data from the farmer's market and and examine if our model fits well.

The Sixth Workshop on Interdisciplinary Sciences (WIS 2024)

Water Environmental Remediation in Organically Polluted Reservoir via Anoxification Recovery Using Underwater LED Irradiation

Dr. Daoluang Honglikith

Natural Resources and Environment Division, Natural Resources and Environment Research Institute, Ministry of Natural Resources and Environment, Vientiane Capital, Laos

Main Supervisors: Assoc.Prof. Masayoshi Harada

Department of Agro-environmental Sciences
Graduate School of Bioresource and Bioenvironmental Sciences, Agriculture Faculty, Kyushu University, Fukuoka, Japan

九州大学
KYUSHU UNIVERSITY

November 29th , 2024

Background: Serious environmental issues

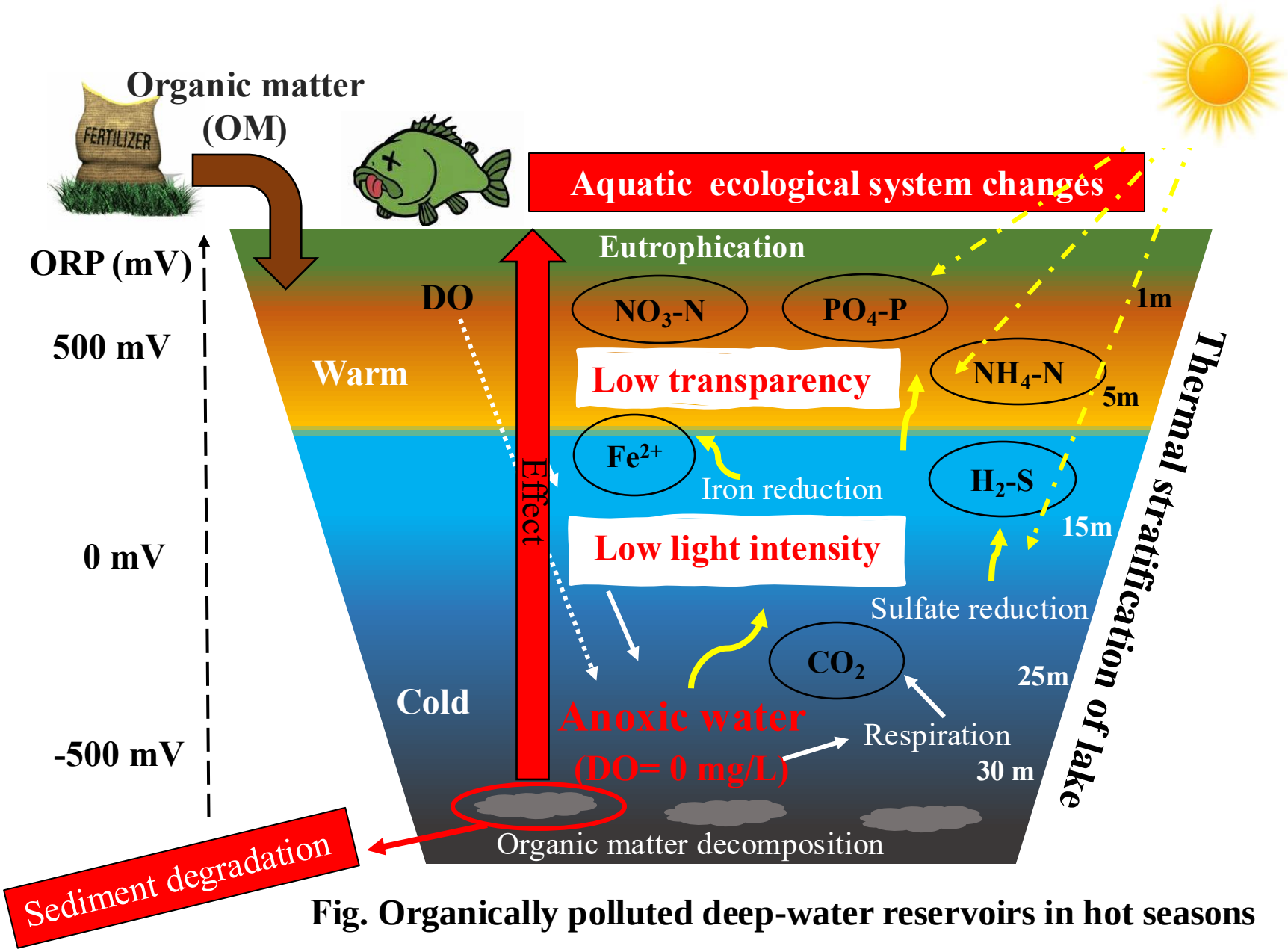

Fig. Organically polluted deep-water reservoirs in hot seasons

Literature Reviews

- **Water quality improvement for anoxic state recovery via using underwater light-emitting diode (LED) :**

Focus

Poor underwater light environment which was caused by dissolved and particulate organic matter, resulting in the occurrence in anoxic water as well as severe DO depletion at the bottom layer of reservoir

Underwater LED irradiation (Artificially improvement of light environment) Minato et al. (2012); Yamanaka et al. (2012); Minato et al. (2014); Harada et al. (2016)

→ Phytoplankton photosynthesis promotion → **Dissolved Oxygen (DO) production** → **Anoxic water elimination**

Dissolved Oxygen (DO) production → Water and bottom sediment quality improvement (Harada et al. 2016)

- **New aquatic environmental conservation technology**
- **This method still not well-known**

Chlorophyll-a (major photosynthetic pigment in plants) ← Absorbed by:

- Blue wavelength (435 nm to 480 nm)
- Red wavelength (610 nm to 750 nm)

→ increase → Chlorophyll production rate and algae growth (Chen et al. 2010)

The relationship photosynthesis rate of phytoplankton and the optical spectrum of the irradiation light were unclear

Previous study

Harada et al. (2016)

“ Quantitatively evaluated the effectiveness of underwater LED irradiation as the water quality improvement technology through a laboratory experiment using a cylindrical water-tank ”

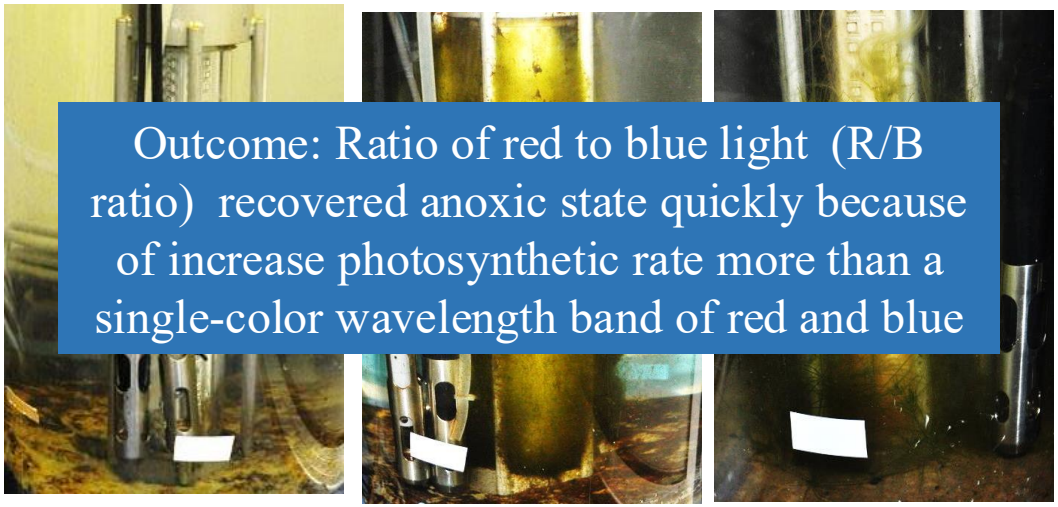

Fig. The overgrowth of filamentous algae in the water-tank experiment

Aim

To examine the influence of the ratio of red to blue light (R/B ratio) on the biochemical changes in DO and Chl-a.

- **Concerning point:**

1) Filamentous algae adhering to LED lamps contributed more strongly to the continuous maintenance of sufficient DO concentration compared to phytoplankton
2) Only a limited space in the vicinity of light source were able to estimate the water environmental remediation

➢ The anoxic state recovery using underwater LEDs where oxygen was produced by photosynthesis of phytoplankton rather than filamentous algae were not yet study

Previous study

Two limitation factors for LED irradiation experiment:

① **Light intensity**
② **Initial water quality parameters**

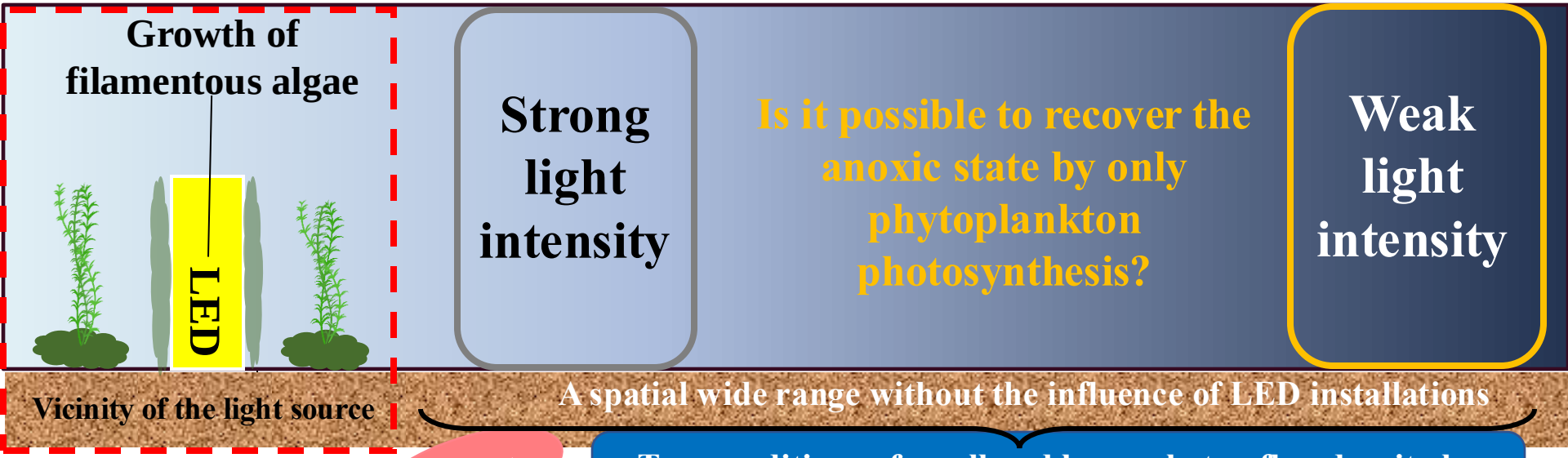

- It is necessary to understand the effects of water environmental remediation under conditions in which the optical intensity is lower than the optimum light quantum for photosynthesis (100 μmol/(m^2 s))

2nd limitation factor: Initial water quality parameters

Initial anaerobic condition with high initial oxidizable substances could affect the anoxic state recovery due to their excessive oxygen consumption via oxidation reactions
(Oniki et al. 2017; Thach et al. 2017; Thach et al. 2018)

→ **Examining the water environmental remediation effects considering the initial anaerobic condition as well as spectral condition of LED irradiation is important**

1st stage: Beaker-scale experiments (Master Research)

Title: Influence of Optical Spectrum on Remediating Anoxic Water Environment by Beaker-scale Experiments

1. Mixed RB:

2. Mixed RGB:

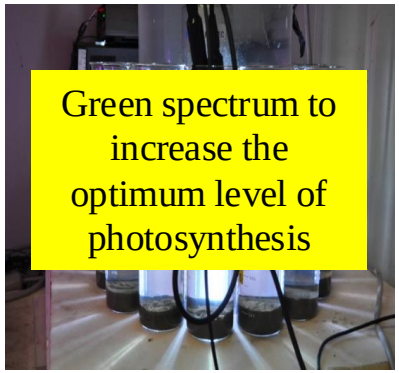

Aim

To evaluate the impacts of the optical spectrum and LED light intensity on the maintenance of healthy aerobic conditions, as well as the anoxic state recovery by promoting oxygen production by phytoplankton photosynthesis

Outcome:

① The photo-responsiveness and photosynthesis rate of phytoplankton could be enhanced in the presence of the green spectrum regardless of light intensity, and the anoxic state could be quickly recovered.

② LED irradiation with mixed RGB spectra was more promote oxygen production than mixed RB spectra under weak light intensity

③ The water environmental remediation by solving the long-term anoxic state under both strong and weak light intensity conditions were reflected in the decrease of TN and TP values upon two months irradiation, regardless of the green spectrum.

2nd stage: Water tank-scale experiments

Title: Influence of RGB Spectra and Initial Anaerobic Conditions on Water Environmental Remediation by Water Tank-scale Experiments

General aim:

To examine the influence of the optical conditions and the initial anaerobic conditions on the water environmental remediation were performed on water tank-scale to enhance the reliability of the experimental results

Series

Specific aims

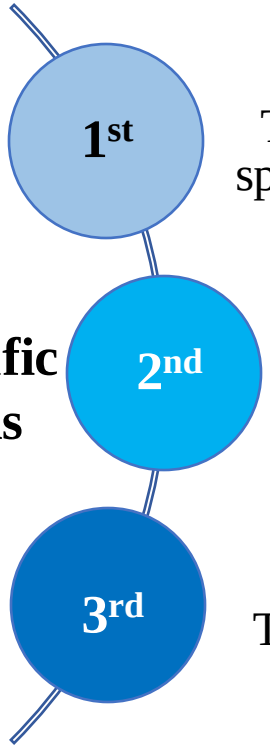

1st: To determine the effects of single-color irradiation (red, green, and blue spectra) on the growth of phytoplankton, fluctuations in DO, and recovery from long-term anoxic state

2nd: To examine the improvement of water quality during the recovery from the anaerobic state under weak light intensity conditions, which was markedly lower than the effective photon flux density for photosynthesis

3rd: To evaluate the influence of initial anaerobic conditions on water environmental remediation effects under weak light intensity

Indoor experimental material

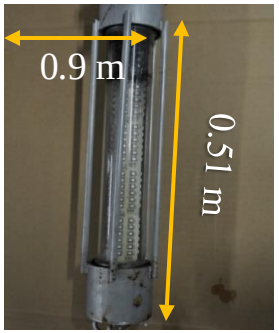

- **Adjustable photon flux density for each component ratio of red, blue, and green color light intensities**

Fig. RGB full color underwater LED lamp (LA1-24RGB, Marintec Inc.). Fish-luring underwater light and has a four-sided structure with 60 LED elements corresponding to RGB color components per side

Physicochemical properties of actual bed mud under anoxic state	
ORP(mV)	-176.5
pH	7.40
EC(mS/cm)	0.068
Sulfide(mg/g)	0.154
ignition loss(%)	11.62

Aim: To examine how much artificial light irradiation could contribute to water environmental remediation in anoxic water through the anaerobic state recovery

Location: Ito campus of Kyushu University, Fukuoka, Japan

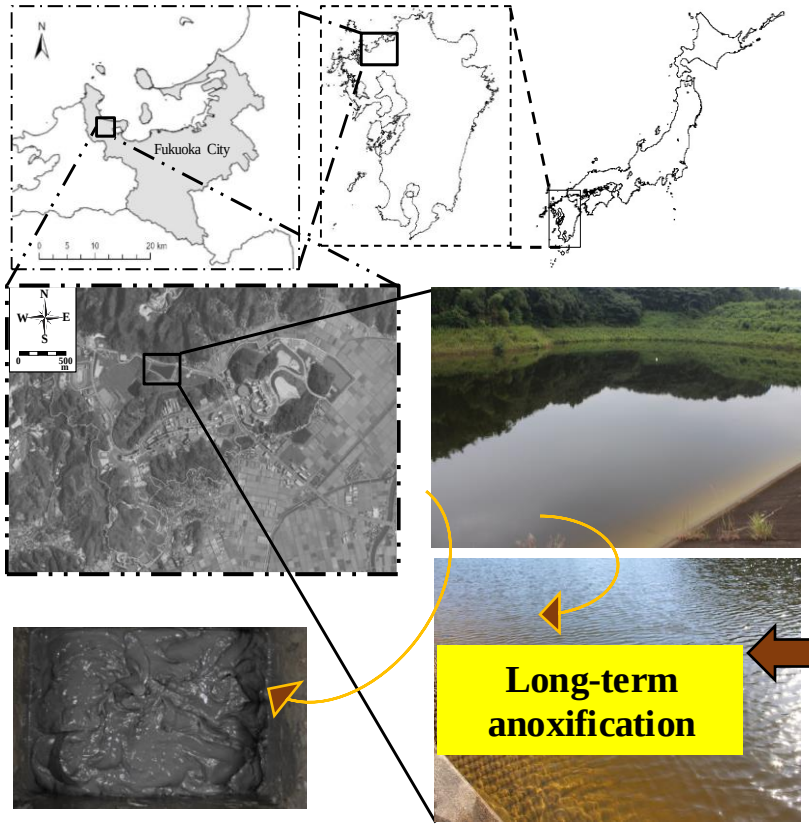

❖ **Characteristics:**

-Area: 13,800 m^2
-Volume: 63,000 m^3
- Storage height: 8 m

Irrigation water resource and a flood control reservoir

Humified logged wood chips by land development

Degraded water quality due to excessive dissolved organic matter (DOM)

Fig. Targeted water body reservoir situated in the Ito campus of Kyushu University, Fukuoka Prefecture

LED irradiation experiments

❑ Water tank-scale experiments:

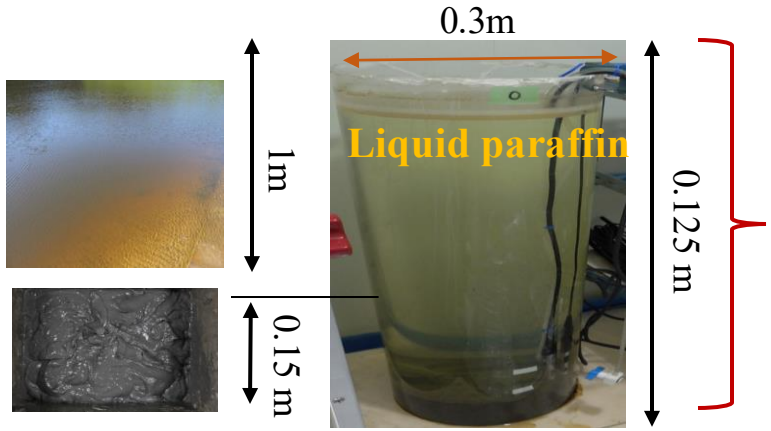

- ✓ Oxygen supply blocking from the atmosphere by liquid paraffin covering
- ✓ Dark room storing
- ✓ Room temperature-control at 20 °C

Fig. Strong anoxic water regeneration in experimental system

❑ Irradiation Experiment setting:

Fig. Water tank irradiation experiments design

- Underwater LED lamp was installed in a transparent acrylic cylinder with a diameter of 0.13 m and a height of 1 m filled with pure water which was set at the center of the water tank to **prevent filamentous and adherent algae growth**
- Surfaces of the bottom mud in the water tank-scale experiments were never irradiated because the LED lamps were pointed upright in the sediment. Therefore, the bottom sediment was unaffected by the LED irradiation.

- ✓ **Two months irradiation**
- ✓ **24h light cycle (12L:12D)**
- ✓ **Room temperature control at 20˚C**

Water quality monitoring

No.	Parameters	Methods	Unit
1	Optical spectrum and light intensity	**Continuous measurement and the data was logged at 20min intervals**	…..
2	Oxidation Reduction Potential (ORP)		mV
3	Dissolved Oxygen (DO)		mg/L
4	Chlorophyll.a by algae class	Multi-wavelength excitation fluorometer (FluoroProbe, bb-Moldaenke)	µg/L
5	Chlorophyll.a (Chl.a)	Extraction by N,N-dimethylformamide (Fluorophotometer)	µg/L
6	Sulfide	Ethylene blue method	µg/L
7	Phosphate (PO_4-P)	Ascorbic acid reduction molybdenum blue method	mg/L
8	Total Phosphorus (TP)		mg/L
9	Total Nitrogen (TN)	**One / twice per week for measurement, the analysis scheduled were conducted at about 11h lapsed from turning on the LED**	mg/L
10	Ammonia (NH_4-N)	Colori	mg/L
11	Sulfate (SO_{42}-)		mg/L
12	Nitrate (NO_3-N)		mg/L
13	Total iron ion (TFe)	2,4,6-tris (2-pyridyl)-1,3,5-triazine method	mg/L
14	Total organic carbon (TOC)	TOC analyzer (Sievers 900, GE Analytical Instruments)	mg/L
15	Dissolved organic carbon (DOC)		mg/L
16	Ultraviolet light absorption at the 254 nm wavelength (E254)	DR5000	……

Experimental conditions of 1st series

- **Anoxic water with a strong reductive potential and subjected to long periods of anoxic state was irradiated under each single-color red, blue or green spectrum**

Case B-1 **Case B-2** **Case B-3**

The photon intensity in this series was adjusted to around **40–50 µmol/(m² s) which was sufficient photon flux density that not inhibit the phytoplankton photosynthesis**

- **Denitrification:** NO_3-N absence
- **Iron reduction:** TFe (Ferrous ion (Fe^{2+})) and PO_4-P release
- **Sulfate reduction:** Sulfide generation
- **Anaerobic decomposition of organic matter:** NH_4-N, PO_4-P generation

Table Optical spectrum and intensity of LED irradiation in the first series

Case	Color	Visible light (360~780 nm) µmol/(m² s)	Blue band (435~480 nm) µmol/(m² s)	Green band (500~570 nm) µmol/(m² s)	Red band (610~710 nm) µmol/(m² s)
B-1	R	46.10	0.39	0.51	45.2
B-2	G	45.61	0.79	44.37	0.45
B-3	B	42.84	42.43	0.25	0.16

- **The initial water quality was determined by long-term anoxic state that characterized by anaerobic biochemical reactions under a strongly reductive state**

Table Initial conditions of main water quality parameters associated with the anaerobic state in the first series

Case	DO (mg/L)	Chl-a (µg/L)	Sulfide (µg/L)	NH_4-N (mg/L)	PO_4-P (mg/L)	NO_3-N (mg/L)	TFe (mg/L)
B-1	0.13	0.17	380.5	1.23	0.279	0.004	1.23
B-2	0.08	0.08	307.0	1.04	0.248	0.002	0.94
B-3	0.19	0.09	237.5	0.97	0.176	0.005	0.63

Results and discussion (Case B)

Water environmental remediation were estimated from viewpoints of anoxic state recovery, maintenance of a healthy DO level, and reductions of nitrogen, phosphorous, and organic matter

The time lag between the start of oxygen production and the recovery from anoxic state was occurred before DO increase. This period was caused by long-term darkness reduced photo-responsiveness of phytoplankton and oxygen production was less than oxygen consumption

- The oxygen production rate between Cases B-1 **(R)** and B-3 **(B)** did not majorly differ
- The oxygen production rate in Case B-2 **(G)** was the lowest during single-color **RGB** irradiation.

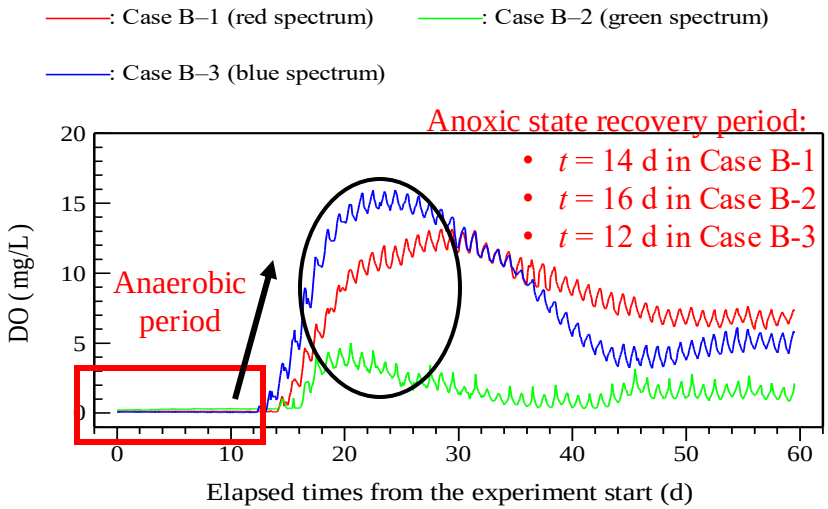

Fig. Continuously monitored DO concentration and saturation in Case B-1 (red spectrum), Case B-2 (green spectrum), and Case B-3 (blue spectrum)

To sum up:

① The time required to recover from the reduced photo-responsiveness of phytoplankton did not differ among the red, green, and blue spectra;
② The time required for anoxic state recovery by LED irradiation with the green spectrum was more because of the low photosynthesis rate than red and blue spectra;
③ The time required for anoxic state recovery between red and blue spectra was not different.

Results and discussion (Case B)

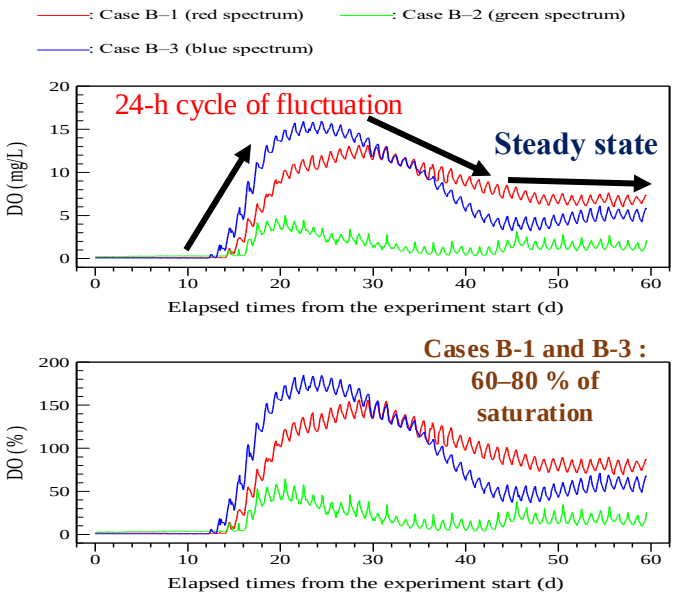

Fig. Continuously monitored DO concentration and saturation in Case B-1 (red spectrum), Case B-2 (green spectrum), and Case B-3 (blue spectrum)

All Cases

Similarities : DO concentration initially reached a peak, gradually decreased, and finally reached a steady state.

Difference :

① Maximum value and steady state in DO;

② Required time of DO to reach the peak value and steady state.

These differences were reflected by each single-spectrum irradiation

- **Case B-1 (R) and B-3 (B): DO > 4mg/L**
- **Case B-2 (G): DO < 4mg/L**

Water quality dynamics in Case B-2 evidently differed from other two cases

In the comparison of red and blue spectra irradiation, blue spectrum irradiation activated photosynthesis and promoted phytoplankton growth more effectively. Thus, DO level under blue irradiation reached a highly oversaturated state early.

To sum up:

- Both red and blue irradiations were extremely effective to properly manage DO level to sustain aquatic life
- The peak DO concentration in Case B-3 was higher than Case B-1, while DO level in the steady state in Case 1 was higher than Case B-3
- The impacts of the green spectrum on oxygen production efficiency and promoting effect of photosynthesis were extremely low compared to red and blue spectra, as consequence, healthy DO levels were not maintained

Results and discussion (Case B)

The temporary change in PO_4-P, TFe, NH_4-N, sulfide, NO_3-N and Chl-a of all cases

Cases B-1 (R) and B-3 (B) (red and blue spectra irradiation) showed nitrogen and phosphorous cycles among planktons, organic substances, and nutrients shifted to an equilibrium state after the anoxic state recovery

Both red and blue spectra irradiations had the same advantages in preserving the aerobic water environment without increasing the amount of phytoplankton

In contrast, Case B-2 (G) did not show a uniform utilization of DIN (Dissolved Inorganic Nitrogen) and DIP (Dissolved Inorganic Phosphorus) for photosynthesis and a balance between nutrient uptake by photosynthesis and their supply into water via aerobic decomposition of organic matter

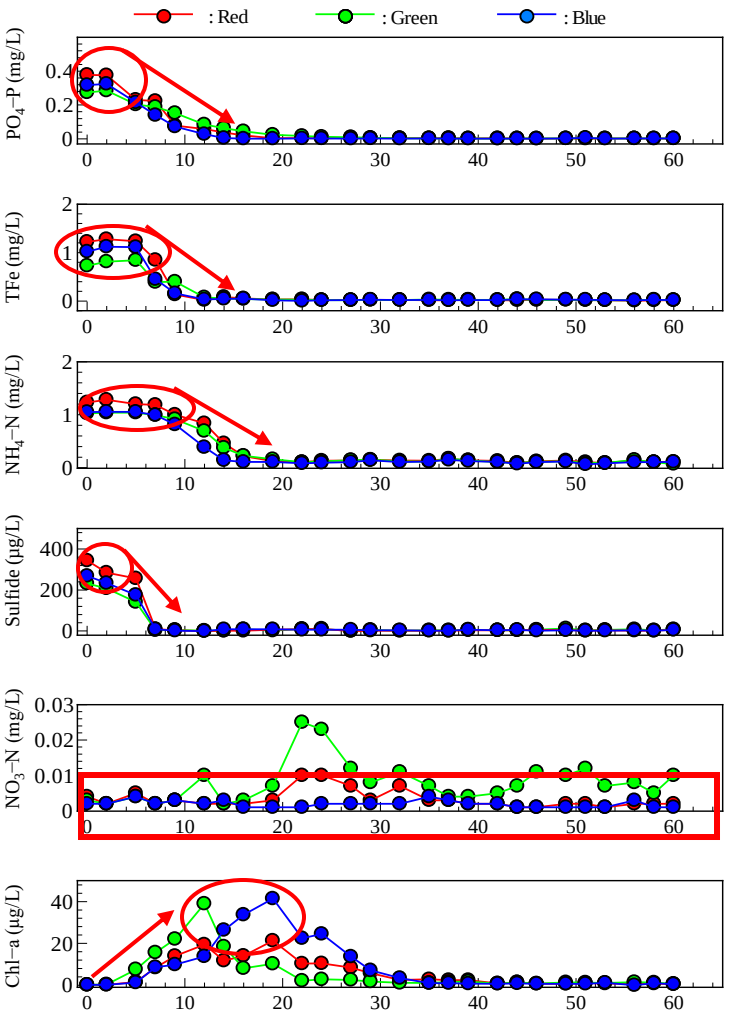

Fig. Scheduled measurements results of PO_4-P, TFe, NH_4-N, sulfide, NO_3-N and Chl-a in Case B-1 to Case B-3

Experimental conditions of 2nd series

Case C-1 **Case C-2**

Case C-BK (Control)

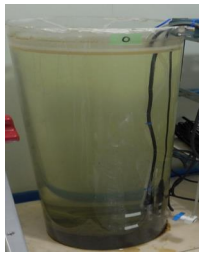

Table Optical spectrum and intensity of LED irradiation in the second series

Case	LED	Intensity (μmol/(m² s)	Visible light 360 ~780 nm	Blue band 435~480 nm	Red band 610 ~710 nm	Green band 500 ~570 nm	R/B ratio
C-1	R:G:B (1:1:1)	Weak	Optimum photon for phytoplankton photosynthesis (increase photosynthesis)				
C-2		Strong	One-fifth of optimum photon for phytoplankton photosynthesis (inhibited photosynthesis)				

Aim: To examine the recovery from anaerobic conditions, in which a strong reductive state caused an increase in NH_4-N, PO_4-P and sulfide like the first series and the beaker-scale experiments

Nutrients and oxidizable substances Increased due to denitrification, iron reduction, and sulfate reduction

Table Initial water quality parameters at the start of LED irradiation in the second series

Case	ORP (mV)	DO (mg/L)	Chl.a (μg/L)	Sulfide (μg/L)	NH_4-N (mg/L)	PO_4-P (mg/L)	NO_3-N (mg/L)	TFe (mg/L)
C-1	-416.7	0.2	1.9	227.0	1.97	0.21	0.00	2.39
C-2	-293.8	0.2	1.5	139.3	2.04	0.19	0.00	2.63
Control	-367.1	0.2	1.5	212.6	1.32	0.20	0.00	2.15

Results and discussion (Case C)

The time lag between the start of oxygen production and the recovery from anoxic state was occurred before DO increase. These occurrence were same as first series

Differences of both cases:

① Recovery time from anoxic state, t= 13 d

② Decrease in photoresponsiveness t=3 d

- **Case C-1 required longer time for anoxic state recovery when compared to Case C-2 due to the influence of low light intensity and high concentrations of oxidizable substances**

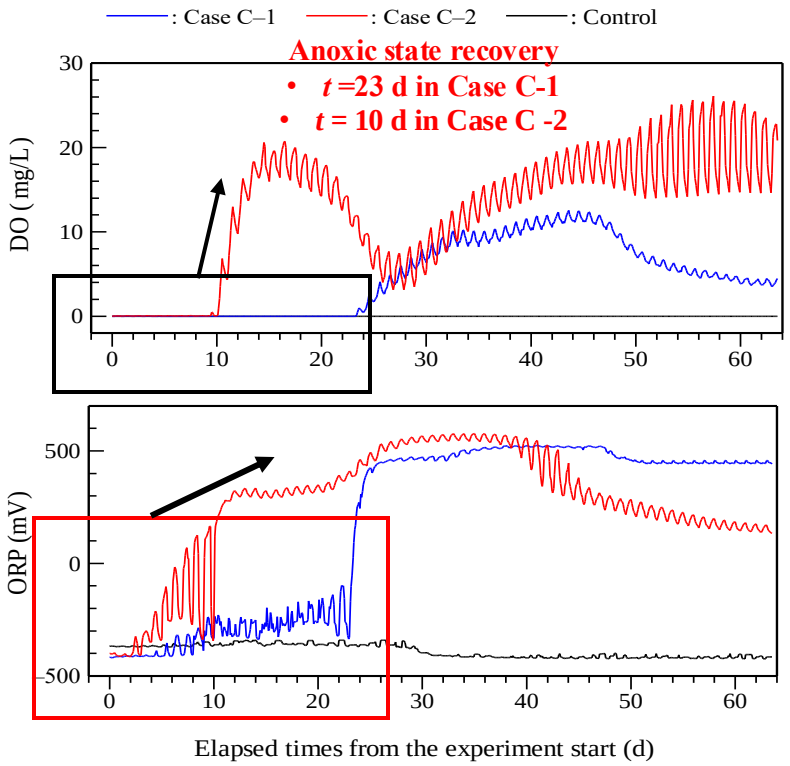

Fig. Continuously measured DO and ORP in Cases C-1 and C-2

The stronger the light intensity, the greater the photosynthetic ability, resulting in the promotion of oxygen production.

The photo-responsiveness and photosynthesis rate of phytoplankton could be enhanced in the presence of the green spectrum regardless of light intensity, and the anoxic state could be quickly recovered

Results and discussion (Case C)

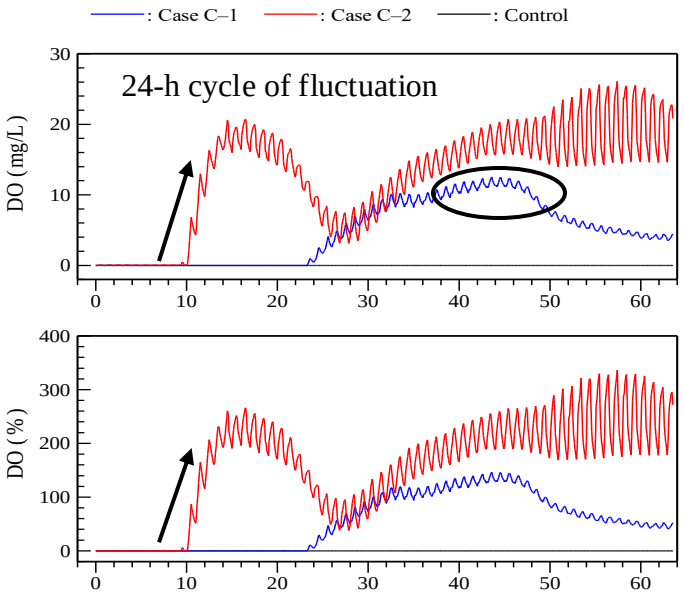

Fig. Continuously measured DO and ORP in Cases C-1 and C-2

The stroke of DO variation in Case C-1 was smaller than Case C-2

Optical limitation on phytoplankton photosynthesis due to weak light intensity

- DO in Case C-1 maintained 60 % saturation (DO = 10 mg/L) with stable fluctuation and without the influence of large oxygen consumption when it reach steady state

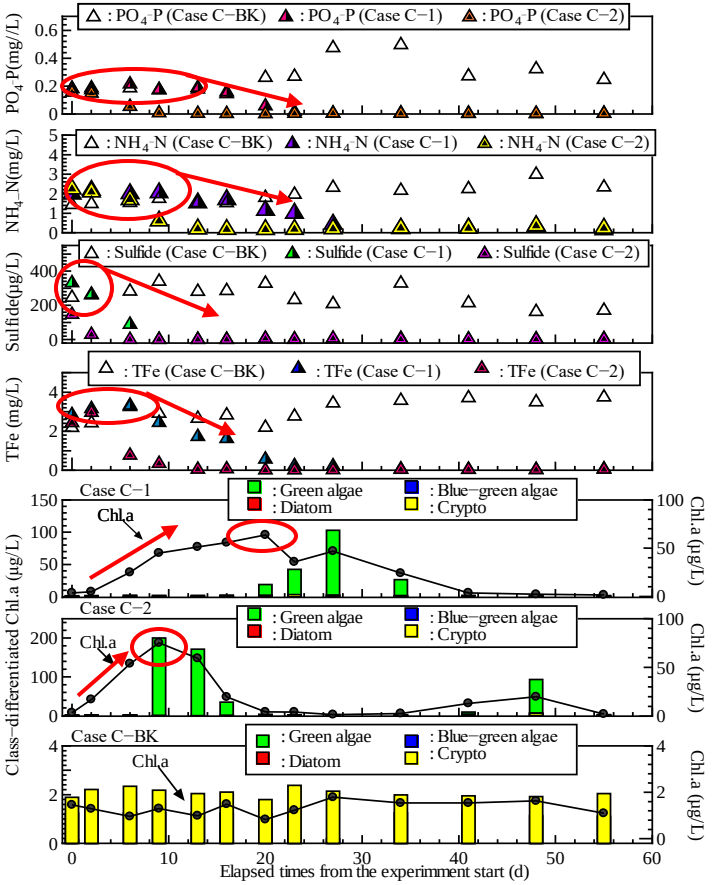

Fig. Periodically measured Chl-a, class-differentiated Chl-a, NH4-N, PO4-P, sulfide, and TFe in Case C-1 and C-2

DO environment was preserved even under weak light intensity of approximately 20 μmol/(m² s) because the matter cycle among planktons, organic substances, and nutrients reached an equilibrium state even

Experimental conditions of 3rd series

To examine the improvement of anoxic water under two different reductive states of anoxic water (strong and a weak reductive potential). The optical conditions were set to low photon intensity, which would strongly affect phytoplankton photosynthesis due to optical limitation

Case D-1

Case D-2

Case D-3

The initial concentrations was a key experimental factor

(High concentrations of NH_4-N, PO_4-P, sulfide, and TFe)

- **Cases D-2 and D-3 (Weak reductive state of initial condition)** started few weeks after the experimental system was set:

(Low concentrations of NH_4-N, PO_4-P, sulfide, and TFe)

Table Optical spectrum and intensity of LED irradiation in the third series

Case	Color	Visible light (360 ~780 nm) μmol/(m² s)	Blue band (435 ~480 nm) μmol/(m² s)	Green band (500 ~570 nm) μmol/(m² s)	Red band (610 ~710 nm) μmol/(m² s)
D-1	RBG	8.12			
D-2	RBG	7.97			
D-3	RBG	3.98			

One-tenth of the lower limit of the optimum light intensity required for photosynthesis

One-twentieth of the lower limit of the optimum photon intensity

Table Initial conditions of main water quality parameters associated with the anaerobic state in the third series

Case	DO (mg/L)	Chl-a (μg/L)	Sulfide (μg/L)	NH_4-N (mg/L)	PO_4-P (mg/L)	NO_3-N (mg/L)	TFe (mg/L)
D-1	0.12	0.6	83.0	1.42	0.51	0.00	2.30
D-2	1.3	0.6	9.0	1.13	0.07	0.01	0.12
D-3	0.01	0.3	5.5	0.61	0.12	0.00	0.17

Results and Discussion of 3rd series

The time lag between the start of oxygen production and the recovery from anoxic state was occurred before DO increase. The reasons of these occurrence were same others series

- **Cases D-1 and Case D-2 required longer time for anoxic state recovery when compared to the cases of the first and second series**

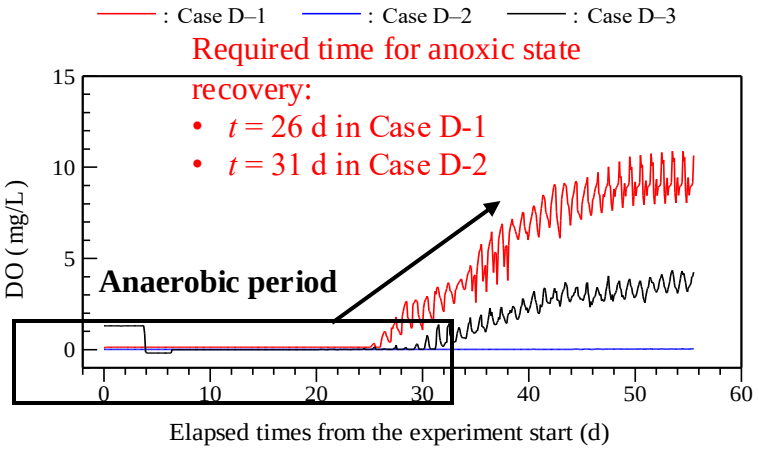

Fig. Continuously monitored DO results of in Cases D-1, D-2, and D-3

Anoxic state recovery was occurred in Cases D-1 and D-2, unlike Case D-3 (DO= 0 mg/L)

The differences between Cases D-1 and D-2:

① The time required for the anoxic state recovery because of differences in the mass balance between oxygen production and oxygen consumption in both cases.

② In Case D-1, having extremely high concentrations of both sulfide and TFe, the oxygen consumption during the oxidation of oxidizable substances was higher than in Case D-2. The anoxic state in Case D-1 recovered faster than that in Case D-2.

The initial high concentrations of NH_4-N and PO_4-P in Case D-1 stimulated the photosynthesis rate more than Case D-2 because of the differences only in the nutrient limiting factor between both cases

Under similar weak light intensities, the time length for anoxic state recovery in both cases depended more strongly on the initial high concentration of nutrients than oxidizable substances

Results and Discussion of 3rd series

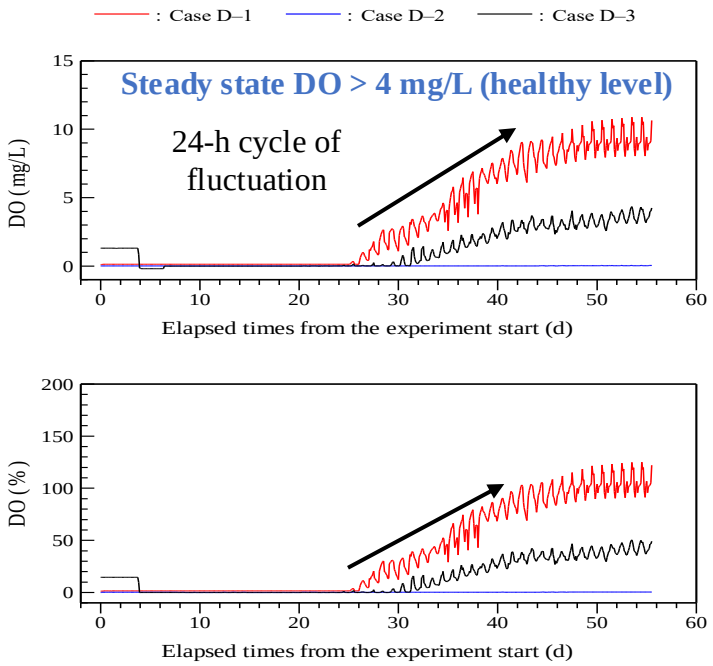

Fig. Continuously monitored DO results of in Cases D-1, D-2, and D-3

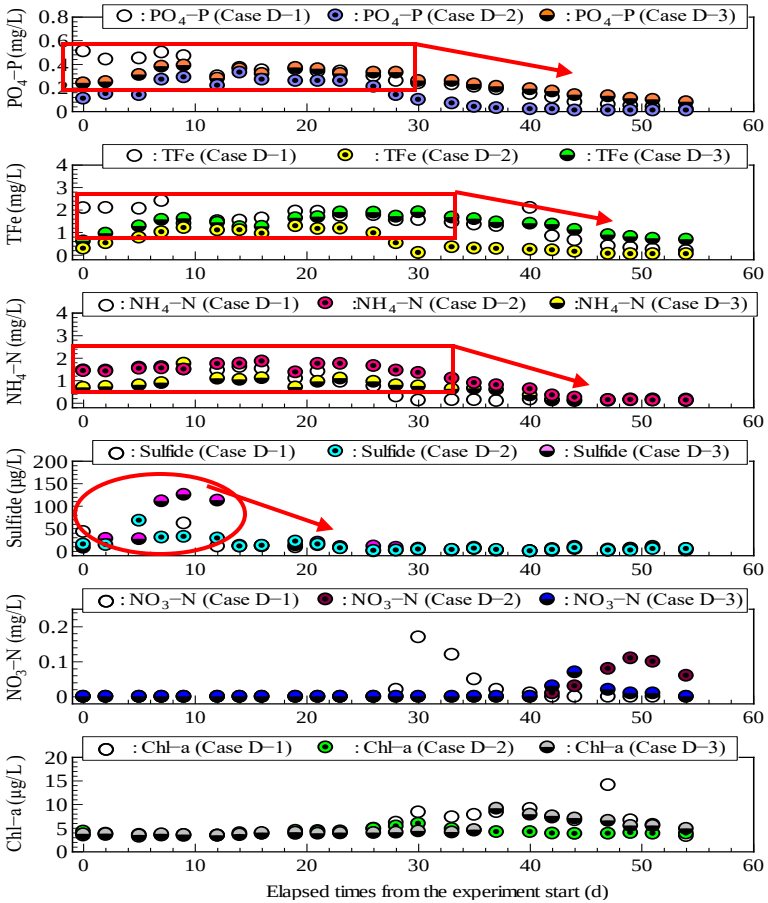

Fig. Time series variation of water quality parameters. (a) PO4-P, (b) TFe, (c) NH4-N, (d) sulfide, (e) NO3-N and (f) Chl-a in Cases D-1, D-2, and D-3

The difference between Cases D-1 and D-2:

① The time required to reach the lower concentration limit (4 mg/L) required for a healthy DO level

② Average increasing rate of DO until the maximum concentration was reached

③ DO concentration at the steady state and daily variation in DO

A healthy DO level could be preserved at a low level of 4 mg/L although the underwater light intensity was one-tenth of the lower limit of the optimum light intensity required for photosynthesis

Results and Discussion of 3rd series

The temporal changes in the water quality of Case D-3 (DO = 0 mg/L) were determined as follows based on the oxidation-reduction reaction

- The oxidizable substances remarkably increased from the initial concentrations as the strong reductive state progressed for $t < 28$ d, consequently, increasing the oxygen consumption since $t > 28$ d.

The anoxic state could not recover in Case D-3 because of the decrease rate of photosynthesis under light limitation and the increase rate of oxidizable substances under strong reductive state

Determining the anoxic state recovery was possible in Case D-3 based on the water quality improvement as sulfide and nutrient contents decreased to nearly zero, although a healthy DO level was not maintained to sustain aquatic life

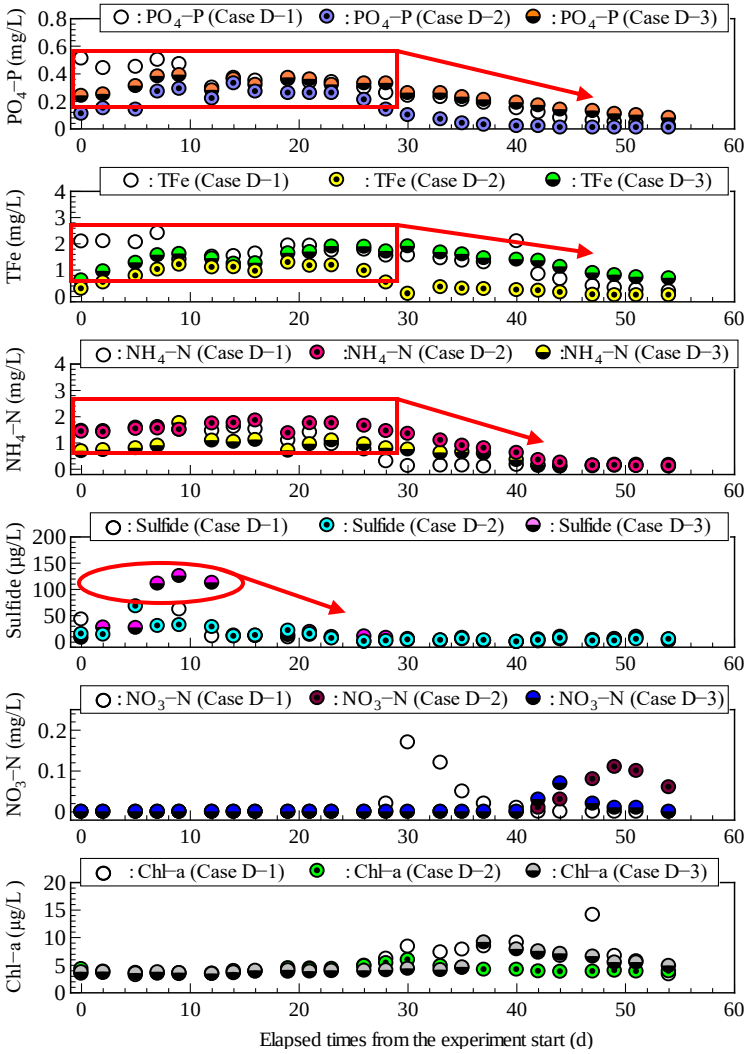

Fig. Time series variation of water quality parameters. (a) PO4-P, (b) TFe, (c) NH4-N, (d) sulfide, (e) NO3-N and (f) Chl-a in Cases D-1, D-2, and D-3

Reduction effects in nitrogen, phosphorous and organic matter for all series

First series

Second series

Third series

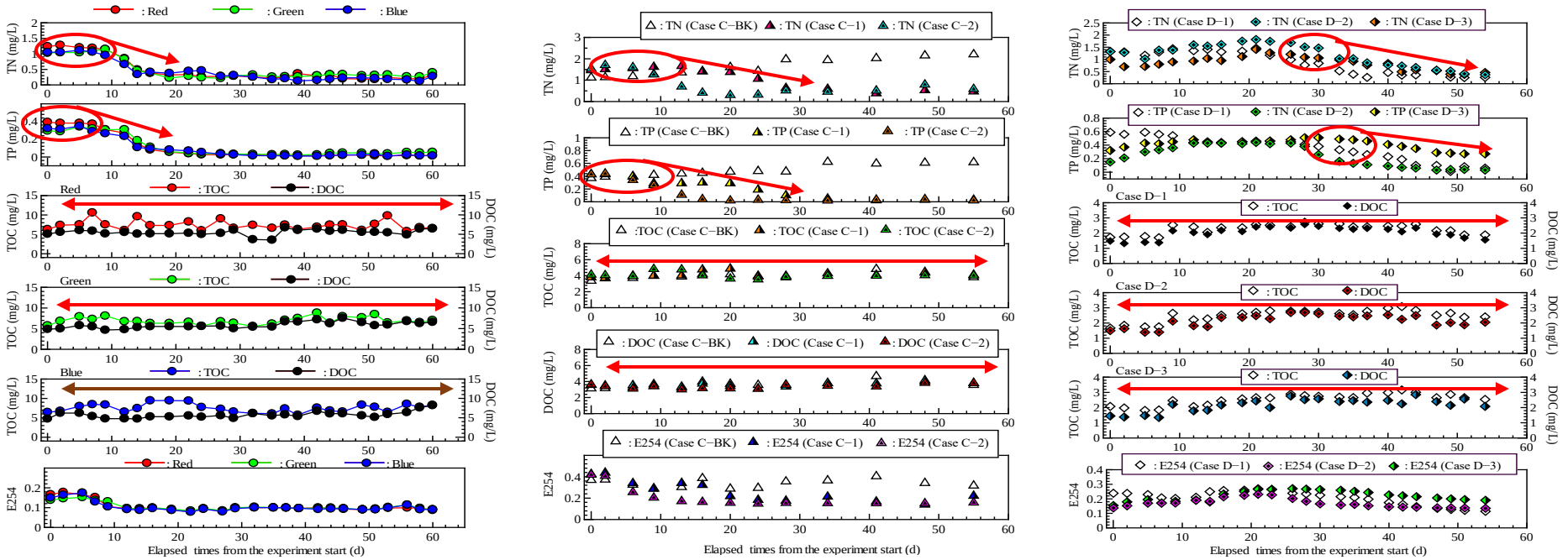

Fig. Time series variation of water quality parameters. (a) TN, (b) TP, (c) TOC, (d) DOC, and (e) E254 in the all series

- TN and TP levels decreased via the aerobic matter cycle
- TOC and DOC levels did not show a remarkably increasing trend
- There was no difference in the decrease rates of TN and TP levels

1st series: The reductions in TN and TP levels were different between the **green spectrum** irradiation, and **red** and **blue** spectra irradiations. This indicated that whether nitrogen or phosphorous cycles among planktons, organic substances, and nutrients were reached an equilibrium state

2nd series: The effect of water environmental remediation under weak light intensity (Case C-1) was same as under strong light intensity(Case C-2).

3rd series: LED irradiation was effective in reducing TN and TP levels even oxygen production was strongly restricted to about **one-tenth** of the lower limit of optimum photon intensity required for photosynthesis

Conclusion

The knowledge and outcomes acquired by underwater LED irradiations was summarized:

1st experimental series:

① In single-color irradiations, under sufficient photon intensity of about 50 μmol/(m^2 s), the green spectrum required more time to recover from the anoxic state because of the lower photosynthesis rate compared to the red and blue spectra.

② Red and blue spectra were essential and largely contributed to the sustainable maintenance of healthy DO level to ensure aquatic environmental conservation even their oxygen production rate, maximum and stationary DO levels were different. Furthermore, green spectrum played an important role in oxygen production via phytoplankton photosynthesis.

2nd experimental series:

① Mixed RGB irradiation assisted healthy aerobic state preservation compared to mixed RB even under weak intensity was about 20 μmol/(m^2 s) as low as **one-fifth** of the optimum photon for phytoplankton photosynthesis

② The spatial effect of water quality improvement via LED irradiation was applicable to a wide range and was not limited to the vicinity of the light source and was reflected in the decreased of TN and TP levels because of the reduction of DIN and DIP through the aerobic matter cycle, in which phytoplankton played a leading role.

Conclusion

3rd experimental series:

① Mixed RGB irradiations maintained a healthy DO level even under weak light intensity of about 10 μmol/(m^2 s) which was **one-tenth** of the lower limit of the optimum photon intensity required for photosynthesis

② Under extremely weak light intensity, which was **one-twentieth** of the optimum intensity, the water quality improvement showed a minimum effects although anoxic state recovery was absent

③ High initial anaerobic condition had advantage on the time required to reach a healthy DO level, average increasing DO rate, maximum, stable concentrations and the oxygen production rate, resulting in early anoxic state recovery

Paddy and Water Environment (2022) 20:153–175
https://doi.org/10.1007/s10333-021-00883-2

ARTICLE

Anoxification recovery using underwater LED irradiation and influence of its optical spectrum on water quality improvement

Daoluang Honglikith[1] · Masayoshi Harada[2] · Kazuaki Hiramatsu[2] · Toshinori Tabata[2] · Akinori Ozaki[3]

Received: 22 August 2021 / Revised: 16 November 2021 / Accepted: 22 November 2021 / Published online: 4 January 2022
© The International Society of Paddy and Water Environment Engineering 2021

Abstract
This study focuses on a method for improving water quality via anoxification recovery using underwater LED treatment in an organically polluted reservoir. The main aim was to evaluate the effects of the optical spectrum and light intensity of LED irradiation on the maintenance of healthy aerobic conditions, as well as anoxification recovery, by promoting oxygen production via phytoplankton photosynthesis. Water quality was monitored via beaker and water tank experiments while using LED irradiation for 24 h (12 h on/12 h off) for 2 months in anoxic water, where the anaerobic decomposition of organic matter progressed under strong reductive conditions. As a result, red–green–blue (RGB) light was advantageous for promoting rapid oxygen production by phytoplankton photosynthesis compared with the mixed red and blue light. In particular, LED irradiation, including the green color, preserved the healthy dissolved oxygen environment without lowering the oxygen level in the dark. In addition, RGB irradiation (R:B:G = 1:1:1) did not only assist in preserving a healthy aerobic state in spite of low light intensities but also evidently decreased concentrations of total nitrogen and total phosphorous. In conclusion, the spatial effect of water quality improvement via LED irradiation was not limited to the vicinity of the light source but was applicable to a wide range, in which the light intensity contributed to one-fifth of the optimum photon intensity for phytoplankton photosynthesis.

Keywords Organic pollution · Dissolved oxygen · Phytoplankton · Dissolved inorganic nitrogen and phosphorous · Optimum light intensity for photosynthesis

Thank you so much for your attention!

A stochastic forest transition model

j.w. Ton Viet Ta and Tianyu Song (Kyushu University.)

Satoshi Kumabe

November, 2024

Self-introduction

- Affiliation : Joint Graduate School of Mathematics for Innovation, Kyushu University, Japan
- 3rd year doctoral student
- Research interests : Mathematics $\cdots$ Number theory, Mathematical modeling (!)

A forest decreasing or increasing?

A forest transition : transition from decreasing to increasing trends in forests.

- The forests in the world are decreasing due to deforestation.
- However, there are reports that, in countries with a per capita GDP of more than \$4,600, forests are changing from decreasing to increasing. (e.g. Kauppi et.al. (2006)[1])

Satake–Rudel (2007) built a mathematical model (called a forest transition model) that captures changes in "forest covering rate". They examine the conditions under which forest transition occurs.

[1] P.E. Kauppi, J.H. Ausubel, J. Fang, A.S. Mather, R.A. Sedjo, P.E. Waggoner, Returning forests analyzed with the forest identity. Proceedings of the National Academy of Sciences 103 (46), 17574-17579

The forest transition model

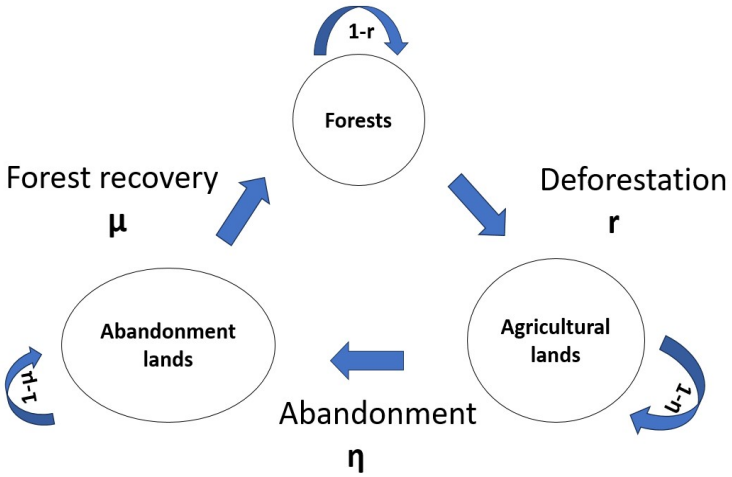

The original forest transition model

Satake–Rudel : They gave the following model (a system of **difference equations**) to capture **the ratio of forest land** $x(t)$ and **that of agricultural land** $y(t)$ $(t = 0, 1, \ldots)$.

$$\begin{cases} x(t+1) = p(x(t))(1 - x(t) - y(t)) + (1 - r)x(t) \\ y(t+1) = r(x(t))x(t) + (1 - \eta)y(t). \end{cases}$$

A goal of our study: We construct a model of stochastic differential equations model based on Satake–Rudel's model.

Toward a stochastic forest transition model

Our strategy :We regard $x(t), y(t)$ as random variables and consider the following "stochastic differential equations".

$$\begin{cases} dx_t = \{p(x_t)(1 - x_t - y_t) - r(x_t)x_t\}dt + \sigma_1 x_t(1 - x_t - y_t)dw_t \\ dy_t = \{r(x_t)x_t - \eta y_t\}dt + \sigma_2 y_t(1 - x_t - y_t)dw_t \end{cases}$$

(p, r:functions of $x = x_t$, $\sigma_1, \sigma_2 > 0$: constant, w_t : the Brownian motion of 1-dimensional, $t \in \mathbb{R}_{>0}$.)

Question: **Why stochastic differential equations?**

$\Rightarrow$ We can capture **influence of random phenomenas in the real world (forest fires, disease outbreaks, economic fluctuations, policy shifts, ...)** to the forest transition model.

The 1st result: Existence and uniqueness Theorem.

For our model

$$\begin{cases} dx_t = \{p(x_t)(1-x_t-y_t) - r(x_t)x_t\}dt + \sigma_1 x_t(1-x_t-y_t)dw_t \\ dy_t = \{r(x_t)x_t - \eta y_t\}dt + \sigma_2 y_t(1-x_t-y_t)dw_t \end{cases},$$

we obtain the following theorem.

Theorem (K. –Song–Ton)

There exists a unique global solution of our model equations in $\Delta := \{(x,y) \in \mathbb{R}^2 \mid x, y > 0, 0 < x+y < 1\}$ a.s. for $0 < t < \infty$.

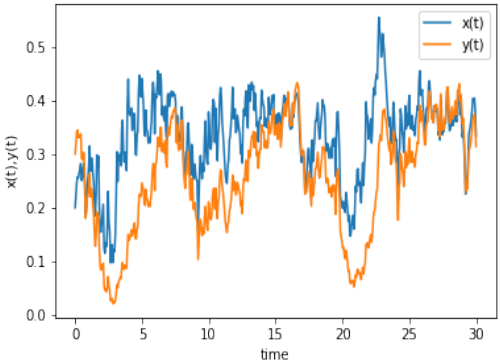

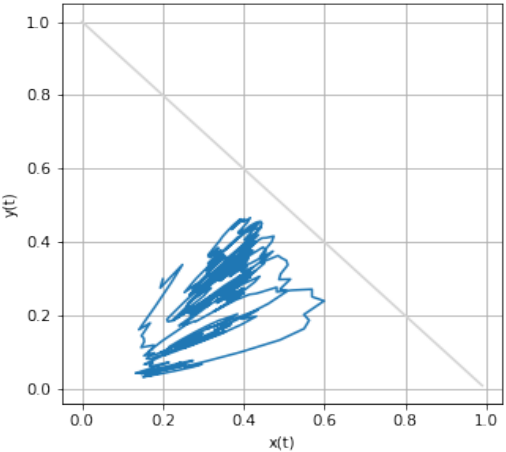

Figure: The values of the solutions (x,y) on $0 \leq t \leq 30$ under FSH.

The 2nd result:Analysis of net expected gain of deforstation

Satake and Rudel introduced a function

$$G(x) = \frac{\alpha[1-\gamma\{1-p(x)\}] - [1-\gamma\{1-\eta-p(x)\}]q(x)}{1-\gamma[2-\eta-p(x)] + \gamma^2(1-\eta)[1-p(x)]}$$

which determine **the sign of the net expected gain of deforestation**.

- If $G(x) > 0$, the owner is likely to deforest to have more land for agriculture.
- if $G(x) \leq 0$ then the owner is likely to increase forest land from agricultural land.

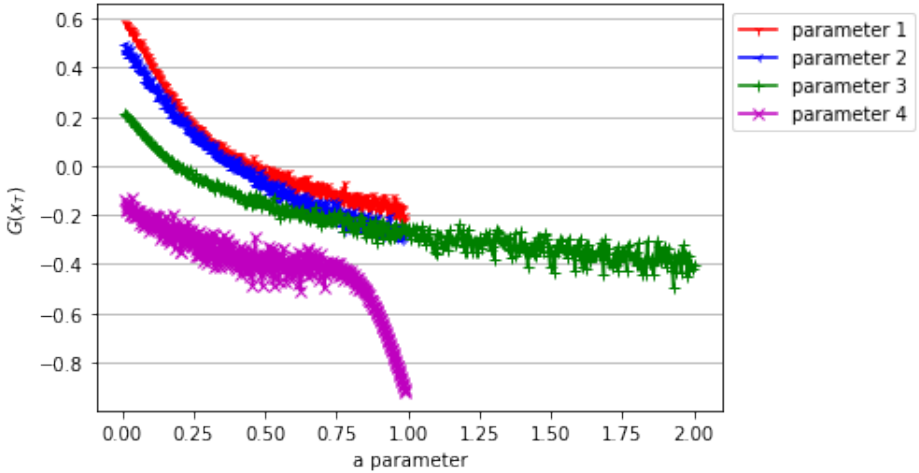

Figure: The value of $G(x_T) = G(x_{30})$ (after $T = 30$ years) as each parameter runs through 0 to 1 under the Forest scarcity hypothesis.

The 3rd result Parameter estimation via deep learning

Following three steps, we predict the parameters giving the stochastic forest transition model.

- **Step 1. Data generation** : We generate a dataset of model parameters (P, σ) through uniform sampling within suitable range.
- **Step 2. Model simulation** : For each model parameter in Step 1, we numerically solve the model equations with a fixed initial value (x_0, y_0). Then we get simulated times series data $(A, F) = ((x_{ij}), (y_{ij}))$.
- **Step 3. Model training** : We train models (RNN, LSTM, SCNN, and Random forest)by datas in Step 2. Then we compare the performances.

Prediction for parameters of the model

- When a numerical data(=the solutions (x_t, y_t)) is given, we will estimate parameters in our stochastic forest transition model. (The inverse problem)
- We apply methods of **deep learning**, RNN, SCNN, LSTM, Random forest model and compare the result.